

**STUDIES IN ASYMMETRIC CATALYSIS FOR
HYDROFORMYLATION REACTIONS**

**A THESIS
SUBMITTED TO THE
UNIVERSITY OF PUNE**

**FOR THE DEGREE OF
DOCTOR OF PHILOSOPHY**

**IN
CHEMISTRY**

**BY
PIPPALADKUMAR S. PANDEY**

**UNDER THE GUIDANCE OF
DR. R. V. CHAUDHARI**

**AT
CHEMICAL ENGINEERING AND PROCESS DEVELOPMENT
DIVISION
NATIONAL CHEMICAL LABORATORY
PUNE – 411 008, INDIA
FEBRUARY 2012**

CERTIFICATE

This is to certify that the work incorporated in the thesis, “**Studies in Asymmetric Catalysis for Hydroformylation Reactions**” submitted by Mr. Pippaladkumar Pandey, for the Degree of Doctor of Philosophy, was carried out by the candidate under my supervision in the National Chemical Laboratory, Pune – 411 008, India. Such material as has been obtained from other sources has been duly acknowledged in the thesis.

Dr. R. V. Chaudhari

Research Supervisor

Declaration by the candidate

I hereby declare that the thesis titled “**Studies in Asymmetric Catalysis for Hydroformylation Reactions**” submitted by me for the degree of Doctor of Philosophy, to the University of Pune, is the record of work carried out by me under the guidance of Dr. R. V. Chaudhari and has not formed the basis for the award of any degree, diploma, associateship, fellowship titles in this or any other university or other institution of higher learning.

I further declare that the material obtained from other sources has been duly acknowledged in this thesis.

February 2012

Pune

Pippaladkumar Pandey

(candidate)

Acknowledgement

I wish to express my sincere gratitude to my research guide, Dr. R. V. Chaudhari for his support, encouragement and guidance during this work. I also wish to express my gratitude to my de-facto co-guides, Dr. Kumar Vanka and Dr. A. A. Kelkar for their continued support which led me in the right direction.

I would like to thank the Director, National Chemical Laboratory for allowing me to carry out this research in this prestigious laboratory. Thanks to the Council of Scientific and Industrial Research for the fellowship.

I would like to gratefully acknowledge the support extended by Dr. S. P. Gupte, Dr. V. H. Rane, Dr. R. M. Deshpande, Dr. Jaganathan, Dr. Sayam Sengupta and Dr. Neelanjana Sengupta during my stay in NCL.

Words cannot express my heartfelt gratitude and appreciation for my friends Dr. Rahul Purandare, Dr. Yogesh Borole, Dr. Nitin Pagar, Dr. Sunil Shinde, Dr. Abhishek Sud, Dr. Kapil Rajurkar, Dr. Makarand Diwakar, Dr. Rashmi Chansarkar, Dr. Charubala Patil, Lalita Kunde, Savita Shingote, Dr. Sunil Tonde, Dr. Deepak Nagargoje, Dr. Jayprakash Nadgeri, Dr. Sangeeta Jagtap, Dr. Amit Chaudhari, Dr. Shashi Bairagi, Dr. Anand Shivarkar, Dr. Nandkumar Patil, Dr. Satyanarayan Reddy, Dr. Sanjay Dhage, Dr. Bibhas Sarkar, Dr. Debdut Roy, Anand Meher, Pravin Jadhav, Harsh Gaikwad, Rajamani, Samadhan Shelke, Chandan, Munshi, Swapna Gade, Vaishali, Kunal, Pradeep, Rakesh, Rajesh, Bharama Malvi and Debasis.

Finally I would like to thank my family for moral support.

February 2012

Pippaladkumar Pandey

List of contents

| | |
|--------------------------|------|
| Chapter index | i |
| List of figures | iv |
| List of tables | vii |
| Abstract of thesis | viii |

Chapter 1: Introduction and literature survey

| | |
|--|-----------|
| 1.1 Asymmetric Catalysis | 1 |
| 1.1.1 Naming Conventions | 1 |
| 1.1.2 Importance of chiral compounds | 2 |
| 1.1.3 Origins of chirality in nature | 3 |
| 1.1.4 Ways of obtaining enantiomerically enriched compounds | 3 |
| 1.1.5 History and basics of asymmetric catalysis | 5 |
| 1.2 Hydroformylation | 7 |
| 1.2.1 Asymmetric hydroformylation | 9 |
| 1.3 Computational chemistry/ Molecular modeling | 22 |
| 1.3.1 Problems faced in molecular modeling | 24 |
| 1.3.2 Finding Transition States (TS) | 25 |
| 1.3.3 Solvation effect | 27 |
| 1.3.4 Literature on DFT studies on asymmetric hydroformylation | 27 |
| 1.4 Scope and objective of the thesis | 28 |

Chapter 2: Asymmetric hydroformylation of styrene using ligand-modified rhodium catalysts (experimental)

| | |
|---|-----------|
| 2.1 Introduction..... | 33 |
| 2.2 Experimental | 33 |
| 2.2.1 Material | 33 |
| 2.2.2 Synthesis of Rh(CO) ₂ (acac)..... | 34 |
| 2.2.3 Experimental set up..... | 34 |
| 2.2.4 Experimental procedure | 35 |
| 2.2.5 Analytical methods | 36 |
| 2.2.6 Separation and identification of the products | 37 |
| 2.3 Results and discussion | 37 |
| 2.3.1 Screening of ligands for rhodium catalyzed asymmetric hydroformylation of styrene | 37 |
| 2.3.2 Effect of solvent..... | 40 |
| 2.3.3 Parametric study..... | 40 |
| 2.3.3.1 Effect of agitation speed | 41 |
| 2.3.3.2 Effect of rhodium concentration | 42 |
| 2.3.3.3 Effect of (<i>R</i>)-BINAP concentration | 45 |
| 2.3.3.4 Effect of CO partial pressure (P _{CO})..... | 46 |
| 2.3.3.5 Effect of H ₂ partial pressure (P _{H2})..... | 48 |
| 2.3.3.6 Effect of styrene concentration | 50 |
| 2.3.3.7 Effect of temperature | 51 |

Chapter 3: Computational study on asymmetric hydroformylation of styrene using (R)-BINAP modified rhodium catalyst

| | |
|---|------------|
| 3.1 Introduction..... | 53 |
| 3.2 Computational..... | 53 |
| 3.3 Results of the computational study | 57 |
| 3.3.1 Conformational search | 57 |
| 3.3.2 Results of DFT study on the catalytic cycle (Heck and Breslow mechanism).... | 60 |
| 3.3.2.1 Energy profile of the catalytic cycle (Heck and Breslow mechanism)..... | 89 |
| 3.3.3 Finding the reasons for the anomalous results of the DFT calculations | 93 |
| 3.3.3.1 Testing the validity of the resolution of identity (RI) approximation..... | 93 |
| 3.3.3.2 Conformational search for the transition states | 93 |
| 3.3.3.3 Testing the validity of use of TZVP and def-TZVP basis sets | 94 |
| 3.3.3.4 Testing the validity of use of Becke-Perdew (b-p) functional | 94 |
| 3.3.3.5 Testing the validity of use of DFT itself..... | 95 |
| 3.3.3.6 Testing the validity of the assumption that (R)-BINAP is a chelating ligand | 95 |
| 3.3.3.7 Testing the validity of use of Heck and Breslow mechanism..... | 104 |
| 3.3.3.8 Investigating the possibility of extra transition states in the Heck and Breslow mechanism | 124 |
| 3.4 Conclusions..... | 128 |

List of figures

Chapter 1: Introduction and literature survey

| | |
|--|----|
| Figure 1: Limonene enantiomers have different smells..... | 2 |
| Figure 2: Synthesis of L-DOPA..... | 5 |
| Figure 3: Representative privileged ligands | 5 |
| Figure 4: The re and si faces of an aldehyde | 6 |
| Figure 5: Reason for asymmetric induction in asymmetric catalysis | 7 |
| Figure 6: General hydroformylation reaction | 8 |
| Figure 7: Heck and Breslow mechanism for hydroformylation reaction | 8 |
| Figure 8: Mechanism proposed by Wilkinson for hydroformylation using modified rhodium catalyst..... | 9 |
| Figure 9: Mechanism of olefin hydroformylation, isomerization and reduction using platinum catalyst..... | 20 |
| Figure 10: Structure of Kelliphite..... | 21 |
| Figure 11: Structure of (<i>R,S</i>)-BINAPHOS..... | 21 |
| Figure 12: Structure of (<i>S,R</i>)-BIPHEMPHOS | 21 |
| Figure 13: Local and global energy minima for butane..... | 25 |
| Figure 14: Saddle point..... | 26 |
| Figure 15: 2-dimensional depiction of reaction coordinate | 26 |

Chapter 2: Asymmetric hydroformylation of styrene using ligand-modified rhodium catalysts (experimental)

| | |
|---|----|
| Figure 1: Ibuprofen | 33 |
| Figure 2: FTIR spectrum of Rh(CO) ₂ (acac) | 34 |
| Figure 3: Schematic diagram of the reactor set up | 35 |
| Figure 4: Typical GC chart | 37 |
| Figure 5: Typical concentration time profile of a batch reactor | 41 |
| Figure 6: Effect of agitation speed on the reaction rate | 42 |

| | |
|--|----|
| Figure 7: Effect of rhodium concentration on the reaction rate | 42 |
| Figure 8: Effect of rhodium concentration on regioselectivity | 43 |
| Figure 9: Effect of rhodium concentration on enantioselectivity | 44 |
| Figure 10: Effect of ligand concentration on reaction rate | 45 |
| Figure 11: Effect of ligand concentration on regioselectivity | 45 |
| Figure 12: Effect of ligand concentration on enantioselectivity | 46 |
| Figure 13: Effect of CO partial pressure on reaction rate | 46 |
| Figure 14: Effect of CO partial pressure on regioselectivity | 47 |
| Figure 15: Effect of CO partial pressure on enantioselectivity | 48 |
| Figure 16: Effect of H ₂ partial pressure on reaction rate | 48 |
| Figure 17: Effect of H ₂ partial pressure on regioselectivity | 49 |
| Figure 18: Effect of H ₂ partial pressure on enantioselectivity | 49 |
| Figure 19: Effect of substrate concentration on reaction rate | 50 |
| Figure 20: Effect of substrate concentration on regioselectivity | 50 |
| Figure 21: Effect of substrate concentration on enantioselectivity | 51 |
| Figure 22: Arrhenius plot | 51 |

Chapter 3: Computational study on asymmetric hydroformylation of styrene using (R)-BINAP modified rhodium catalyst

| | |
|---|----|
| Figure 1: Heck and Breslow mechanism for asymmetric hydroformylation of styrene using (R)-BINAP modified rhodium catalyst | 54 |
| Figure 2: n-decane | 57 |
| Figure 3: Plot of strain energy and electronic energy versus the conformer number of n-decane | 57 |
| Figure 4: Plot of strain energy and electronic energy versus the conformer number of the “step 2” molecule (in the catalytic cycle that gives rise to 3-phenylpropanal) | 58 |
| Figure 5: The two conformers of (R)-BINAP ligand | 59 |
| Figure 6: Cis and trans-chelating ligands | 59 |
| Figure 7: Berry pseudorotation in Iron pentacarbonyl | 60 |
| Figure 8: Free energy profile (gas phase) for formation of (S)-2-phenylpropanal | 89 |

| | |
|---|-----|
| Figure 9: Free energy profile (gas phase) for formation of (<i>R</i>)-2-phenylpropanal..... | 90 |
| Figure 10: Free energy profile (gas phase) for formation of 3-phenylpropanal | 90 |
| Figure 11: Free energy profile (solvated in toluene) for formation of (<i>S</i>)-2-phenylpropanal..... | 91 |
| Figure 12: Free energy profile (solvated in toluene) for formation of (<i>R</i>)-2-phenylpropanal..... | 92 |
| Figure 13: Free energy profile (solvated in toluene) for formation of 3-phenylpropanal | 92 |
| Figure 14: Complex that can be formed by insertion of styrene in the Rh-CO bond of HRh(CO) ₂ (<i>R</i>)-BINAP] | 105 |
| Figure 15: The structure of the "resting state" when H is added to C ₃ in figure 14..... | 105 |
| Figure 16: "Mechanism 2" for hydroformylation..... | 106 |
| Figure 17: Free energy profile (solvated in toluene) for formation of (<i>S</i>)-2-phenylpropanal ("mechanism 2") | 122 |
| Figure 18: Free energy profile (solvated in toluene) for formation of (<i>R</i>)-2-phenylpropanal ("mechanism 2") | 123 |
| Figure 19: Free energy profile (solvated in toluene) for formation of 3-phenylpropanal ("mechanism 2")..... | 123 |
| Figure 20: Complex that can be formed by insertion of styrene in the Rh-CO bond of HRh(CO)(<i>R</i>)-BINAP]..... | 124 |
| Figure 21: Styrene uptake transition states | 125 |
| Figure 22: Modified free energy profile (gas phase) for formation of (<i>S</i>)-2-phenylpropanal..... | 126 |
| Figure 23: Modified free energy profile (gas phase) for formation of (<i>R</i>)-2-phenylpropanal..... | 126 |
| Figure 24: Modified free energy profile (gas phase) for formation of 3-phenylpropanal | 127 |

List of tables

Chapter 1: Introduction and literature survey

| | |
|---|----|
| Table 1: Representative catalysts for asymmetric hydroformylation | 11 |
|---|----|

Chapter 2: Asymmetric hydroformylation of styrene using ligand-modified rhodium catalysts (experimental)

| | |
|---|----|
| Table 1: Standard GC conditions | 36 |
| Table 2: Screening of chiral ligands for asymmetric hydroformylation of styrene | 38 |
| Table 3: Effect of solvent on asymmetric hydroformylation of styrene | 40 |

Chapter 3: Computational study on asymmetric hydroformylation of styrene using (R)-BINAP modified rhodium catalyst

| | |
|---|-----|
| Table 1: Description of optimized geometries of lowest free energy stable molecules (Heck and Breslow mechanism) | 61 |
| Table 2: Description of optimized geometries of transition states (Heck and Breslow mechanism) | 70 |
| Table 3: Structures of molecules described in table 1 and table 2 | 80 |
| Table 4: Description of optimized geometries of styrene insertion transition states with monodentate (R)-BINAP – rhodium catalyst | 96 |
| Table 5: Structures of molecules described in table 4 | 101 |
| Table 6: Description of optimized geometries of TS(A), the lowest free energy "step A" molecules and TS(B) in "mechanism 2" | 108 |
| Table 7: Structures of molecules described in table 6 | 117 |

Abstract of the Thesis

Title: “Studies in Asymmetric Catalysis for Hydroformylation Reactions”

This thesis is being presented in three chapters, a brief summary of which is given below:

Chapter 1: Introduction and literature survey

Most biological systems are chiral. Natural sugars – the building blocks of carbohydrates, are almost exclusively right handed (dextro). On the other hand, natural amino acids, which are the building blocks of proteins, are almost exclusively left handed (leavo). Because most biological systems are chiral, most biologically active molecules like drugs, agricultural chemicals, flavors, fragrances are also chiral. The demand for chiral compounds, often as single enantiomers, has escalated sharply in recent years, driven particularly by the demands of the pharmaceutical industry. Two-thirds of prescription drugs are chiral, with the majority of new chiral drugs being single enantiomers. Although the most obvious applications are bio-related, materials science also relies on the properties imparted by chirality, notably in chiral polymers and liquid crystals. This widespread demand for chiral compounds has stimulated intensive research to develop improved methods for synthesizing such compounds ^[1].

Asymmetric catalysis or enantioselective catalysis is one of the ways to produce enantiomerically enriched compounds. In asymmetric catalysis, small amounts of chiral, enantiomerically pure (or enriched) catalysts are used to promote reactions and lead to the formation of large amounts of enantiomerically pure or enriched product ^[2].

Asymmetric hydroformylation has not reached the level of sophistication of its hydrogenation counterpart (asymmetric hydrogenation) yet. The reasons are unsatisfactory selectivity, activity and low catalyst stability. To achieve the highest levels of activity and selectivity (the prime performance criteria of any catalyst) in asymmetric hydroformylation, several reaction parameters must be optimized, the most crucial of which is perhaps the design of the chiral ligand ^[3]. Because hydroformylation seems to be attainable only with man-made catalysts, extensive efforts have been made by people to develop new chiral transition-metal catalysts ^[4].

This thesis also presents computational (DFT) study on asymmetric hydroformylation. Computational chemistry is a branch of chemistry that uses principles of computer science to assist in solving chemical problems. It uses the results of theoretical chemistry, incorporated into efficient computer programs, to calculate the structures and properties of molecules and solids. Very few literature reports are available on DFT studies on asymmetric hydroformylation ^[5]. Even for achiral hydroformylation, most full DFT studies (entire catalytic cycle) are limited to model reaction systems ^[6].

The main aim of this thesis is to model the asymmetric hydroformylation reaction system to get a deeper insight in the mechanism so that the activity/ selectivity of new catalysts can be predicted beforehand.

Chapter 2: Asymmetric hydroformylation of styrene using ligand-modified rhodium catalysts (experimental)

Styrene is an important substrate for hydroformylation because analogous substrates can be hydroformylated (and later oxidized) to form “profen” drugs. Profen drugs are nonsteroidal anti-inflammatory drugs (NSAIDs) with analgesic and antipyretic (fever-reducing) effects. As analgesics, NSAIDs are unusual in that they are non-narcotic. Most of the NSAIDs classified as propionic acid derivatives (e.g. Ibuprofen, Naproxen, Fenoprofen, Ketoprofen, Dexketoprofen, Flurbiprofen, Loxoprofen) can be synthesized by hydroformylation of substrates analogous to styrene. Most of the profen drugs are chiral and are either marketed as racemic mixtures (e.g. Ibuprofen) or as enantiopure compounds [e.g. (*S*)-Naproxen]. Asymmetric hydroformylation can be one of the ways to synthesize enantiomerically enriched or enantiopure profen drugs.

Chapter 2 presents experimental study on asymmetric hydroformylation of styrene. Various commercially available chiral ligands were screened for this study. Out of the screened ligands, (*R*)-BINAP was chosen and a parametric study on the reaction system was done. Effects of parameters like agitation speed, rhodium concentration, (*R*)-BINAP concentration, CO partial pressure, H₂ partial pressure and styrene concentration on the rate and selectivity (regio and enantio) of the reaction were studied. The activation energy (34.2 kcal/mol) was calculated using the Arrhenius plot.

Chapter 3: Computational study on asymmetric hydroformylation of styrene using (R)-BINAP modified rhodium catalyst

Chapter 3 describes a DFT study on the entire catalytic cycle of asymmetric hydroformylation of styrene. The catalyst is (R)-BINAP modified rhodium. Styrene can be hydroformylated to give three different products – (S)-2-phenylpropanal, (R)-2-phenylpropanal and 3-phenylpropanal. The overall mechanism of styrene hydroformylation can be imagined as a superimposition of three distinct catalytic cycles, each giving rise to one of the three aldehyde products.

Because the metal-complex molecules on which this computational study has been done are very large and can have many conformers, a conformational search (using torsion angle driving) was done on stable molecules. At least five of the lowest energy conformers so obtained from the conformational search were subjected to DFT calculations for geometry optimization. Thus the conformers were screened using molecular mechanics (MM) before subjecting them to quantum mechanical (QM) calculations. The solvation effect was calculated for important molecules using COSMO. The transition states (saddle points on the energy hypersurface) were derived from the optimized geometries of the stable molecules in the catalytic cycle.

The DFT studies done for the Heck and Breslow mechanism^[7] gave results (for regioselectivity and enantioselectivity) that were in contradiction to the experimental results in chapter 2. To find out the reasons for the anomalous results of the DFT calculations, some of the assumptions and approximations (used during the calculations) were tested for their validity. The possibility of the reaction following alternate mechanisms was also explored. It was found that the uptake barrier for styrene (and not the alkene insertion) was the rate determining step.

References:

- [1] J. Halpern, B. M. Trost, *Proceedings of the National Academy of Sciences of the United States of America* **2004**, *101*, 5347.
- [2] aI. Ojima, *Catalytic asymmetric synthesis*, Wiley, **2010**; bH. U. Blaser, E. Schmidt, *Introduction*, Wiley Online Library, **2004**; cM. Heitbaum, F. Glorius, I. Escher, *Angewandte Chemie International Edition* **2006**, *45*, 4732-4762; dE. N. Jacobsen, A. Pfaltz, H. Yamamoto, *Comprehensive asymmetric catalysis*, Vol. 2, Springer, **2004**.
- [3] P. Leeuwen, P. Kamer, C. Claver, O. Pàmies, M. Diéguez, *Chemical Reviews* **2010**.
- [4] K. Nozaki, N. Sakai, T. Nanno, T. Higashijima, S. Mano, T. Horiuchi, H. Takaya, *Journal of the American Chemical Society* **1997**, *119*, 4413-4423.
- [5] aC. J. Copley, R. D. J. Froese, J. Klosin, C. Qin, G. T. Whiteker, K. A. Abboud, *Organometallics* **2007**, *26*, 2986-2999; bJ. Meeuwissen, A. J. Sandee, B. de Bruin, M. A. Siegler, A. L. Spek, J. N. H. Reek, *Organometallics* **2010**, *29*, 2413-2421.
- [6] aM. Sparta, K. J. Børve, V. R. Jensen, *Journal of the American Chemical Society* **2007**, *129*, 8487-8499; bJ. da Silva, R. P. Dias, W. B. de Almeida, W. R. Rocha, *Journal of Computational Chemistry* **2010**, *31*, 1986-2000; cC.-F. Huo, Y.-W. Li, M. Beller, H. Jiao, *Chemistry--A European Journal* **2005**, *11*, 889-902.
- [7] R. F. Heck, D. S. Breslow, *Journal of the American Chemical Society* **1961**, *83*, 4023-4027.



CHAPTER 1

Introduction and Literature Survey

1.1 Asymmetric Catalysis

Asymmetric catalysis or enantioselective catalysis is one of the ways to produce enantiomerically enriched compounds. An enantiomer is one of the two stereoisomers that are non-superposable mirror images of each other. An enantiomerically enriched compound is a mixture of the two enantiomers, where the concentration of one enantiomer is in excess to the other. The extent of enantiomeric enrichment is measured in terms of “enantiomeric excess” (ee).

$$ee (\%) = \frac{[R] - [S]}{[R] + [S]} * 100$$

Here, [R] and [S] represent the concentrations of R and S enantiomers of a “chiral” compound. The term “chiral” in general is used to describe an object that is non-superposable on its mirror image (Greek word for hand – “cheir”). A chiral object lacks an internal plane of symmetry. An achiral (non-chiral) object is one which is identical to its mirror image.

An ee of 0 % corresponds to a racemic mixture (derived from the Latin word “racemus” for “bunch of grapes”. This term has its origins in the work of Louis Pasteur who isolated racemic tartaric acid from wine). An ee of 100 % corresponds to enantiopure compounds, i.e., compounds having molecules of only one chirality ^[1] (within the limits of detection).

1.1.1 Naming Conventions: The R / S system is the most important nomenclature system for denoting enantiomers. It labels each chiral center R or S according to a system by which its substituents are each assigned a priority, according to the Cahn–Ingold–Prelog priority rules (CIP), based on atomic number ^[2]. If the center is oriented so that the lowest-priority of the four is pointed away from a viewer, the viewer will then see two possibilities: If the priority of the remaining three substituents decreases in clockwise direction, it is labeled R (for Rectus, Latin for right), if it decreases in counterclockwise direction, it is S (for Sinister, Latin for left).

Besides the R / S system of nomenclature, there are D / L and (+) / (-) systems. The D / L nomenclature is generally used for biomolecules and is based on relating the chiral molecule with glyceraldehyde. The (+) / (-) nomenclature indicates that the enantiomer rotates the plane of polarized light (as seen by a viewer towards whom the light is traveling), clockwise or anti-clockwise respectively. There is no fixed relation between the three nomenclature systems. An R isomer can be either (+) or (-), or it can be D or L.

1.1.2 Importance of chiral compounds: Most biological systems are chiral. Natural sugars – the building blocks of carbohydrates, are almost exclusively right handed (dextro). On the other hand, natural amino acids, which are the building blocks of proteins, are almost exclusively left handed (leavo). Two enantiomers of limonene give oranges (R) and lemons (S) quite different and characteristic flavors ^[3].

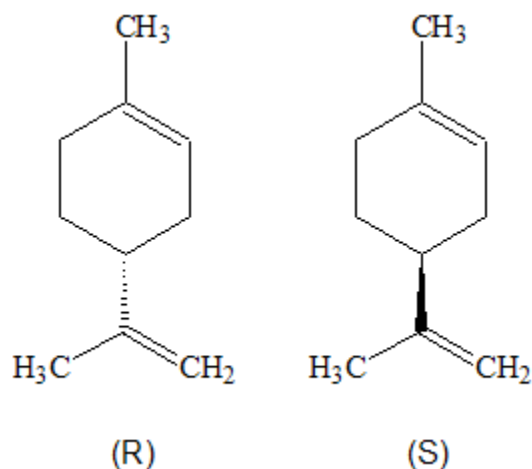


Figure 1: Limonene enantiomers have different smells.

Caraway (S) and Spearmint (R) flavors are enantiomers. North American Pine trees contain one enantiomer of pinene, but the European Pines contain the other.

Because most biological systems are chiral, most biologically active molecules like drugs, agricultural chemicals, flavors, fragrances are also chiral. The demand for chiral compounds, often as single enantiomers, has escalated sharply in recent years, driven particularly by the demands of the pharmaceutical industry. Two-thirds of prescription drugs are chiral, with the majority of new chiral drugs being single enantiomers.

Although the most obvious applications are bio-related, materials science also relies on the properties imparted by chirality, notably in chiral polymers and liquid crystals. This widespread demand for chiral compounds has stimulated intensive research to develop improved methods for synthesizing such compounds ^[4].

1.1.3 Origins of chirality in nature: In biology homochirality is a common property of amino acids and sugars. A molecule is said to be homochiral if all the molecule's constituent units are of the same chiral form. It is unclear if homochirality has a purpose, however it appears to be a form of information storage ^[5]. Some scientists believe that Earth life's "choice" of chirality was purely random, and that if carbon-based life forms exist elsewhere in the universe, their chemistry could theoretically have opposite chirality. However, there is some suggestion that early amino acids could have formed in comet dust. In this case, circularly polarized radiation (which makes up 17% of stellar radiation) could have caused the selective destruction of one chirality of amino acids, leading to a selection bias which ultimately resulted in all life on Earth being homochiral ^[6].

1.1.4 Ways of obtaining enantiomerically enriched compounds: One has to understand why it is difficult to obtain enantiomerically enriched compounds. Enantiomers have the same physical properties, viz., boiling points, melting points, solubilities, etc., so many of the techniques used to separate other compounds don't work on racemic mixtures. Enantiomers behave identically in an achiral environment. The solution to this problem is to separate enantiomers in a chiral environment, where they interact differently.

There are two main strategies for obtaining enantiomerically enriched compounds:

- **Chiral resolution** ^[7]: It is a process for the separation of racemic compounds into their enantiomers. Typically 5-10% of all racemates are known to crystallize as mixtures of enantiopure crystals, so-called conglomerates ^[8]. Louis Pasteur was the first to conduct chiral resolution when he discovered the concept of optical activity in the first place by the manual separation of left-handed and right-handed tartaric acid crystals in 1849. Besides the crystallization method, one can also use

chiral resolving agents. The method was introduced (again) by Louis Pasteur in 1853 by resolving racemic tartaric acid with optically active (+)-cinchotoxine. One modern-day method of chiral resolution is used in the organic synthesis of the drug Duloxetine^[9]. Besides these methods, one can also use chiral column chromatography. In chiral resolution techniques, 50 % of the compound (the unwanted enantiomer) is either discarded or has to undergo the Resolution-Racemization-Recycle (RRR) pathway. Thus, chiral resolution is a very inefficient method for enantiomeric enrichment.

- **Asymmetric synthesis:** To obtain enantiomerically enriched compounds, at least one component in the reaction system has to be chiral. Either the substrate, the catalyst, the solvent, the source of energy (circularly or elliptically polarized light) or the space where the reaction takes place (nanoreactor) has to be chiral.
 - (i) Chiral pool synthesis is a method where a chiral substrate is manipulated through successive reactions using achiral reagents that retain its chirality to obtain the desired target molecule. This method uses stoichiometric amount of enantiopure substrate.
 - (ii) Chiral solvents^[10] can be used in some cases where they influence the solubility of the enantiomers of the product in a differential way.
 - (iii) Circularly or elliptically polarized light can be used for inducing chirality^[11]. It can also be used to selectively destroy the unwanted enantiomer. Circular dichroism (CD) refers to the differential absorption of left and right circularly polarized light^[12]. This phenomenon was discovered by Jean-Baptiste Biot, Augustin Fresnel, and Aimé Cotton in the first half of the 19th century^[13].
 - (iv) Chiral reactor can induce enantiomeric asymmetry, provided the size of the reactor is not too large compared to the size of the reacting molecules. Chiral nanoreactors can be useful in this case^[14]. Mesoporous materials synthesized using chiral templates can also act as chiral reactors^[15].
 - (v) Asymmetric catalysis employ small amounts of chiral, enantiomerically pure (or enriched) catalysts to promote reactions and lead to the formation of large amounts of enantiomerically pure or enriched product^[10b, 16]. Chiral catalysts can be broadly divided into metal-ligand complexes derived from chiral ligands,

chiral organocatalysts ^[17] and biocatalysts (enzymes). The scope of the present thesis is limited to metal-ligand complexes derived from chiral ligands.

1.1.5 History and basics of asymmetric catalysis: The first methods were pioneered by William S. Knowles and Ryōji Noyori (Nobel Prize in Chemistry 2001). Knowles in 1968 replaced the achiral triphenylphosphine ligands in Wilkinson's catalyst by the chiral phosphine ligands P(phenyl)(methyl)(propyl), thus creating the first asymmetric catalyst. Knowles' method was used in industrial production of L-DOPA.

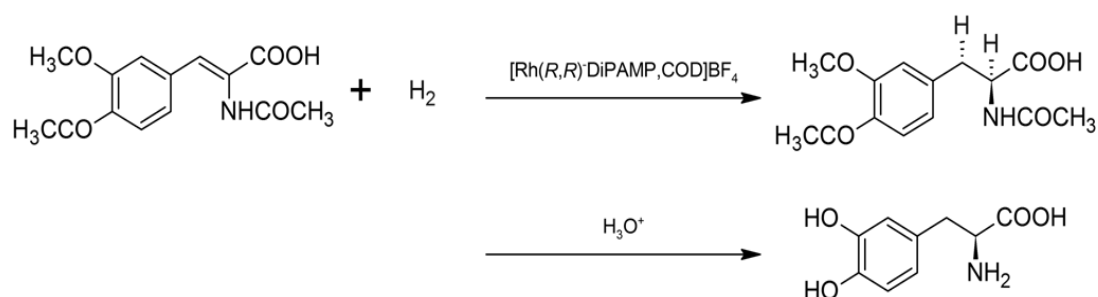


Figure 2: Synthesis of L-DOPA

In the same year, Noyori ^[18] published his chiral ligand for a cyclopropanation reaction of styrene.

Many thousands of chiral ligands have been prepared and tested since then but only several compound classes have been found to have a general scope. These ligands are therefore called privileged ligands ^[19].

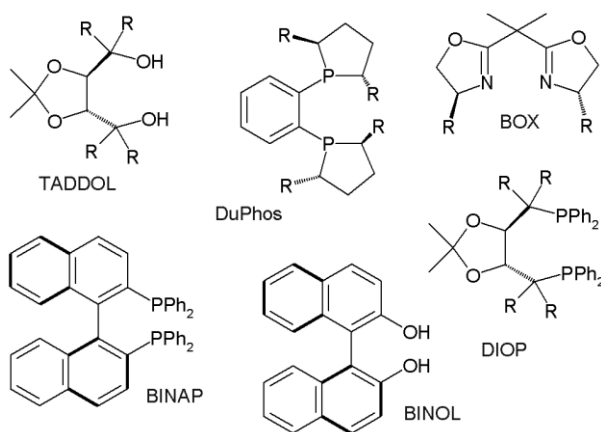


Figure 3: Representative privileged ligands

Most of the chiral ligands in literature are huge molecules and are often referred to as “chemzymes” (analogous to enzymes) ^[20]. Catalysts synthesized using these chemzymes can be called biomimetic catalysts ^[21] because they imitate mode of action by natural enzymes. Most of the models applied to enzymes (for example, Emil Fischer’s “lock and key” ^[22] model and Daniel Koshland’s “induced fit” ^[23] model) can also be applied to chemzymes. A large number of chiral ligands are bidentate because bidentate ligands provide rigidity to the structure of the metal-ligand complex (this is in contrast to monodentate ligands which can freely rotate along the metal-ligand axis).

If one looks at the structures of BINOL and BINAP ligands, these don’t have a “point chirality” (there is no single stereogenic atom). This is because it is possible for a molecule to be chiral without having actual point chirality. Common examples include 1,3-dichloro-allene, which has axial chirality, (*E*)-cyclooctene, which has planar chirality, and certain calixarenes and fullerenes, which have inherent chirality. BINOL and BINAP show axial chirality because rotation along the bond joining the two naphthyl moieties is restricted.

To carry out asymmetric catalysis, one needs a prochiral substrate and a chiral catalyst. Prochiral molecules are those that can be converted from achiral to chiral in a single step. Prochirality depends not only on the structure of the substrate but also the type of reaction under study. For example, styrene is a prochiral substrate for asymmetric hydroformylation [because it can give rise to (*R*)-2-phenylpropanal and (*S*)-2-phenylpropanal during the reaction], but it is not a prochiral substrate for asymmetric hydrogenation (because it will hydrogenate to give ethylbenzene – an achiral product).

A prochiral molecule typically has two faces – the *re*-face and the *si*-face.

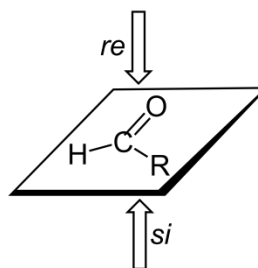


Figure 4: The *re* and *si* faces of an aldehyde

The following figure 5 shows the reason for asymmetric induction in asymmetric catalysis.

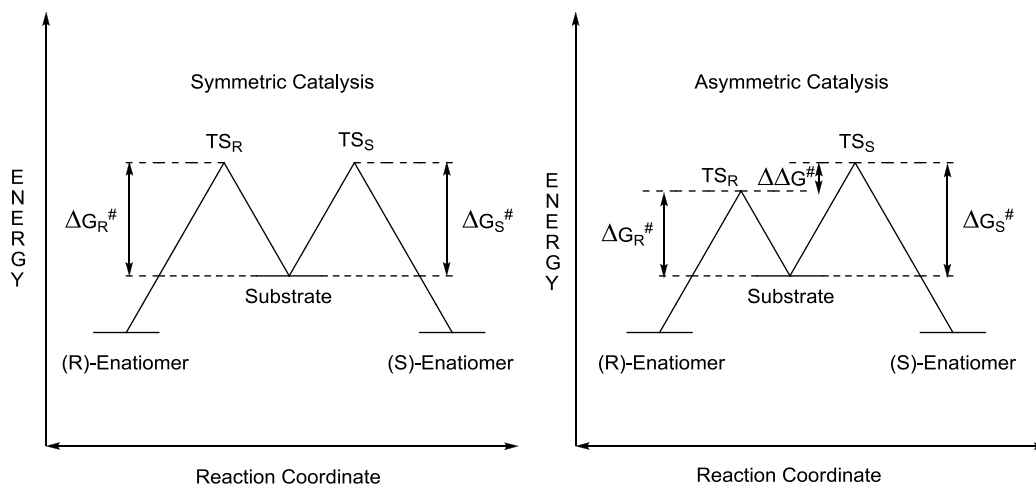


Figure 5: Reason for asymmetric induction in asymmetric catalysis

In case of symmetric catalysis, the prochiral substrate interacts with the achiral catalyst to form enantiomeric transition states. These enantiomeric transition states have the same stability (and therefore the same activation energy). This leads to formation of a racemic mixture. On the other hand, in the case of asymmetric catalysis, the prochiral substrate interacts with the chiral catalyst to form diastereomeric transition states. Diastereomers are stereoisomers that are not enantiomers, and so they have different stability, which is depicted in the differentiation of the activation energies ($\Delta\Delta G^\ddagger \neq 0$). This is how one can get a non-thermodynamic/ non-racemic mixture of the enantiomers of the product. The enantiomeric excess obtained in a reaction can be correlated with $\Delta\Delta G^\ddagger$ (and vice versa) using the Arrhenius equation.

1.2 Hydroformylation

Hydroformylation is an important industrial process for the production of aldehydes from alkenes ^[24]. This chemical reaction entails the addition of a formyl group (CHO) and a hydrogen atom to a carbon-carbon double bond. This is an excellent example of a potentially 100 % atom efficient ^[25] reaction, and has been extensively used in the industrial synthesis of simple linear aldehydes ^[26]. This process has undergone

continuous growth since its invention in the 1930s: Production capacity reached 6.6×10^6 tons in 1995. It is important because the resulting aldehydes are easily converted into many secondary products. For example, the resulting aldehydes are hydrogenated to alcohols that are converted to detergents. Hydroformylation is also used in specialty chemicals, relevant to the organic synthesis of fragrances and natural products. The development of hydroformylation, which originated within the German coal-based industry, is considered one of the premier achievements of 20th-century industrial chemistry.

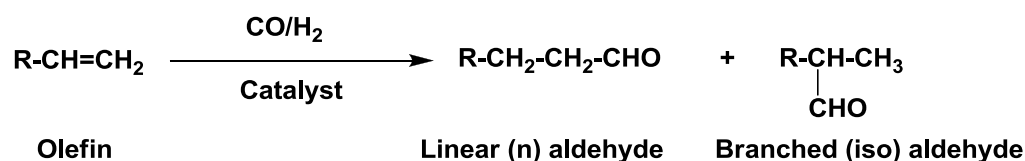


Figure 6: General hydroformylation reaction

The original catalyst was $\text{HCo}(\text{CO})_4$, discovered by Otto Roelen^[27]. Subsequent work demonstrated that the ligand tributylphosphine (PBU_3) improved the selectivity of the cobalt-catalyzed process. Since the 1970s, most hydroformylation relies on catalysts based on rhodium^[28].

Heck and Breslow proposed a mechanism for hydroformylation in 1961^[29]. This mechanism was proposed for the cobalt catalyzed hydroformylation reaction. However, the basic steps in this mechanism are valid also for rhodium catalyzed hydroformylation.

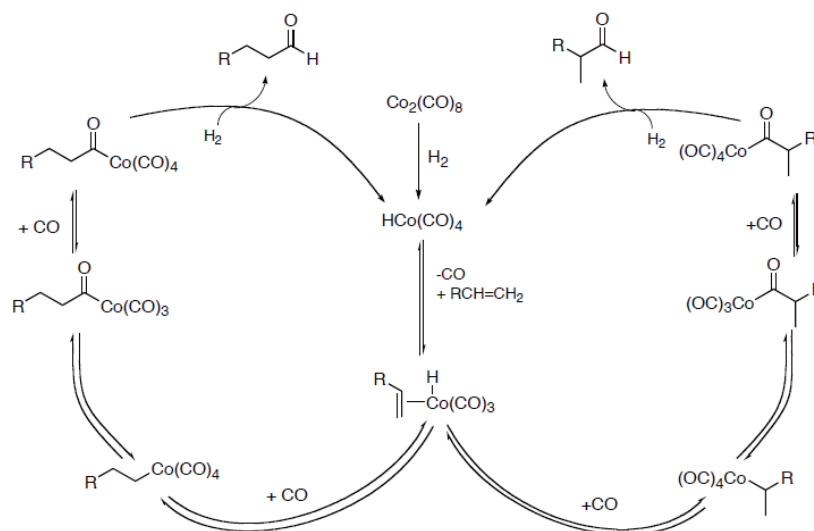


Figure 7: Heck and Breslow mechanism for hydroformylation reaction

The following figure 8 describes the mechanism for rhodium catalyzed hydroformylation, as proposed by Wilkinson^[30].

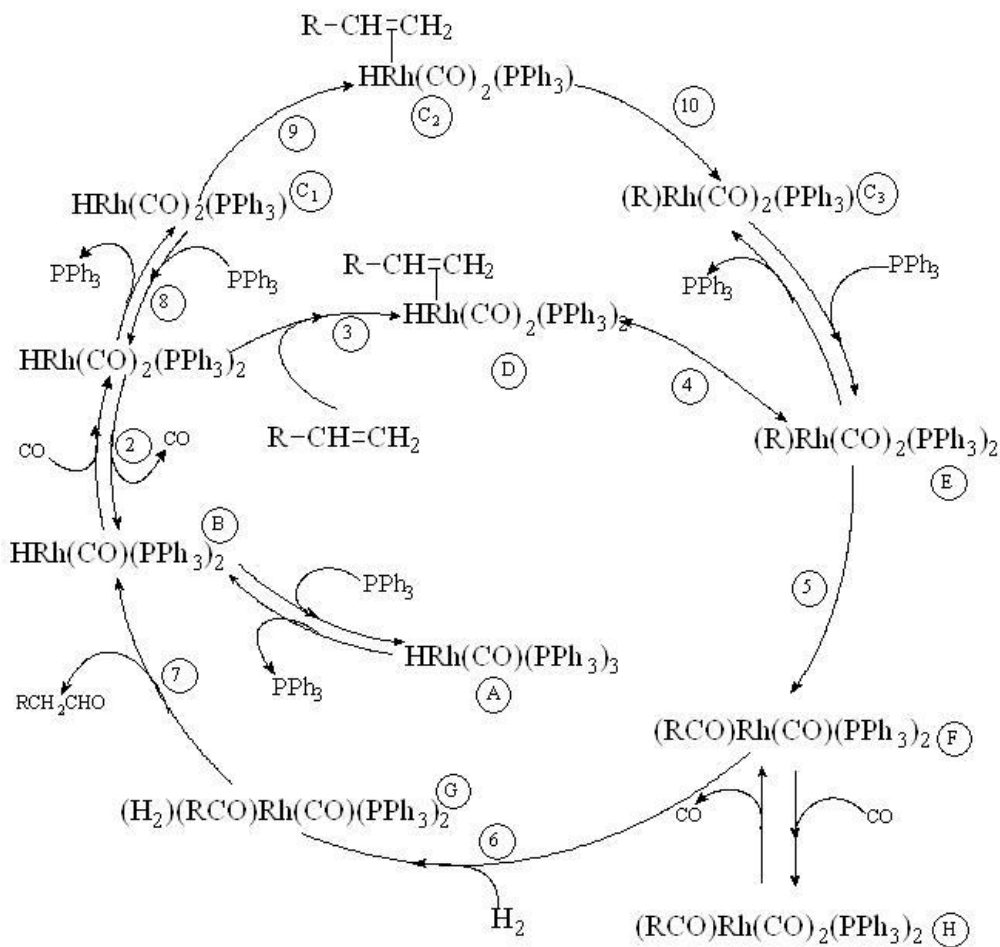


Figure 8: Mechanism proposed by Wilkinson for hydroformylation using modified rhodium catalyst

1.2.1 Asymmetric hydroformylation: Asymmetric hydroformylation has not reached the level of sophistication of its hydrogenation counterpart (asymmetric hydrogenation) yet. The reasons are unsatisfactory selectivity, activity and low catalyst stability.

To achieve the highest levels of activity and selectivity (the prime performance criteria of any catalyst) in asymmetric hydroformylation, several reaction parameters must be optimized, the most crucial of which is perhaps the design of the chiral ligand^[31]. Because hydroformylation seems to be attainable only with man-made catalysts, extensive efforts have been made to develop new chiral transition-metal catalysts^[32].

The activity of a catalyst is measured in terms of “turn over frequency” (TOF) which is “turn over number”^[33] (TON) per unit time. The selectivity of a catalyst is its ability to direct a reaction to yield preferentially a particular product. For asymmetric hydroformylation of molecules like styrene and vinyl acetate, the hierarchy of selectivity can be represented as below:

- Chemoselectivity
- Regioselectivity
- Enantioselectivity

Most hydroformylation catalysts can also carry out hydrogenation. The selectivity towards hydroformylation products (as against hydrogenation products) is termed chemoselectivity. The regioselectivity refers to preference towards formation of either the branched aldehyde or the linear aldehyde. Regioselectivity is normally measured in terms of the branched/ linear (b/l) or the branched/ normal (b/n) ratio. One must take into account the fact that the branched aldehyde is more preferred in asymmetric hydroformylation because the branched aldehyde is chiral whereas the linear aldehyde is achiral. This is in contrast to achiral hydroformylation where the linear aldehyde is preferred. The enantioselectivity is measured in terms of enantiomeric excess (ee). One has to remember that the calculation for enantiomeric excess does not take into account the chemoselectivity and the regioselectivity. To enhance the overall selectivity, all the three selectivities should be maximized. (In some substrates, there is an extra layer of selectivity – the diastereoselectivity – which has to be considered for finding the overall selectivity.)

Substrates like styrene and vinyl acetate have a tendency to give high b/l ratio (as compared to substrates like 1-butene and 1-pentene). So these (with their derivatives) are amongst the popular substrates studied for asymmetric hydroformylation.

The following table 1 enlists some representative ligands in the literature that have been used for asymmetric hydroformylation:

Table 1: Representative catalysts for asymmetric hydroformylation

| Sr. No. | Catalyst | | Substrate | Selectivity | | | Rf. |
|---------|----------|---------------------------------------|---------------|-------------------------------|---------------------|---------------|------|
| | Metal | Ligand | | Chemo/ % conv. or yield | Regio/ b/l ratio | Enantio/ ee % | |
| 1 | Rh | (<i>R,R</i>)- DIOP | Styrene | - | 2.1 | 12 % (R) | [34] |
| 2 | Rh | (<i>R,R</i>)- DIOP- DBP | Styrene | - | 8.1 | 25 % (R) | [34] |
| 3 | Rh | (<i>R,R</i>) DIPHOL | Vinyl Acetate | - | - | 51 % (R) | [35] |
| 4 | Rh | (<i>R,R</i>) DIOP | Vinyl Acetate | - | - | 40 % (S) | [35] |
| 5 | Rh | (<i>R,R</i>) 1-Naphthalene DIOP | Vinyl Acetate | - | - | 6 % (S) | [35] |
| 6 | Rh | (<i>R,R</i>) 2-Naphthalene DIOP | Vinyl Acetate | - | - | 39 % (S) | [35] |
| 7 | Rh | (<i>R,R</i>) m-CF ₃ DIOP | Vinyl Acetate | - | - | 42 % (S) | [35] |
| 8 | Rh | (<i>R,R</i>) DMPP- DIOP | Vinyl Acetate | - | - | 18 % (R) | [35] |
| 9 | Rh | (<i>R,R</i>) DIPH- DIOP | Vinyl Acetate | - | - | 29 % (S) | [35] |
| 10 | Pt | (<i>R,R</i>)- DIOP- DBP | Styrene | > 59 % | 4.5 | 80 % (S) | [36] |
| 11 | Rh | (<i>S,S</i>)- CHIRAPHOS | Styrene | 80 % | 15.7 | 24 % (R) | [37] |
| 12 | Pt | (<i>R,R</i>)- DIOP | Styrene | 35 % | 0.6 | 4 % (S) | [37] |
| 13 | Pt | (<i>S,S</i>)- CHIRAPHOS | Styrene | 47 % | 0.6 | 45 % (R) | [37] |
| 14 | Pt | (<i>2S, 4S</i>)- BPPM | Styrene | > 98 % | 1.0 | > 96 % (S) | [38] |
| 15 | Pt | (<i>R,S</i>)- EPHOS | Styrene | 50 % | 0.7 | 36 % (S) | [39] |
| 16 | Rh | (<i>R,S</i>)- EPHOS | Styrene | 63 % | 9.0 | 31 % (R) | [40] |
| 17 | Rh | (<i>R,R</i>)- DIOP-Et | Styrene | 58 % | 100 | 0.2 % (S) | [41] |

| Sr. No. | Catalyst | | Substrate | Selectivity | | | Rf. |
|---------|----------|--|-------------------------------|-------------------------------|---------------------|---------------|------|
| | Metal | Ligand | | Chemo/ % conv. or yield | Regio/ b/l ratio | Enantio/ ee % | |
| 18 | Pt | 1-(tert- Butoxycarbonyl)- (2 <i>S</i> ,4 <i>S</i>)-2- [(dibenzo phospholyl) methyl]-4- (dibenzo phospholyl) pyrrolidine | Styrene | 56 % | 3.3 | > 96 % | [42] |
| 19 | Pt | (-) BPPM | Styrene | 100 % | 0.5 | > 96 % | [42] |
| 20 | Pt | 1-(tert- Butoxycarbonyl)- (2 <i>S</i> ,4 <i>S</i>)-2- [(diphenyl phosphino) methyl]-4- (dibenzo phospholyl) pyrrolidine | Styrene | 26 % | 1.2 | > 96 % | [42] |
| 21 | Pt | 1-(tert- Butoxycarbonyl)- (2 <i>S</i> ,4 <i>S</i>)-2- [(dibenzo phospholyl) methyl]-4- (diphenyl phosphino) pyrrolidine | Styrene | 90 % | 0.9 | > 96 % | [42] |
| 22 | Pt | 1-(tert- Butoxycarbonyl)- (2 <i>S</i> ,4 <i>S</i>)-2- [(dibenzo phospholyl) methyl]-4- (dibenzo phospholyl) pyrrolidine | 2-Vinyl Naphthalene | 73 % | 3.4 | > 96 % (S) | [42] |
| 23 | Pt | 1-(tert- Butoxycarbonyl)- (2 <i>S</i> ,4 <i>S</i>)-2- [(dibenzo phospholyl) methyl]-4- (dibenzo phospholyl) pyrrolidine | 3-Ethenylphenyl Phenyl Ketone | 34 % | 3.3 | > 96 % (S) | [42] |
| 24 | Pt | 1-(tert- Butoxycarbonyl)- (2 <i>S</i> ,4 <i>S</i>)-2- [(dibenzo phospholyl) methyl]-4- (dibenzo phospholyl) pyrrolidine | 4-Ethenylphenyl Phenyl Ketone | 15 % | 3.0 | > 96 % (S) | [42] |

| Sr. No. | Catalyst | | Substrate | Selectivity | | | Rf. |
|---------|----------|--|---|-------------------------------|---------------------|---------------|------|
| | Metal | Ligand | | Chemo/ % conv. or yield | Regio/ b/l ratio | Enantio/ ee % | |
| 25 | Pt | 1-(tert- Butoxycarbonyl)- (2 <i>S</i> ,4 <i>S</i>)-2- [(dibenzo phospholyl) methyl]-4- (dibenzo phospholyl) pyrrolidine | 2-Ethenyl- 5- benzoyl thiophene | 38 % | 25.0 | > 96 % (S) | [42] |
| 26 | Pt | 1-(tert- Butoxycarbonyl)- (2 <i>S</i> ,4 <i>S</i>)-2- [(dibenzo phospholyl) methyl]-4- (dibenzo phospholyl) pyrrolidine | 4-Ethenylphenyl 2- Thienyl Ketone | 15 % | 3.4 | > 96 % (S) | [42] |
| 27 | Pt | 1-(tert- Butoxycarbonyl)- (2 <i>S</i> ,4 <i>S</i>)-2- [(dibenzo phospholyl) methyl]-4- (dibenzo phospholyl) pyrrolidine | 4-Ethenyl- 2-fluoro biphenyl | 20 % | 3.4 | > 96 % (S) | [42] |
| 28 | Pt | 1-(tert- Butoxycarbonyl)- (2 <i>S</i> ,4 <i>S</i>)-2- [(dibenzo phospholyl) methyl]-4- (dibenzo phospholyl) pyrrolidine | 4-(1,3- Dihydro- 1-oxo- 2H- isoindol- 2-yl) styrene | 60 % | Only Branched | 60 % (S) | [42] |
| 29 | Pt | 1-(tert- Butoxycarbonyl)- (2 <i>S</i> ,4 <i>S</i>)-2- [(dibenzo phospholyl) methyl]-4- (dibenzo phospholyl) pyrrolidine | p-iso butyl styrene | 8 % | 2.0 | > 96 % (S) | [42] |
| 30 | Pt | 1-(tert- Butoxycarbonyl)- (2 <i>S</i> ,4 <i>S</i>)-2- [(dibenzo phospholyl) methyl]-4- (dibenzo phospholyl) pyrrolidine | m-phenoxy styrene | 33 % | 1.3 | > 96 % (S) | [42] |
| 31 | Pt | 1-(tert- Butoxycarbonyl)- (2 <i>S</i> ,4 <i>S</i>)-2- [(dibenzo phospholyl) methyl]-4- (dibenzo phospholyl) pyrrolidine | 6-methoxy- 2-vinyl naphthalene | 50 % | 3.4 | > 96 % (S) | [42] |

| Sr. No. | Catalyst | | Substrate | Selectivity | | | Rf. |
|---------|----------|---|---------------------|-------------------------------|---------------------|------------------------|------|
| | Metal | Ligand | | Chemo/ % conv. or yield | Regio/ b/l ratio | Enantio/ ee % | |
| 32 | Pt | (<i>S</i>)- BINAP | Styrene | 36 % | 0.5 | 69 % | [43] |
| 33 | Pt | (<i>R,R</i>)- BCO | Styrene | 90 % | 0.8 | 25 % (<i>S</i>) | [44] |
| 34 | Pt | (<i>R,R</i>)- BCO- DBP | Styrene | 71 % | 4.0 | 85 % (<i>S</i>) | [44] |
| 35 | Pt | <i>S</i> - PROLOPHOS | Styrene | 95 % | 1.2 | 29 % (<i>R</i>) | [45] |
| 36 | Rh | (<i>R,S</i>)- BINAPHOS | Vinyl Acetate | > 99 % | 6.1 | 92 % (<i>S</i>)- (-) | [46] |
| 37 | Rh | (<i>R,R</i>)- BINAPHOS | Vinyl Acetate | 46 % | 11.5 | 73 % (<i>S</i>)- (-) | [46] |
| 38 | Rh | (<i>R,S</i>)- 3,5- Me ₂ BINAPHOS | Vinyl Acetate | 72 % | 5.7 | 90 % (<i>S</i>)- (-) | [46] |
| 39 | Rh | (<i>S,R</i>)- BINAPHOS | p-methyl styrene | 97 % | 6.1 | 95 % (+) | [46] |
| 40 | Rh | (<i>S,R</i>)- BINAPHOS | 4-methoxy styrene | > 99 % | 6.7 | 88 % (+) | [46] |
| 41 | Rh | (<i>S,R</i>)- BINAPHOS | 4-chloro styrene | > 99 % | 6.7 | 93 % (+) | [46] |
| 42 | Rh | (<i>S,R</i>)- BINAPHOS | p-iso butyl styrene | > 99 % | 7.3 | 92 % (<i>S</i>)- (+) | [46] |
| 43 | Rh | (<i>R,S</i>)- BINAPHOS | n-butyl styrene | 90 % | 0.3 | 75 % (<i>R</i>)- (-) | [46] |
| 44 | Rh | (+) BINAS + PPh ₃ | Styrene | 100 % | 11.5 | 7 % (<i>S</i>) | [47] |
| 45 | Rh | (+) Me ₂ BINAS | Styrene | 100 % | 5.3 | 15 % (<i>S</i>) | [47] |
| 46 | Rh | (-) DIOS + PPh ₃ | Styrene | 97 % | 10.1 | 4 % (<i>S</i>) | [48] |
| 47 | Rh | <i>S</i> -methyl (<i>R</i>)-2-diphenyl phosphino-1,1'-binaphthyl-2'-thiol | Styrene | 100 % | 24.0 | 14 % | [49] |
| 48 | Rh | (<i>S</i>)-4-phenyl-4,5-dihydro-3H-dinaphtho[2,1-c;1',2'-e] phosphepine | Styrene | 96 % | 13.3 | 12 % | [50] |
| 49 | Rh | (isoBHA-P) ₂ -2 <i>R</i> ,4 <i>R</i> - pentanediol | Styrene | - | 49.2 | 90 % (<i>S</i>) | [51] |

| Sr. No. | Catalyst | | Substrate | Selectivity | | | Rf. |
|---------|----------|---|----------------|-------------------------------|---------------------|---------------|------|
| | Metal | Ligand | | Chemo/ % conv. or yield | Regio/ b/l ratio | Enantio/ ee % | |
| 50 | Rh | (isoBHA-P) ₂ -2 <i>R</i> ,4 <i>R</i> -pentanediol | Vinyl Acetate | - | - | 50 % (S) | [51] |
| 51 | Rh | (<i>S,R</i>)- BIPHEMPHOS | Styrene | > 99 % | 9.0 | 94 % (S) | [52] |
| 52 | Rh | (<i>S,R</i>)- BIPHEMPHOS | Vinyl Acetate | 65 % | 5.7 | 90 % (R) | [52] |
| 53 | Rh | (<i>S,R</i>)- BIPHEMPHOS | 1- Hexene | 51 % | 0.3 | 85 % (S) | [52] |
| 54 | Rh | (<i>S,R</i>)- BIPHEMPHOS | Indene | 62 % | 11.5 | 88 % (+) | [52] |
| 55 | Rh | (<i>S,R</i>)- BIPHEMPHOS | Acenaphthylene | 74 % | 19.0 | 96 % (+) | [52] |
| 56 | Rh | 3,5- Bis [(4,4',6,6'- tetra- t- butyl- 2, 2'- biphenyl- 1,1'- diy) phosphite]- 1,2- <i>O</i> - isopropylidene- D- xylo- furanose | Styrene | 47 % | 19.0 | 40 % (S) | [53] |
| 57 | Rh | 3,5- Bis [(4,4'-di- t- butyl- 6,6'- dimethoxy- 2, 2'- biphenyl- 1,1'- diy) phosphite]- 1,2- <i>O</i> - isopropylidene- D- xylo- furanose | Styrene | 99 % | 11.5 | 43 % (S) | [53] |
| 58 | Rh | Methyl- 4,6- bis [(4,4',6,6'- tetra- t- butyl- 2, 2'- biphenyl- 1,1'- diy) phosphite]- 2,3- <i>O</i> - isopropylidene- α - D- manno pyranoside | Styrene | 67 % | 32.3 | 31 % (R) | [53] |
| 59 | Rh | Methyl- 4,6- bis [(4,4'-di- t- butyl- 6,6'- dimethoxy- 2, 2'- biphenyl- 1,1'- diy) phosphite]- 2,3- <i>O</i> - isopropylidene- α - D- manno pyranoside | Styrene | 42 % | 19.0 | 53 % (R) | [53] |
| 60 | Rh | PYDIPHOS | Styrene | 15 % | 9.0 | 28 % (R) | [54] |

| Sr. No. | Catalyst | | Substrate | Selectivity | | | Rf. |
|---------|----------|--|--|-------------------------------|---|-------------------|------|
| | Metal | Ligand | | Chemo/ % conv. or yield | Regio/ b/l ratio | Enantio/ ee % | |
| 61 | Pt | (<i>S</i>)- MOBIPH | Styrene | 53 % | 1.0 | 72 % (<i>S</i>) | [55] |
| 62 | Rh | (<i>R</i>)-2-di (3,5-dimethyl phenyl) phosphino-2'-dimethyl phosphinoxy-1,1'-binaphthalene | (1 <i>R</i> , 3 <i>S</i> , 4 <i>R</i>)-vinyl azetidin-2-one | - | 2.6 | 90 % (<i>S</i>) | [56] |
| 63 | Rh | (iPr) ₂ BINAS | Styrene | 100 % | 5.7 | 20 % | [57] |
| 64 | Rh | (<i>R,S</i>)- BINAPHOS | 2,5-Dihydro furan | 75 % | 100 % THF- 3-carbaldehyde | 57 % (<i>R</i>) | [58] |
| 65 | Rh | (<i>R,S</i>)- 3,3'- Me ₂ - BINAPHOS | 2,5-Dihydro furan | > 99 % | 100 % THF- 3-carbaldehyde | 64 % (<i>R</i>) | [58] |
| 66 | Rh | (<i>R,S</i>)- BINAPHOS | N- (tert- Butoxy carbonyl)- 3- pyrroline | 98 % | 100 % N- (tert- Butoxy carbonyl) pyrrolidine- 3- carbaldehyde | 47 % (<i>R</i>) | [58] |
| 67 | Rh | (<i>R,S</i>)- 3,3'- Me ₂ - BINAPHOS | N- (tert- Butoxy carbonyl)- 3- pyrroline | 99 % | 100 % N- (tert- Butoxy carbonyl) pyrrolidine- 3- carbaldehyde | 73 % (<i>R</i>) | [58] |
| 68 | Rh | (<i>R,S</i>)- BINAPHOS | N- Acetyl- 3- pyrroline | 92 % | 100 % N- Acetyl pyrrolidine- 3- carbaldehyde | 66 % (-) | [58] |
| 69 | Rh | (<i>R,S</i>)- 3,3'- Me ₂ - BINAPHOS | N- Acetyl- 3- pyrroline | 97 % | 100 % N- Acetyl pyrrolidine- 3- carbaldehyde | 65 % (-) | [58] |

| Sr. No. | Catalyst | | Substrate | Selectivity | | | Rf. |
|---------|----------|--|---|-------------------------------|--|---------------|------|
| | Metal | Ligand | | Chemo/ % conv. or yield | Regio/ b/l ratio | Enantio/ ee % | |
| 70 | Rh | (<i>R,S</i>)- BINAPHOS | Cis-4, 7- dihydro-1, 3- dioxepin | > 99 % | 100 % 1,3- dioxepane- 5- carbaldehyde | 76 % (-) | [58] |
| 71 | Rh | (<i>R,S</i>)- 3,3'- Me ₂ - BINAPHOS | Cis-4, 7- dihydro-1, 3- dioxepin | 99 % | 100 % 1,3- dioxepane- 5- carbaldehyde | 56 % (-) | [58] |
| 72 | Rh | (<i>R,S</i>)- BINAPHOS | Cis-2,2- dimethyl-4, 7- dihydro-1, 3- dioxepin | 77 % | 100 % 2,2- Dimethyl- 1,3- dioxepane- 5- carbaldehyde | 73 % (R) | [58] |
| 73 | Rh | (<i>R,S</i>)- 3,3'- Me ₂ - BINAPHOS | Cis-2,2- dimethyl-4, 7- dihydro-1, 3- dioxepin | > 99 % | 100 % 2,2- Dimethyl- 1,3- dioxepane- 5- carbaldehyde | 68 % (R) | [58] |
| 74 | Pt | (2 <i>R,4R</i>)-2, 4-Bis[(4 <i>R,6R</i>)- 4, 6- dimethyl-1, 3, 2- dioxa phosphorinan- 2- yloxy]- pentane | Styrene | 60 % | 2.4 | 40 % (S) | [59] |
| 75 | Pt | (2 <i>S,4S</i>)-2, 4-Bis[(4 <i>R,6R</i>)- 4, 6- dimethyl-1, 3, 2- dioxa phosphorinan- 2- yloxy]- pentane | Styrene | 85 % | 2.4 | 26 % (R) | [59] |
| 76 | Pt | (1 <i>S,3S</i>)-1, 3-Diphenyl-1, 3-Bis[(4 <i>R,6R</i>)- 4, 6- dimethyl-1, 3, 2- dioxa phosphorinan- 2- yloxy]- propane | Styrene | 21 % | 3.2 | 35 % (S) | [59] |
| 77 | Pt | (1 <i>S,3S</i>)-1, 3-Diphenyl-1, 3-Bis[(4 <i>S,6S</i>)- 4, 6- dimethyl-1, 3, 2- dioxa phosphorinan- 2- yloxy]- propane | Styrene | 32 % | 2.3 | 12 % (S) | [59] |

| Sr. No. | Catalyst | | Substrate | Selectivity | | | Rf. |
|---------|----------|---|-------------------|-------------------------------|---------------------|---------------|------|
| | Metal | Ligand | | Chemo/ % conv. or yield | Regio/ b/l ratio | Enantio/ ee % | |
| 78 | Rh | (2 <i>R</i> ,4 <i>R</i>)-2, 4-Bis[(4 <i>R</i> ,6 <i>R</i>)- 4, 6- dimethyl-1, 3, 2-dioxa phosphorinan- 2- yloxy]- pentane | Styrene | 69 % | 4.9 | 15 % (R) | [59] |
| 79 | Rh | CBDTS | Styrene | 67 % | 3.2 | 17 % (S) | [60] |
| 80 | Rh | CpTi + TFBB + (+)-BINAP | Styrene | 18 % | 10.1 | 15 % (S) | [61] |
| 81 | Rh | (<i>S,S</i>)-2,4-bis (diphenyl phosphine) pentane | Styrene | >99 % | 15.7 | 50 % (S) | [62] |
| 82 | Rh | (<i>S</i>)-([1,1'-binaphthalene]-2,2'-diyl-bis(oxy)) bis-(<i>S</i>)-dinaphtho [2,1-d:1',2'-f] [1,3,2] dioxaphosphine | Styrene | 100 % | 3.0 | 23 % (S) | [63] |
| 83 | Rh | (<i>R,S</i>) nBu- QUINAPHOS | Styrene | 75 % | 29.3 | 74 % (S) | [64] |
| 84 | Rh | (1 <i>R</i> ,2 <i>S</i>)-2-N- methyl-N-(n-butyl phenyl phosphino)-2-amino-1-phenyl-1 -(diphenyl phosphinoxy) propane | Styrene | - | 49.0 | 75 % (S) | [65] |
| 85 | Rh | Chiral Polyether – Phosphite ligands derived from (<i>S</i>)-binaphthol & polyethylene glycol-methyl ether (Mn ca. 750) | Styrene | > 99 % | 4.9 | 25 % (S) | [66] |
| 86 | Rh | (<i>S,S</i>) 1,1'-bis(1-naphthyl phenylphosphino) ferrocene | Styrene | 85 % | 1.5 | 41 % (S) | [67] |
| 87 | Rh | (<i>S,S</i>)-(+)-1,1'-Bis((4-methoxy phenyl) (1-naphthyl) phosphino) ferrocene | 4-methoxy styrene | - | 1.2 | 51 % (S) | [67] |
| 88 | Rh | (<i>R,S</i>)-3-H ² F ⁶ - BINAPHOS | Vinyl Acetate | 73 % | 12.0 | 95 % (S) | [68] |
| 89 | Rh | BDPP | 2,5-dihydro-furan | 91 % | - | 14 % (S) | [69] |

| Sr. No. | Catalyst | | Substrate | Selectivity | | | Rf. |
|---------|----------|--|---------------|-------------------------------|---------------------|---------------|------|
| | Metal | Ligand | | Chemo/ % conv. or yield | Regio/ b/l ratio | Enantio/ ee % | |
| 90 | Pt | (2 <i>S</i> ,4 <i>S</i>)-2,4-bis[(<i>S</i>)-5,5',6,6',7,7',8,8'-octahydro-dinaphtho [2,1-d:1',2'-f][1,3,2] dioxaphosphepin-2-yloxy]-pentane | Styrene | 62 % | 5.3 | 88 % (R) | [70] |
| 91 | Pt | (2 <i>S</i> ,4 <i>S</i>)- BDPP | Styrene | - | 1.5 | 60 % (S) | [71] |
| 92 | Rh | Kelliphite | Vinyl Acetate | - | 40 | 95 % | [72] |
| 93 | Rh | Kelliphite | Styrene | - | 30 | 89 % | [72] |
| 94 | Rh | Kelliphite | Allyl Cyanide | - | 4.8 | 87 % | [72] |

It is evident from the literature that rhodium and platinum metals and phosphine and phosphite ligands have been extensively studied for asymmetric hydroformylation. Use of tin (II) chloride cocatalyst is important when platinum is used for hydroformylation. Schwager and Knifton used platinum^[73] for hydroformylation for the first time. Platinum shows lower activity and chemoselectivity for hydroformylation, as compared to rhodium. The following figure 9 shows mechanism for platinum catalyzed hydroformylation as described by Schwager and Knifton^[74].

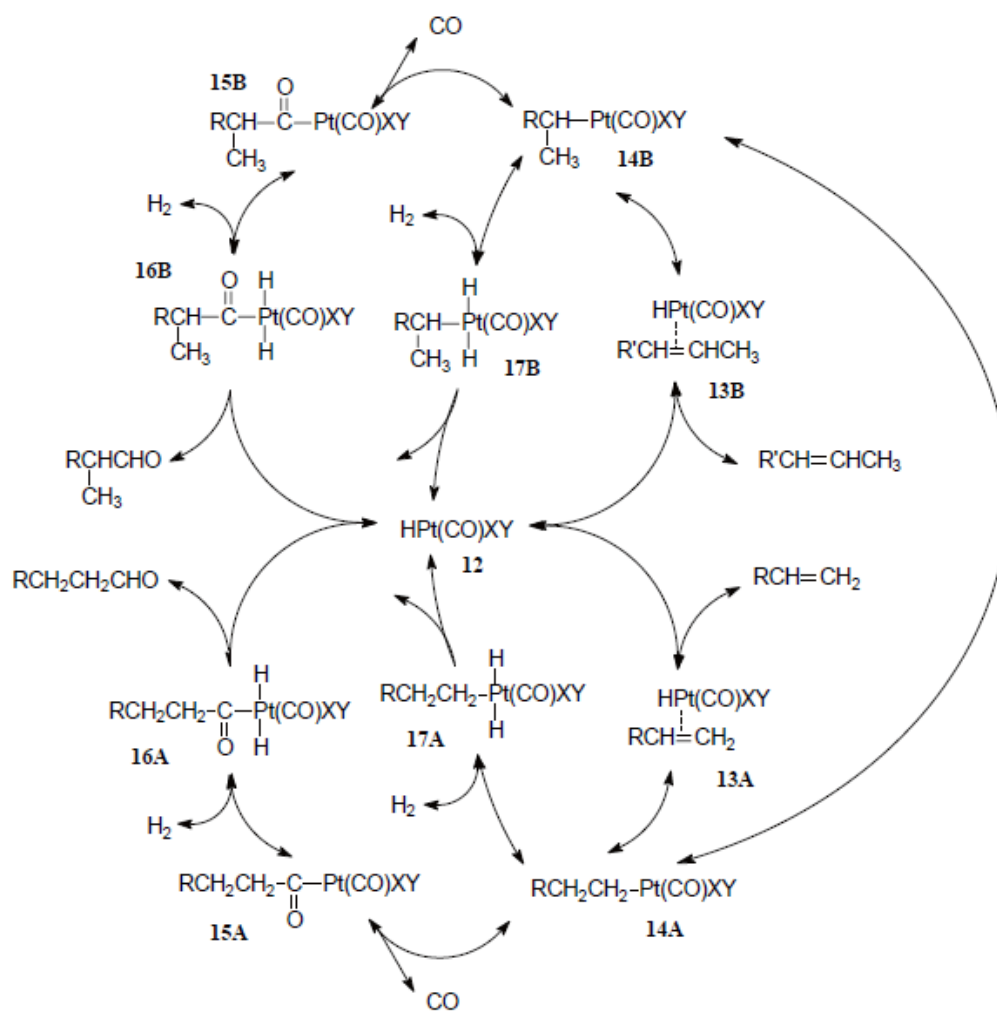


Figure 9: Mechanism of olefin hydroformylation, isomerization and reduction using platinum catalyst

Amongst the ligands, BINAPHOS, BIPHEMPHOS and Kelliphite show the best overall selectivity for asymmetric hydroformylation. Following are the structures of these ligands:

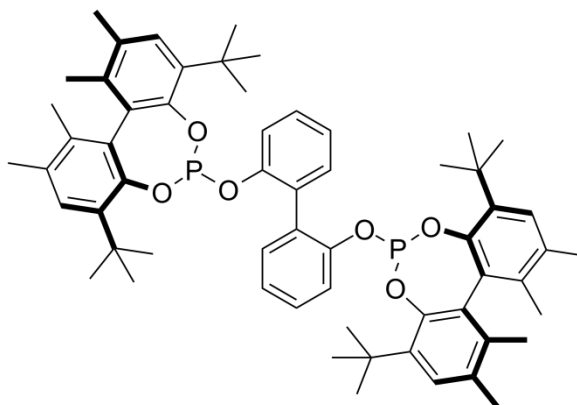


Figure 10: Structure of Kelliphite

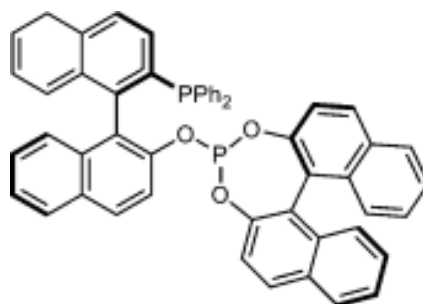


Figure 11: Structure of (*R,S*)-BINAPHOS

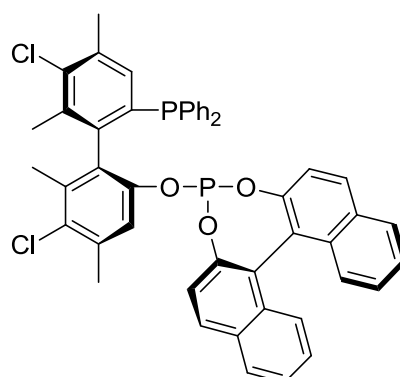


Figure 12: Structure of (*S,R*)-BIPHEMPHOS

1.3 Computational chemistry/ Molecular modeling

Computational chemistry is a branch of chemistry that uses principles of computer science to assist in solving chemical problems. It uses the results of theoretical chemistry, incorporated into efficient computer programs, to calculate the structures and properties of molecules and solids. Molecular modeling encompasses all theoretical methods and computational techniques used to model or mimic the behavior of molecules. Molecular modeling can be done using molecular mechanics or quantum mechanics. A typical molecular modeling job is to minimize the energy of a molecule (also called energy optimization or geometry optimization). Here the input is the “initial guess structure” of a molecule. Mathematical procedures are used on the initial guess structure and the atoms are moved in such a way that the overall energy of the molecule is minimized. The principle behind this method is that nature always prefers minimum energy configuration. Lesser is the energy, higher is the stability.

- **Molecular mechanics** (MM) uses Newtonian/ classical mechanics to model molecular systems. Here the molecule is assumed to be a ball and spring model, where the balls represent the atoms and the springs represent the bonds between the atoms. The spring constants/ force constants of the springs are derived from a database called “force field”. Force field functions and parameter sets are derived from both experimental work (for example, infra red spectra) and high-level quantum mechanical calculations. Here geometry optimization involves minimizing the strain in the molecule (strain caused due to elongation or compression of the “springs”). Because of the numerous approximations involved in MM calculations, they are called “empirical”. Various popular force fields include MM2, MM3, MM4, MM+, AMBER, CHARMM, UFF, etc. ^[75] MM calculations are less compute intensive as compared to quantum mechanical calculations. MM calculations for small molecules can be carried out on desktop computers. This is in contrast to quantum mechanical calculations which almost exclusively are carried out on high performance clusters (HPCs – often called “supercomputers”). Because the bonds are predefined in MM, transition states involving making and breaking of bonds cannot be modeled using MM.

- **Quantum mechanics** (QM) provides mathematical description of the dual particle-like and wave-like behavior and interactions of energy and matter. In most QM calculations, using the Born–Oppenheimer approximation ^[76], the electronic and nuclear wavefunctions are separated and then the electrons are treated as quantum mechanical objects and the nuclei are treated as classical objects. When an initial guess structure is submitted for a typical calculation, the electronic energy is minimized by fixing the positions of the nuclei (this is called a “single point” calculation). Then the positions of the nuclei are changed and the electronic energy is minimized again. This procedure is continued till no more changes in the positions of nuclei reduce the electronic energy. Accuracy of the calculations can be improved by incurring higher computational cost. It is important to note that very few aspects of chemistry can be computed exactly. However, almost every aspect of chemistry can be described in a qualitative or approximate quantitative computational scheme.

Density functional theory (DFT) ^[77] is the most popular QM method applied to real life chemistry problems because it provides good accuracy with low computational cost. With this theory, the properties of a many-electron system can be determined by using functionals, i.e. functions of another function, which in this case is the spatially dependent electron density. Hence the name density functional theory comes from the use of functionals of the electron density. DFT methods are often considered to be ab initio methods (methods based entirely on theory from first principles), even though many of the most common functionals use parameters derived from empirical data, or from more complex calculations. For carrying out a DFT calculation, one needs to provide an initial guess structure of the molecule, the functional to be used for the calculation and the “basis set” for the atoms in the molecule. The basis set is nothing but the definition of the atom as input in the calculation. There are different “qualities” of basis sets available, for example SVP (split valence with polarization), DZVP (Double Zeta Valence with Polarization), TZVP (Triple Zeta Valence with Polarization), etc. The higher the quality of basis set, higher is the computational cost and higher is the accuracy.

- **Truncated models and hybrid models** are used to reduce the time/ cost of computation. An example of a truncated model is replacement of the phenyl rings in triphenylphosphine ligand, by methyl or ethyl groups. This will greatly reduce the number of atoms in the structure (and hence the computation time) and provide results with acceptable accuracy. An example of a hybrid method is the QM/MM ^[78] method where QM is applied to the core atoms and MM is applied to the peripheral atoms.

The initial guess structure is generally drawn using any of the free or commercially available software packages (eg. Molden ^[79], ChemDraw ^[80], etc). The structure is generally saved in the xyz file format (that contains Cartesian coordinates of the atoms) or the z-matrix ^[81] (provides a description of each atom in a molecule in terms of its atomic number, bond length, bond angle, and dihedral angle, the so-called internal coordinates). Use of z-matrix format significantly reduces the computational cost because chemical structures are highly coupled systems ^[82].

1.3.1 Problems faced in molecular modeling: Most real life molecules are composed of many nuclei and electrons. One has to deal with an “n-body problem” while carrying out any geometry optimization. An exact solution or analytical solution is not possible in this case and therefore, approximate iterative calculations become necessary. These iterative calculations are compute-intensive. Moreover, the potential energy surface (which is a multidimensional hypersurface) of a molecule has many minima and maxima. One can get trapped in a local minimum depending on the initial guess structure. Because the final output of the calculation depends on the input, one can call these calculations as Monte Carlo methods ^[83]. Every conformer of a molecule is a local minimum on the potential energy surface (and large molecules can have many conformers). Nature, however, prefers the global minimum. The following figure 13 depicts local and global minima for the butane molecule:

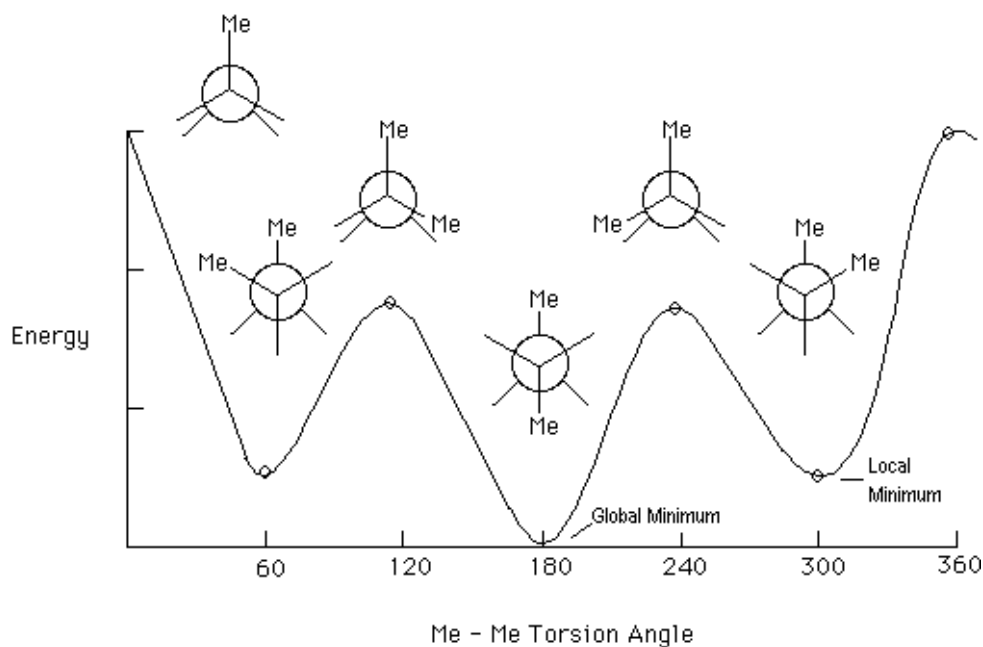


Figure 13: Local and global energy minima for butane

One can avoid the local minima trap by using methods like simulated annealing or torsion angle/ dihedral angle driving.

1.3.2 Finding Transition States (TS): A stationary point is a geometry such that the derivative of the energy with respect to all displacements of the nuclei is zero. A local (energy) minimum is a stationary point where all such displacements lead to an increase in energy (a stable molecule). A transition state however is a structure where one particular coordinate change leads to a decrease in the total energy in both directions. This coordinate is called the reaction coordinate. According to the transition state theory, the transition state is a “saddle point” on the potential energy surface. A saddle point can also be visualized as the highest point on a mountain pass.

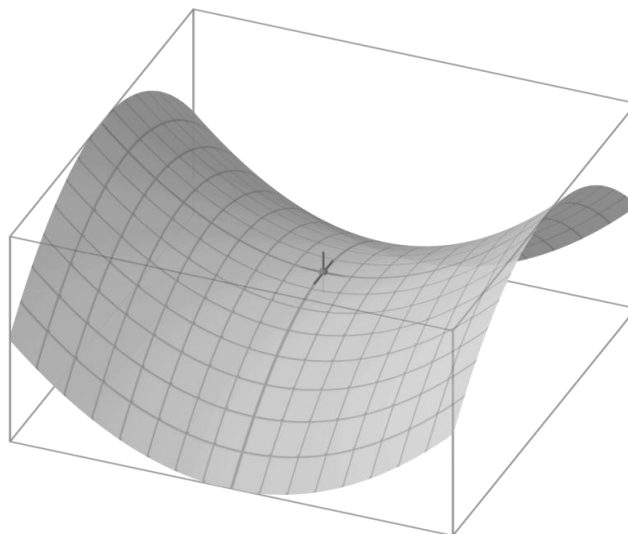


Figure 14: Saddle point

When a reaction coordinate is depicted in a two dimensional space, there are “mountains” above and below the plane of the paper.

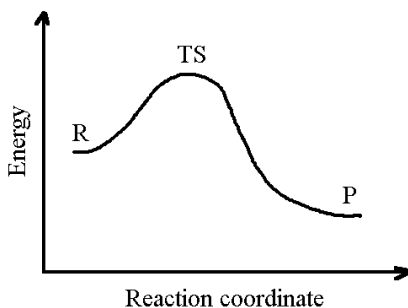


Figure 15: 2-dimensional depiction of reaction coordinate

The determination of molecular structure by geometry optimization became routine only after efficient methods for calculating the first derivatives of the energy with respect to all atomic coordinates became available. Evaluation of the related second derivatives allows the prediction of vibrational frequencies if harmonic motion is estimated. More importantly, it allows for the characterization of stationary points. The frequencies are related to the eigenvalues of the Hessian matrix, which contains second derivatives. If the eigenvalues are all positive, then the frequencies are all real and the stationary point is a local minimum. If one eigenvalue is negative (i.e., an imaginary frequency), then the

stationary point is a transition structure. Because nature prefers the path of least resistance, a transition state is a geometry which has one and only one negative eigenvalue (imaginary frequency).

Finding transition states is essential to study the kinetics of a reaction *in silico*. The activation energy of the reaction is calculated by finding the difference in energies of the reactant and the transition state. However transition state calculation is the most difficult job in computational chemistry and is still considered by many as more of an art than science. The free energy profile of a typical catalytic reaction consists of many transition states and intermediates.

1.3.3 Solvation effect: In a typical geometry optimization job, the molecule is assumed to be surrounded by empty space. In other words, the molecule is assumed to be in gas phase and so the calculations are called gas-phase calculations. In a real life situation however, the molecules are likely to be surrounded by solvent and because we know the importance of solvents in chemical reactions, it is important to take into account the “solvation effect”. COSMO is a popular method for study of solvation effect in computational chemistry. COSMO is the abbreviation for "COnductor-like Screening MOdel". It determines the electrostatic interaction of a molecule with a solvent. In COSMO the solvent is treated as a continuum with a permittivity ϵ , and therefore belongs to the "continuum solvation" group of models. As in all these models COSMO approximates the solvent by a dielectric continuum, surrounding the solute molecules outside of a molecular cavity.

1.3.4 Literature on DFT studies on asymmetric hydroformylation: Very few literature reports are available on DFT studies on asymmetric hydroformylation^[84]. Even for achiral hydroformylation, most full DFT studies (entire catalytic cycle) are limited to model reaction systems^[85].

1.4 Scope and objective of the thesis

To achieve the highest levels of activity and selectivity (the prime performance criteria of any catalyst) in asymmetric hydroformylation, several reaction parameters must be optimized, the most crucial of which is perhaps the design of the chiral ligand. The problem however is – most chiral ligands are huge molecules that are difficult to synthesize. The synthesis process is tedious and involves multiple steps. Moreover one can never be sure that the new ligand/ catalyst will give acceptable activity/ selectivity. To overcome this problem, a methodology for prediction of activity/ selectivity of any chiral catalyst needs to be developed:

- Study of asymmetric hydroformylation reaction using easily available catalysts (laboratory bench work).
- Computational study of one of the catalysts and matching of the experimental results with computational results.
- Development of a method of prediction where the activity/ selectivity of a catalyst can be quickly and accurately predicted even before the catalyst is synthesized in the lab. The input data for this prediction would be the structure of the catalyst/ ligand. In this way, structures of catalysts can be screened computationally and only the best few amongst them need to be actually synthesized and tested in the lab (for the “proof of pudding”).

After all, the acid test of human knowledge is the ability to predict the outcome of a “thought experiment”. (A thought experiment or Gedanken experiment considers some hypothesis, theory, or principle for the purpose of thinking through its consequences.) An ideal situation for a chemist would be one where he/she can carry out *in silico* “experiments” at the speed of thought leaving only the final synthesis to be done using bench work. With Moore’s law ^[86] in place, it seems this may not be so distant in the future. This thesis can push the current state of art and can be a small step towards that ideality.

References

- [1] aA. D. McNaught, A. Wilkinson, *IUPAC compendium of chemical terminology*, Vol. 2, Blackwell Scientific Publications, **1997**; bP. Cintas, *Angewandte Chemie International Edition* **2007**, *46*, 4016-4024.
- [2] M. Smith, J. March, *March's advanced organic chemistry: reactions, mechanisms, and structure*, Wiley, **2007**.
- [3] K. G. Fahlbusch, F. J. Hammerschmidt, J. Panten, W. Pickenhagen, D. Schatkowski, K. Bauer, D. Garbe, H. Surburg, *Ullmann's Encyclopedia of Industrial Chemistry* **2002**.
- [4] J. Halpern, B. M. Trost, *Proceedings of the National Academy of Sciences of the United States of America* **2004**, *101*, 5347.
- [5] aJ. D. Carroll, *Chirality* **2009**, *21*, 354-358; bU. Meierhenrich, *Amino acids and the asymmetry of life: caught in the act of formation*, Springer Verlag, **2008**.
- [6] M. Quack, *Angewandte Chemie International Edition* **2002**, *41*, 4618-4630.
- [7] W. H. Porter, *Pure Appl. Chem* **1991**, *63*, 1119.
- [8] E. L. Eliel, S. H. Wilen, *Stereochemistry of organic compounds*, Wiley-India, **2008**.
- [9] Y. Fujima, M. Ikunaka, T. Inoue, J. Matsumoto, *Organic process research & development* **2006**, *10*, 905-913.
- [10] aW. H. Laarhoven, T. J. H. M. Cuppen, *J. Chem. Soc., Perkin Trans. 2* **1978**, 315-318; bI. Ojima, *Catalytic asymmetric synthesis*, Wiley, **2010**; cJ. Ding, D. W. Armstrong, *Chirality* **2005**, *17*, 281-292.
- [11] R. J. Cave, *Science* **2009**, *323*, 1435.
- [12] aP. W. Atkins, J. De Paula, *Elements of physical chemistry*, WH Freeman & Co, **2009**; bA. Lever, E. Dodsworth, by *EI Solomon and ABP Lever*, John Wiley & Sons, Inc., New York **1999**, 2.
- [13] G. D. Fasman, *Circular dichroism and the conformational analysis of biomolecules*, Springer, **1996**.
- [14] Y. Yin, R. M. Rioux, C. K. Erdonmez, S. Hughes, G. A. Somorjai, A. P. Alivisatos, *Science* **2004**, *304*, 711.
- [15] Z. Guo, Y. Du, Y. Chen, S. C. Ng, Y. Yang, *The Journal of Physical Chemistry C* **2010**.
- [16] aH. U. Blaser, E. Schmidt, *Introduction*, Wiley Online Library, **2004**; bM. Heitbaum, F. Glorius, I. Escher, *Angewandte Chemie International Edition* **2006**, *45*, 4732-4762; cE. N. Jacobsen, A. Pfaltz, H. Yamamoto, *Comprehensive asymmetric catalysis*, Vol. 2, Springer, **2004**.
- [17] aA. Berkessel, H. Gröger, *Asymmetric organocatalysis*, Wiley Online Library, **2005**; bB. List, *Chemical Reviews* **2007**, *107*, 5413-5415; cP. I. Dalko, L. Moisan, *Angewandte Chemie International Edition* **2004**, *43*, 5138-5175; dM. J. Gaunt, C. C. Johansson, A. McNally, N. T. Vo, *Drug Discovery Today* **2007**, *12*, 8-27; eD. Enders, C. Grondal, M. R. M. Hüttl, *Angewandte Chemie International Edition* **2007**, *46*, 1570-1581; fP. I. Dalko, L. Moisan, *Angewandte Chemie International Edition* **2001**, *40*, 3726-3748.
- [18] H. Nozaki, H. Takaya, S. Moriuti, R. Noyori, *Tetrahedron* **1968**, *24*, 3655-3669.

- [19] aA. Pfaltz, W. J. Drury III, *Proceedings of the National Academy of Sciences* **2004**, *101*, 5723-5726; bT. P. Yoon, E. N. Jacobsen, *Science* **2003**, *299*, 1691.
- [20] aJ. Bjerre, C. Rousseau, L. Marinescu, M. Bols, *Applied microbiology and biotechnology* **2008**, *81*, 1-11; bJ. Xiao, F. X. Xu, Y. P. Lu, T. P. Loh, *Organic Letters* **2010**, *12*, 1220-1223.
- [21] aD. Mansuy, *Pure Appl. Chem* **1990**, *62*, 741-746; bJ. F. V. Vincent, O. A. Bogatyreva, N. R. Bogatyrev, A. Bowyer, A. K. Pahl, *Journal of the Royal Society Interface* **2006**, *3*, 471-482; cJ. Lee, S. Bernard, X. C. Liu, *Reactive and Functional Polymers* **2009**, *69*, 650-654.
- [22] E. Fischer, *Berichte der deutschen chemischen Gesellschaft* **1894**, *27*, 2985-2993.
- [23] D. Koshland Jr, *Proceedings of the National Academy of Sciences of the United States of America* **1958**, *44*, 98.
- [24] I. Ojima, C. Y. Tsai, M. Tzamarioudaki, D. Bonafoux, *Organic Reactions* **2000**.
- [25] B. M. Trost, *Angewandte Chemie International Edition in English* **1995**, *34*, 259-281.
- [26] M. L. Clarke, G. J. Roff, *Chemistry-A European Journal* **2006**, *12*, 7978-7986.
- [27] B. Cornils, W. A. Herrmann, M. Rasch, *Angewandte Chemie International Edition in English* **1994**, *33*, 2144-2163.
- [28] D. Evans, J. Osborn, G. Wilkinson, *J. Chem. Soc. A* **1968**, 3133-3142.
- [29] R. F. Heck, D. S. Breslow, *Journal of the American Chemical Society* **1961**, *83*, 4023-4027.
- [30] G. Yagupsky, C. Brown, G. Wilkinson, *J. Chem. Soc. A* **1970**, 1392-1401.
- [31] P. Leeuwen, P. Kamer, C. Claver, O. Pàmies, M. Diéguez, *Chemical Reviews* **2010**.
- [32] K. Nozaki, N. Sakai, T. Nanno, T. Higashijima, S. Mano, T. Horiuchi, H. Takaya, *Journal of the American Chemical Society* **1997**, *119*, 4413-4423.
- [33] J. Hagen, *Industrial catalysis: a practical approach*, Vch Verlagsgesellschaft Mbh, **2006**.
- [34] T. Hayashi, M. Tanaka, Y. Ikeda, I. Ogata, *Bulletin of the Chemical Society of Japan* **1979**, *52*, 2605-2608.
- [35] C. F. Hobbs, W. S. Knowles, *The Journal of Organic Chemistry* **1981**, *46*, 4422-4427.
- [36] G. Consiglio, P. Pino, L. I. Flowers, C. U. Pittman, *J. Chem. Soc., Chem. Commun.* **1983**, 612-613.
- [37] G. Consiglio, F. Morandini, M. Scalone, P. Pino, *Journal of organometallic chemistry* **1985**, *279*, 193-202.
- [38] G. Parrinello, J. Stille, *Journal of the American Chemical Society* **1987**, *109*, 7122-7127.
- [39] S. Mutez, A. Mortreux, F. Petit, *Tetrahedron letters* **1988**, *29*, 1911-1914.
- [40] Y. Pottier, A. Mortreux, F. Petit, *Journal of organometallic chemistry* **1989**, *370*, 333-342.
- [41] G. Consiglio, F. Rama, *Journal of Molecular Catalysis* **1991**, *66*, 1-5.
- [42] J. K. Stille, H. Su, P. Brechot, G. Parrinello, L. S. Hegedus, *Organometallics* **1991**, *10*, 1183-1189.
- [43] L. Kollar, P. Sandor, G. Szalontai, *Journal of Molecular Catalysis* **1991**, *67*, 191-198.

- [44] G. Consiglio, S. C. A. Nefkens, A. Borer, *Organometallics* **1991**, *10*, 2046-2051.
- [45] A. L. Bandini, G. Banditelli, E. Cesarotti, G. Minghetti, B. Bovio, *Inorganic Chemistry* **1992**, *31*, 391-398.
- [46] N. Sakai, S. Mano, K. Nozaki, H. Takaya, *Journal of the American Chemical Society* **1993**, *115*, 7033-7034.
- [47] C. Claver, S. Castellón, N. Ruiz, G. Delogu, D. Fabbri, S. Gladiali, *J. Chem. Soc., Chem. Commun.* **1993**, 1833-1834.
- [48] A. Masdeu, A. Orejon, A. Ruiz, S. Castillon, C. Claver, *Journal of Molecular Catalysis* **1994**, *94*, 149-156.
- [49] S. Gladiali, D. Antonio, F. Davide, *Tetrahedron: Asymmetry* **1994**, *5*, 1143-1146.
- [50] S. Gladiali, A. Dore, D. Fabbri, O. De Lucchi, M. Manassero, *Tetrahedron: Asymmetry* **1994**, *5*, 511-514.
- [51] J. E. Babin, G. T. Whiteker, Google Patents, **1994**.
- [52] T. Higashizima, N. Sakai, K. Nozaki, H. Takaya, *Tetrahedron letters* **1994**, *35*, 2023-2026.
- [53] G. J. H. Buisman, M. E. Martin, E. J. Vos, A. Klootwijk, P. C. J. Kamer, P. W. N. M. van Leeuwen, *Tetrahedron: Asymmetry* **1995**, *6*, 719-738.
- [54] G. Chelucci, M. A. Cabras, C. Botteghi, C. Basoli, M. Marchetti, *Tetrahedron: Asymmetry* **1996**, *7*, 885-895.
- [55] A. Scrivanti, V. Beghetto, A. Bastianini, U. Matteoli, G. Menchi, *Organometallics* **1996**, *15*, 4687-4694.
- [56] T. Saito, K. Matsumura, T. Miura, H. Kumobayashi, A. Yoshida, EP Patent 0,755,937, **2002**.
- [57] N. Ruiz, A. Aaliti, J. Fornies-Camer, A. Ruiz, C. Claver, C. J. Cardin, D. Fabbri, S. Gladiali, *Journal of organometallic chemistry* **1997**, *545*, 79-87.
- [58] T. Horiuchi, T. Ohta, E. Shirakawa, K. Nozaki, H. Takaya, *The Journal of Organic Chemistry* **1997**, *62*, 4285-4292.
- [59] S. Cserépi-Szűcs, I. Tóth, L. Párkányi, J. Bakos, *Tetrahedron: Asymmetry* **1998**, *9*, 3135-3142.
- [60] M. D. Miquel-Serrano, A. M. Masdeu-Bulto, C. Claver, D. Sinou, *Journal of Molecular Catalysis A: Chemical* **1999**, *143*, 49-55.
- [61] M. A. Casado, M. A. Ciriano, A. J. Edwards, F. J. Lahoz, L. A. Oro, J. J. Pérez-Torrente, *Organometallics* **1999**, *18*, 3025-3034.
- [62] M. Dieguez, M. M. Pereira, A. M. Masdeu-Bulto, C. Claver, J. C. Bayon, *Journal of Molecular Catalysis A: Chemical* **1999**, *143*, 111-122.
- [63] S. Cserépi-Szűcs, G. Huttner, L. Zsolnai, A. Szolossy, C. Hegedus, J. Bakos, *Inorganica chimica acta* **1999**, *296*, 222-230.
- [64] G. Franciò, F. Faraone, W. Leitner, *Angewandte Chemie International Edition* **2000**, *39*, 1428-1430.
- [65] R. Ewalds, E. B. Eggeling, A. C. Hewat, P. C. J. Kamer, P. W. N. M. van Leeuwen, D. Vogt, *Chemistry-A European Journal* **2000**, *6*, 1496-1504.
- [66] J. A. J. Breuzard, M. L. Tommasino, M. C. Bonnet, M. Lemaire, *Journal of organometallic chemistry* **2000**, *616*, 37-43.
- [67] U. Nettekoven, P. C. J. Kamer, M. Widhalm, P. W. N. M. van Leeuwen, *Organometallics* **2000**, *19*, 4596-4607.

- [68] G. Francio, K. Wittmann, W. Leitner, *Journal of organometallic chemistry* **2001**, *621*, 130-142.
- [69] I. del Río, P. W. N. M. van Leeuwen, C. Claver, *Canadian Journal of Chemistry* **2001**, *79*, 560-565.
- [70] J. Bakos, S. Cserepi-Szucs, Á. Gömöry, C. Hegedüs, L. Marko, Á. Szöllosy, *Canadian Journal of Chemistry* **2001**, *79*, 725-730.
- [71] C. P. Casey, S. C. Martins, M. A. Fagan, *Journal of the American Chemical Society* **2004**, *126*, 5585-5592.
- [72] T. P. Clark, C. R. Landis, S. L. Freed, J. Klosin, K. A. Abboud, *Journal of the American Chemical Society* **2005**, *127*, 5040-5042.
- [73] I. Schwager, J. F. Knifton, (Texaco Development Corp.). Application: DE DE, **1973**, p. 53 pp.
- [74] I. Schwager, J. Knifton, *Journal of Catalysis* **1976**, *45*, 256-267.
- [75] aN. L. Allinger, *Journal of the American Chemical Society* **1977**, *99*, 8127-8134; bN. L. Allinger, Y. H. Yuh, J. H. Lii, *Journal of the American Chemical Society* **1989**, *111*, 8551-8566; cJ. H. Lii, N. L. Allinger, *Journal of the American Chemical Society* **1989**, *111*, 8576-8582; dJ. H. Lii, N. L. Allinger, *Journal of the American Chemical Society* **1989**, *111*, 8566-8575; eW. D. Cornell, P. Cieplak, C. I. Bayly, I. R. Gould, K. M. Merz, D. M. Ferguson, D. C. Spellmeyer, T. Fox, J. W. Caldwell, P. A. Kollman, *Journal of the American Chemical Society* **1995**, *117*, 5179-5197; fB. R. Brooks, R. E. Bruccoleri, B. D. Olafson, S. Swaminathan, M. Karplus, *Journal of Computational Chemistry* **1983**, *4*, 187-217; gA. Rappe, C. Casewit, K. Colwell, W. Goddard Iii, W. Skiff, *Journal of the American Chemical Society* **1992**, *114*, 10024-10035.
- [76] M. Born, R. Oppenheimer, *Annalen der Physik* **1927**, *389*, 457-484.
- [77] P. Hohenberg, W. Kohn, *Physical Review* **1964**, *136*, B864.
- [78] A. Warshel, M. Levitt, *Journal of molecular biology* **1976**, *103*, 227-249.
- [79] G. Schaftenaar, J. H. Noordik, *Journal of Computer-Aided Molecular Design* **2000**, *14*, 123-134.
- [80] N. Mills, *Journal of the American Chemical Society* **2006**, *128*, 13649-13650.
- [81] M. Gordon, J. Pople, *The Journal of Chemical Physics* **1968**, *49*, 4643.
- [82] J. Parsons, J. B. Holmes, J. M. Rojas, J. Tsai, C. E. M. Strauss, *Journal of Computational Chemistry* **2005**, *26*, 1063-1068.
- [83] H. L. Anderson, *Los Alamos Science* **1986**, *14*, 96-108.
- [84] aC. J. Copley, R. D. J. Froese, J. Klosin, C. Qin, G. T. Whiteker, K. A. Abboud, *Organometallics* **2007**, *26*, 2986-2999; bJ. Meeuwissen, A. J. Sandee, B. de Bruin, M. A. Sieglar, A. L. Spek, J. N. H. Reek, *Organometallics* **2010**, *29*, 2413-2421.
- [85] aM. Sparta, K. J. Børve, V. R. Jensen, *Journal of the American Chemical Society* **2007**, *129*, 8487-8499; bJ. da Silva, R. P. Dias, W. B. de Almeida, W. R. Rocha, *Journal of Computational Chemistry* **2010**, *31*, 1986-2000; cC.-F. Huo, Y.-W. Li, M. Beller, H. Jiao, *Chemistry--A European Journal* **2005**, *11*, 889-902.
- [86] aG. E. Moore, *Proceedings of the IEEE* **1998**, *86*, 82-85; bR. W. Keyes, *Solid-State Circuits Newsletter, IEEE* **2006**, *20*, 25-27; cM. Kanellos, *CNET News.com* **2005**; dP. Gelsinger, *Solid-State Circuits Newsletter, IEEE* **2006**, *20*, 18-20.



CHAPTER 2

**Asymmetric hydroformylation of
styrene using ligand-modified rhodium
catalysts (experimental)**

2.1 Introduction

Styrene is an important substrate for hydroformylation because analogous substrates can be hydroformylated (and later oxidized) to form “profen” drugs. Profen drugs are nonsteroidal anti-inflammatory drugs (NSAIDs) with analgesic and antipyretic (fever-reducing) effects. As analgesics, NSAIDs are unusual in that they are non-narcotic. Most of the NSAIDs classified as propionic acid derivatives (e.g. Ibuprofen, Naproxen, Fenoprofen, Ketoprofen, Dexketoprofen, Flurbiprofen, Loxoprofen) can be synthesized by hydroformylation of substrates analogous to styrene.

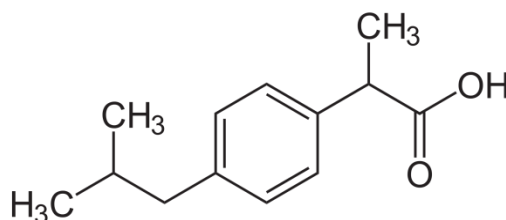


Figure 1: Ibuprofen

Most of the profen drugs are chiral and are either marketed as racemic mixtures (e.g. Ibuprofen) or as enantiopure compounds [e.g. (*S*)-Naproxen]. Asymmetric hydroformylation can be one of the ways to synthesize enantiomerically enriched or enantiopure profen drugs.

2.2 Experimental

2.2.1 Material: Rhodium chloride trihydrate (RhCl₃·3H₂O, 40% Rh) was obtained from Hindustan Platinum and was used as received. Styrene, (*R*)-tolyl-BINAP, (*R*)-xylyl-BINAP, (*R*)-BINAP, (-)-(*R,R*)-DIOP, (*S,S*)-BDPB were procured from Sigma-Aldrich, USA and were used without further purification. Toluene and methyl ethyl ketone were obtained from Merck, India and were freshly distilled and dried prior to use. Hydrogen gas and nitrogen gas supplied by Indian Oxygen, Mumbai and carbon monoxide gas

(>99.8% pure, Matheson gas, USA) were used directly from the cylinders. The syn gas mixture (CO + H₂) was prepared by mixing H₂ and CO in a reservoir vessel.

2.2.2 Synthesis of Rh(CO)₂(acac): Rh(CO)₂(acac) was prepared by a method described by Varshavskii and Cherkasova ^[1]. Acetylacetone (12 ml) was added to a solution of RhCl₃ · 3H₂O (3.0 g, 1.14 × 10⁻² moles) in DMF (60 ml) with stirring. The solution was refluxed for 30 minutes and then cooled. It was diluted to twice the volume with distilled water. The addition of water resulted in a voluminous crimson precipitate. The precipitate was filtered and washed with alcohol and ether. The complex was recrystallized from a hexane solution at room temperature. Needle shaped red green crystals were obtained by slow cooling of the hexane solution. The yield (2.4 g) was about 81%. The elemental analysis of Rh(CO)₂(acac) showed C=32.6%, H=2.7%. Calculated: C=32.5%; H=3.0%. Characteristic IR shifts for this complex at 2065 cm⁻¹, 2006 cm⁻¹ and 1525 cm⁻¹ are shown in the following figure 2.

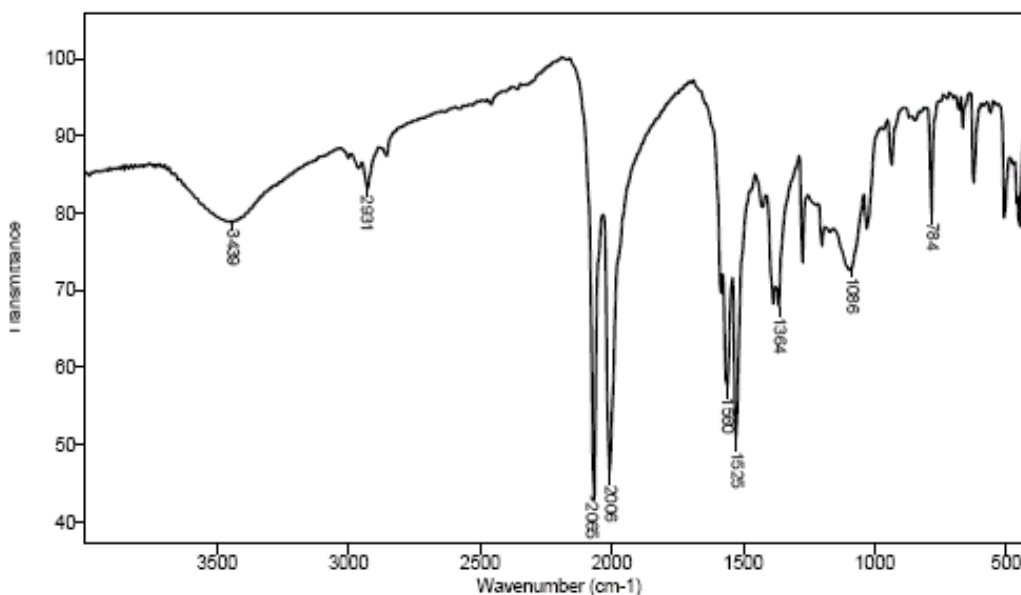


Figure 2: FTIR spectrum of Rh(CO)₂(acac)

2.2.3 Experimental set up: All the hydroformylation reactions were carried out in a 50 ml Parr Autoclave made of stainless steel (Maximum pressure capacity of 20.7 MPa at 548 K), having facilities for gas inlet, outlet, intermediate sampling, temperature

controlled heating ($\pm 1\text{K}$) and variable agitation speed (0 to 33.3 Hz). The typical reaction set-up is shown in the following figure. As a safety precaution, a rupture disc (gold faced), which can withstand a maximum pressure of 20.7 MPa was attached to the reactor. Gas was fed through constant pressure regulator attached to the syn gas reservoir. The syn gas reservoir was always maintained at a minimum of 1.5 MPa higher pressure compared to the reactor pressure. Ice water-cooled condensers were used for intermediate sampling.

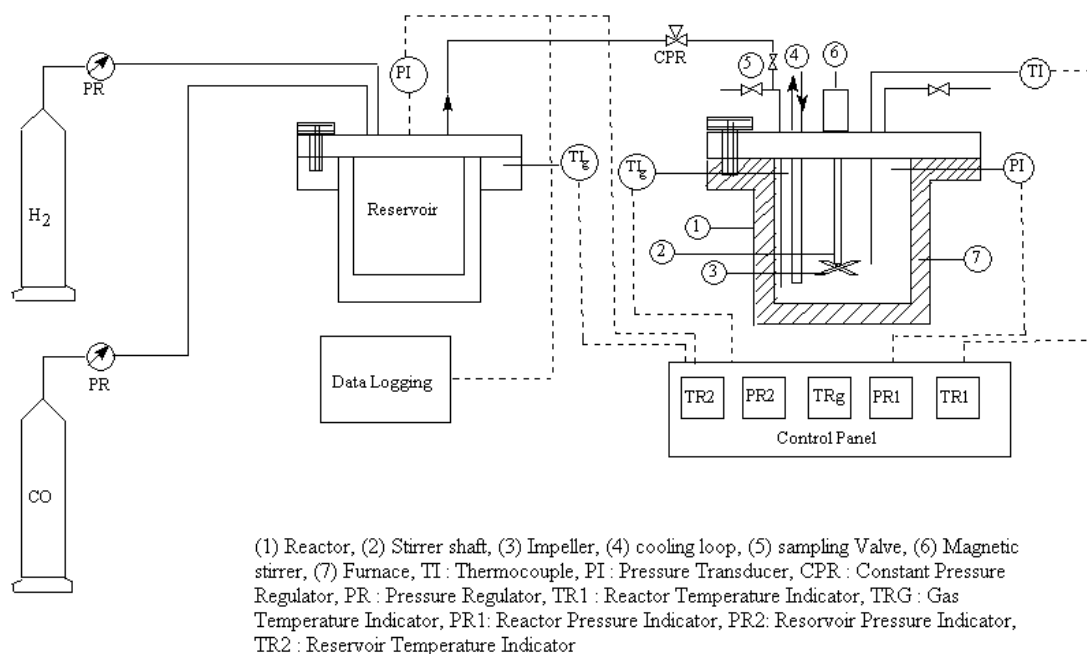


Figure 3: Schematic diagram of the reactor set up

2.2.4 Experimental procedure: In a typical experiment, known quantities of $\text{Rh}(\text{CO})_2(\text{acac})$, ligand, olefin (styrene), and the solvent were charged into the autoclave and the reactor was flushed with nitrogen. The contents were then flushed with a mixture of CO and H_2 and were heated to a desired temperature. A mixture of CO and H_2 , in the required ratio (e.g. 1:1), was introduced into the autoclave, a sample of liquid withdrawn, and the reaction was started by switching the stirrer on. The reaction was then continued at a constant pressure by supply of $\text{CO}+\text{H}_2$ (1:1) from the reservoir vessel. Because the major products formed were aldehydes, supply of $\text{CO}+\text{H}_2$ at a ratio of 1:1 (as per the stoichiometry) was adequate to maintain a constant composition of CO and H_2 in the

autoclave, as introduced in the beginning. This was confirmed in a few cases by analysis of the CO content in the gas phase at the end of the reaction. In each run, samples were withdrawn at regular intervals of time and analyzed for reactants and products in order to check the material balance. The reproducibility of the experiments was found to be in a range of 4-6%.

2.2.5 Analytical methods: FT-IR spectrum was recorded on a Bio-Rad Spectrophotometer 175C. The reaction products were identified using GC-MS (Agilent GC 6890N with 5973 mass selective detector instrument). The quantitative analysis of the reactant and hydroformylation products was carried out by gas chromatography (GC) using an external standard method. For this purpose, HP 6850 gas chromatograph controlled by the HP Chemstation software and equipped with an auto sampler unit, fitted with β -DEX 225 (chiral) capillary column [non-bonded; 25% 2,3-di-O-acetyl-6-O-TBDMS- β -cyclodextrin in SPB-20 poly (20% phenyl/80% dimethylsiloxane) phase; column dimensions 30 m \times 0.25 mm; film thickness 0.25 μ m] and FID detector was used. Authentic standards were prepared in the range of concentrations studied, and a calibration-table was constructed for the quantification. Standard GC conditions for analysis were as shown in the following table 1:

Table 1: Standard GC conditions

| | | | |
|---------------------------------------|----------------|----------------|-----------------|
| Injector (split) Temperature | 250°C | | |
| Flame ionization detector Temperature | 250°C | | |
| Inlet flow–total (He) | 96.7 ml/min | | |
| Split ratio for Injector | 150:1 | | |
| Column Temperature | Rate (°C/min) | T (°C) | Hold time (min) |
| | | 100 | 30 |
| | 30 | 200 | 5 |
| Column Pressure | Rate (psi/min) | Pressure (psi) | Hold time (min) |
| | | 10 | 38.33 |

A typical GC chart shows (from left to right), the solvent (toluene), reactant (styrene) and the products [(*R*)-2-phenylpropanal, (*S*)-2-phenylpropanal and 3-phenylpropanal]:

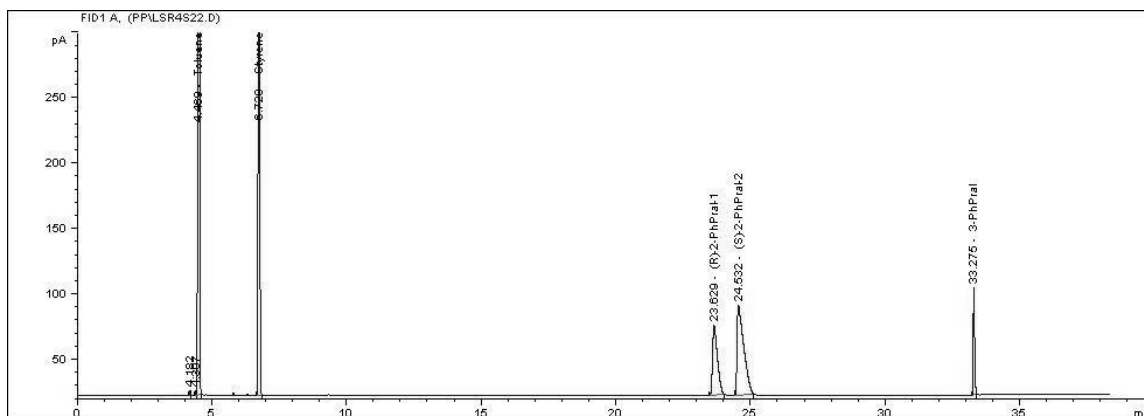


Figure 4: Typical GC chart

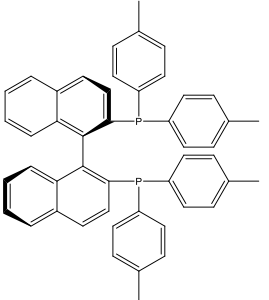
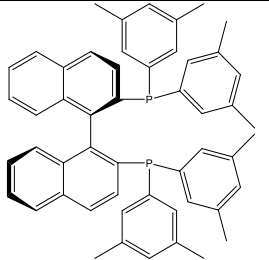
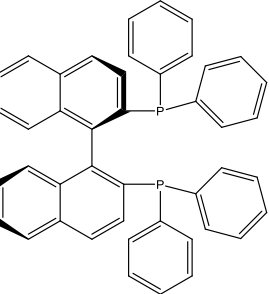
Complete mass balance of the liquid phase components was obtained from quantitative GC analysis. The observed syn gas absorption was found to match with the products formed within ~ 7 % error. Thus, the complete mass balance of liquids and gases was established.

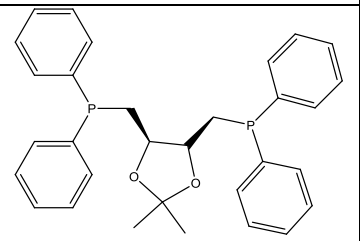
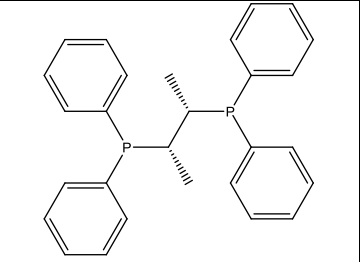
2.2.6 Separation and identification of the products: The styrene hydroformylation products - 2-phenylpropanal and 3-phenylpropanal were identified using GC-MS. The enantiomers of the branched aldehyde [(*R*)-2-phenylpropanal, (*S*)-2-phenylpropanal] were identified by carrying out an asymmetric hydroformylation reaction of styrene using the (*R*)-BINAP modified rhodium catalyst, and by comparing the product profile (using GC) of this reaction with literature ^[2].

2.3 Results and discussion

2.3.1 Screening of ligands for rhodium catalyzed asymmetric hydroformylation of styrene: Various commercially available chiral ligands were tested as per the table 2 below:

Table 2: Screening of chiral ligands for asymmetric hydroformylation of styrene

| Sr. No. | Ligand | Structure | Time of Reaction | Conversion | Activity, TOF/ hour ⁻¹ | Selectivity | |
|---------|--------------------------|---|------------------|------------|--------------------------------------|---------------|-------------------|
| | | | | | | Regio, b/l | Enantio, % ee |
| 1 | (<i>R</i>)-tolyl-BINAP |  | 20 hours | 48.7 % | 8.5 | 7.5 | 27.2 (<i>S</i>) |
| 2 | (<i>R</i>)-xylyl-BINAP |  | 20 hours | 50.8 % | 8.5 | 6.6 | 27.1 (<i>S</i>) |
| 3 | (<i>R</i>)-BINAP |  | 20 hours | 64.9 % | 11.3 | 8.4 | 24.4 (<i>S</i>) |

| Sr. No. | Ligand | Structure | Time of Reaction | Conversion | Activity, TOF/ hour ⁻¹ | Selectivity | |
|---------|----------------|---|------------------|------------|--------------------------------------|---------------|------------------|
| | | | | | | Regio, b/l | Enantio, % ee |
| 4 | (-)-(R,R)-DIOP |  | 10 hours | 100 % | 34.9 | 1.5 | 14.2 (R) |
| 5 | (S,S)-BDPB |  | 9 hours 35 min | 100 % | 35.7 | 41 | 0.4 (R) |

Reaction conditions: Rh(CO)₂(acac) – 15.6 mg (0.06 mmol); Ligand: 0.24 mmol; Styrene: 2.08 g (20 mmol); Solvent: Toluene; Total charge: 15 ml; Syn gas (CO:H₂ = 1:1) pressure: 147 psi (10 atm); Temperature: 65 °C (338 K); Agitation speed: 900 rpm

The ligand screening study shows that the bulky ligands (BINAP and BINAP derivatives) gave higher enantioselectivity and lower activity compared to DIOP and BDPB. The regioselectivity seems to be dependent on the bite angle, which in turn is dependent on the distance between phosphorus atoms in the ligand molecule. The lower the distance between the phosphorus atoms in the ligand, lower is the bite angle and higher is the selectivity for branched aldehyde.

2.3.2 Effect of solvent: Solvents are known to influence activity and selectivity of the hydroformylation reaction. To understand the role of polarity of the solvent in asymmetric hydroformylation, two reactions were carried out: one with a polar solvent (methyl ethyl ketone) and one with a non-polar solvent (toluene).

Table 3: Effect of solvent on asymmetric hydroformylation of styrene

| Sr. No. | Solvent | Conversion | Activity, TOF/hour ⁻¹ | Selectivity | |
|---------|---------------------|------------|-------------------------------------|---------------|------------------|
| | | | | Regio, b/l | Enantio, % ee |
| 1 | Toluene | 64.9 % | 11.3 | 8.4 | 24.4 (S) |
| 2 | Methyl Ethyl Ketone | 39.1 % | 6.35 | 7.7 | 15.6 (S) |

Reaction Conditions: Rh(CO)₂(acac) – 15.6 mg (0.06 mmol); (*R*)-BINAP: 150 mg (0.24 mmol); Styrene: 2.08 g (20 mmol); Total charge: 15 ml; Syn gas (CO:H₂ = 1:1) pressure: 147 psi (10 atm); Temperature: 65 °C (338 K); Reaction time: 20 hours; Agitation speed: 900 rpm

The dielectric constant of methyl ethyl ketone is 18.5 at 20 °C and that of toluene is 2.379 at 25 °C. The increase in polarity of the solvent decreases the activity and selectivity (regio and enantio) of the reaction.

2.3.3 Parametric study: The effect of different parameters on the activity and selectivity of asymmetric hydroformylation reaction were studied.

A typical concentration time profile, used to calculate activity and selectivity, is shown in the following figure 5:

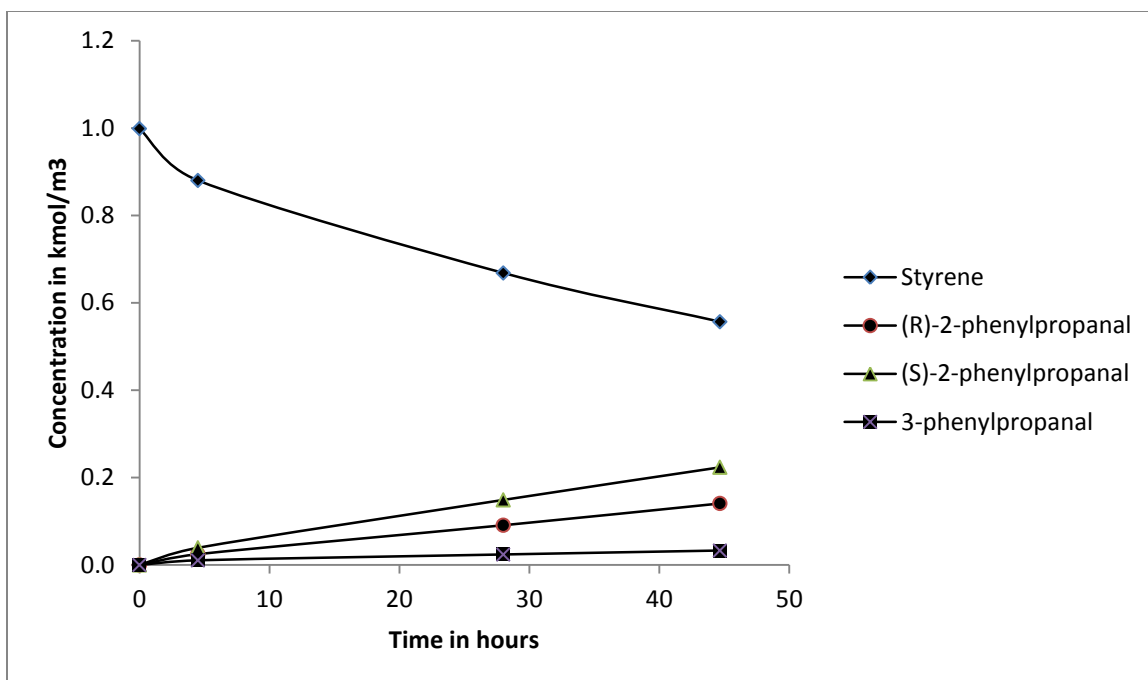


Figure 5: Typical concentration time profile of a batch reactor

Reaction Conditions: Rh(CO)₂(acac) – 19.2 mg (0.074 mmol); (*R*)-BINAP: 94 mg (0.15 mmol); Styrene: 2.61 g (25 mmol); Solvent: Toluene; Total charge: 25 ml; Syn gas (CO:H₂ = 1:1) pressure: 147 psi (10 atm); Temperature: 60 °C (333 K); Reaction time: 45 hours; Agitation speed: 900 rpm

The rate of the reaction was calculated in terms of conversion of styrene per unit time. However, the concentration of styrene itself is a parameter that affects the reaction rate (and styrene concentration reduces in the batch reactor as more and more styrene is converted to products). Therefore, only the data collected till 15 to 20 % of styrene conversion occurred, was used to calculate the reaction rate, and it was assumed that the styrene concentration remains constant during the collection of this data.

2.3.3.1 Effect of agitation speed: To be sure that the reaction is in the chemical kinetics regime and that the observed reaction rate is not the rate of mass transfer (rate of dissolution/diffusion of syn gas in the solvent), the effect of agitation speed on the reaction rate was studied.

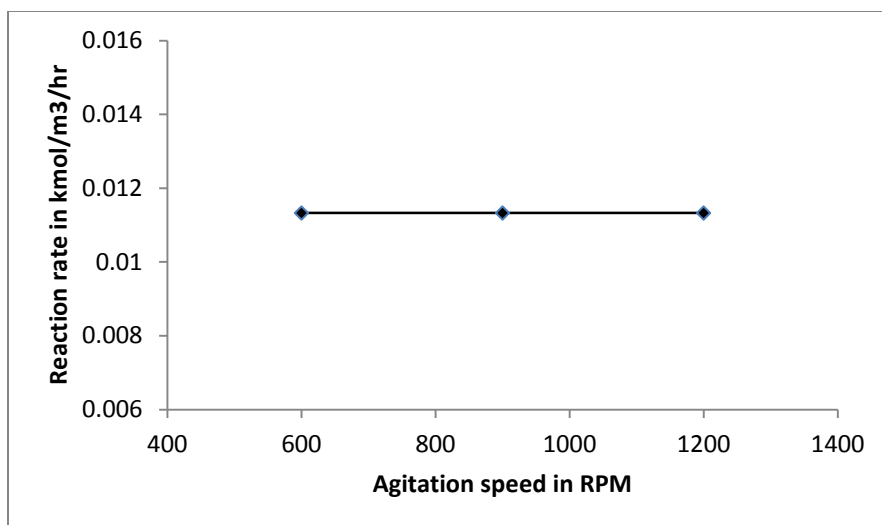


Figure 6: Effect of agitation speed on the reaction rate

Reaction Conditions: Rh(CO)₂(acac) – 19.2 mg (0.074 mmol); (*R*)-BINAP: 94 mg (0.15 mmol); Styrene: 2.61 g (25 mmol); Solvent: Toluene; Total charge: 25 ml; Syn gas (CO:H₂ = 1:1) pressure: 147 psi (10 atm); Temperature: 60 °C (333 K)

The agitation speed does not affect the rate of reaction, which indicates that the observed rate is the true intrinsic rate of the chemical reaction.

2.3.3.2 Effect of rhodium concentration: A plot of reaction rate versus rhodium concentration is given below.

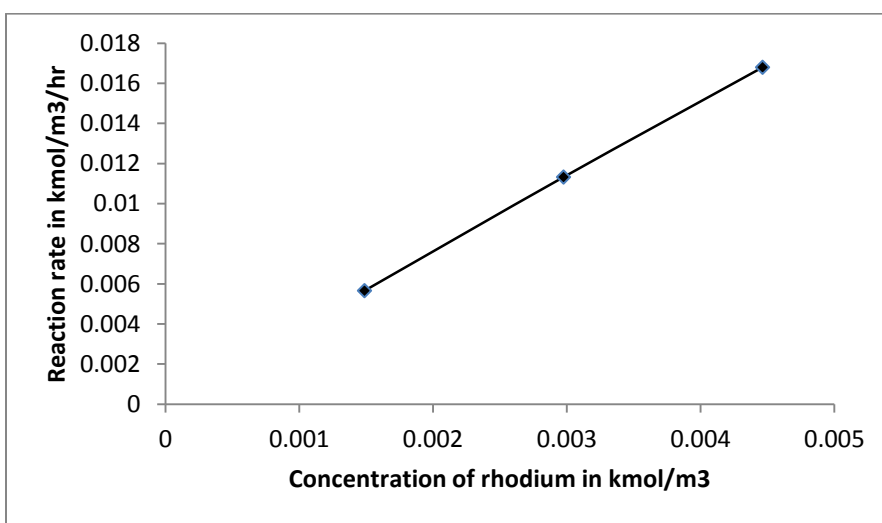


Figure 7: Effect of rhodium concentration on the reaction rate

Reaction Conditions: (*R*)-BINAP: 150 mg (0.24 mmol); Styrene: 2.08 g (20 mmol); Total charge: 15 ml; Syn gas (CO:H₂ = 1:1) pressure: 147 psi (10 atm); Temperature: 60 °C (333 K); Agitation speed: 900 rpm

The reaction rate was found to be linearly dependent of the rhodium concentration indicating first order kinetics.

Plots of regioselectivity and enantioselectivity versus rhodium concentrations (for the same reaction conditions) are given below.

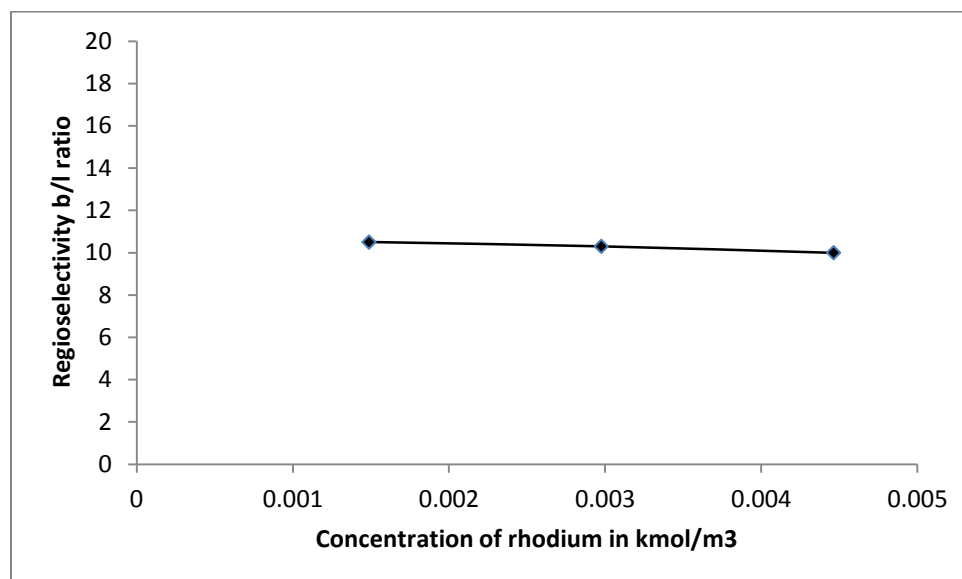


Figure 8: Effect of rhodium concentration on regioselectivity

The b/l ratio decreases marginally with increase in rhodium concentration.

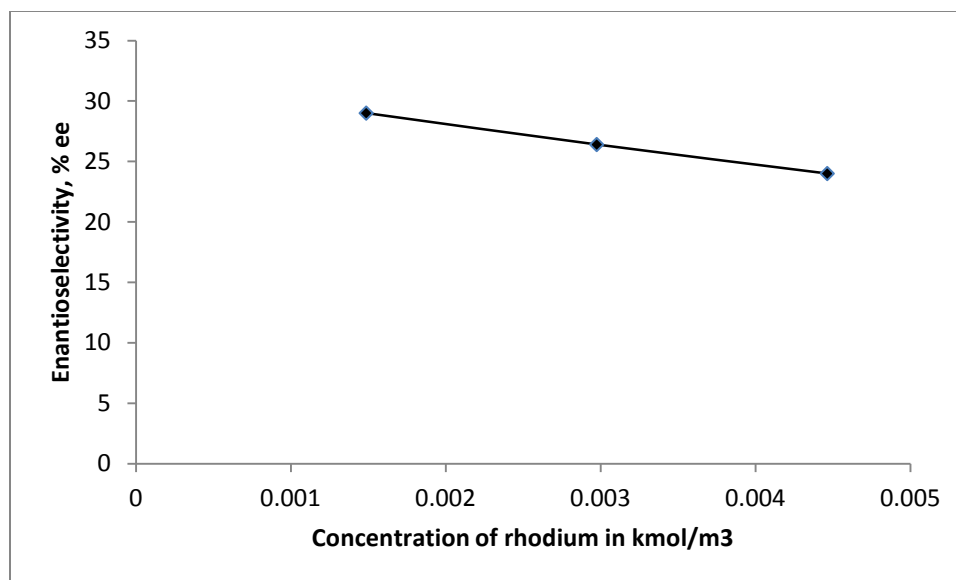


Figure 9: Effect of rhodium concentration on enantioselectivity

The enantioselectivity decreases with increase in the rhodium concentration. This is because the rhodium concentration rises whereas the (*R*)-BINAP concentration remains constant, thereby changing the ligand/metal ratio. The higher this ratio, higher is the enantioselectivity.

It is important to note that the ligand is in substantial stoichiometric excess to the metal (ligand/metal ratio is more than one) in case of all the three data points in the plot. This was determined after a test run with the ligand/metal ratio of 1.1 showed a sudden increase in the reaction rate after about 10 hours of reaction time. This sudden increase in reaction rate was accompanied by a steep drop in enantiomeric excess, indicating that the chiral phosphine catalyst had degraded ^[3] and that the more active symmetric catalysis had taken over. A substantial stoichiometric excess of (*R*)-BINAP (over rhodium) was necessary to maintain the reaction in the asymmetric catalysis regime.

2.3.3.3 Effect of (*R*)-BINAP concentration:

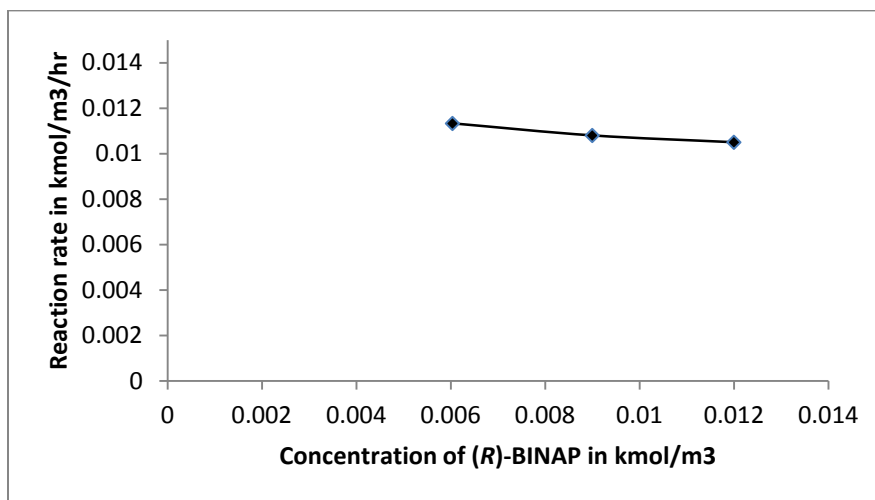


Figure 10: Effect of ligand concentration on reaction rate

Reaction Conditions: Rh(CO)₂(acac) – 19.2 mg (0.074 mmol); Styrene: 2.61 g (25 mmol); Solvent: Toluene; Total charge: 25 ml; Syn gas (CO:H₂ = 1:1) pressure: 147 psi (10 atm); Temperature: 60 °C (333 K); Agitation speed: 900 rpm

The rate of the reaction decreases marginally with increase in the concentration of (*R*)-BINAP.

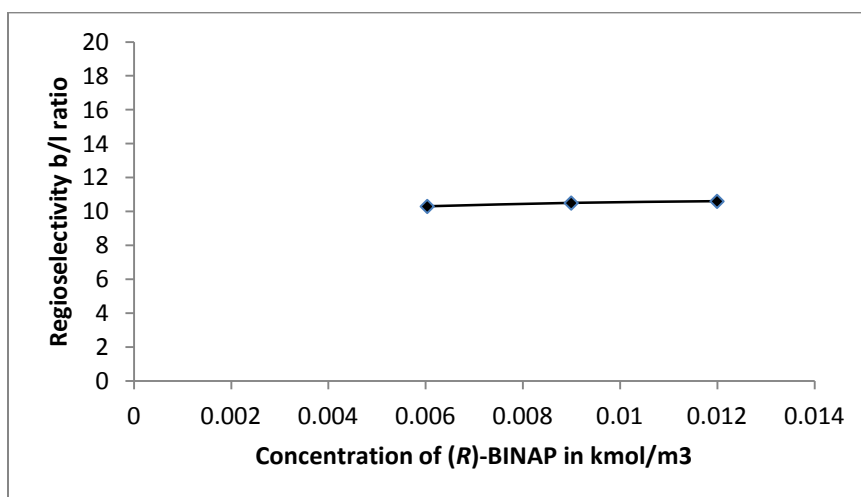


Figure 11: Effect of ligand concentration on regioselectivity

Increase in (*R*)-BINAP concentration increases the b/l ratio marginally.

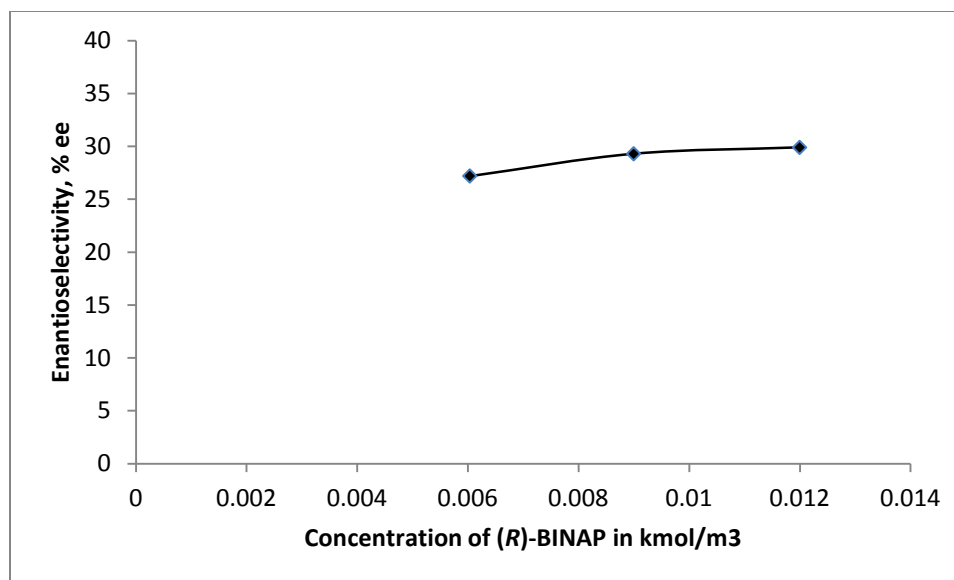


Figure 12: Effect of ligand concentration on enantioselectivity

The increase in (*R*)-BINAP concentration increases the enantioselectivity of the reaction. This effect is similar to the effect of decrease in rhodium concentration because in both cases the ligand/metal ratio increases.

2.3.3.4 Effect of CO partial pressure (P_{CO}):

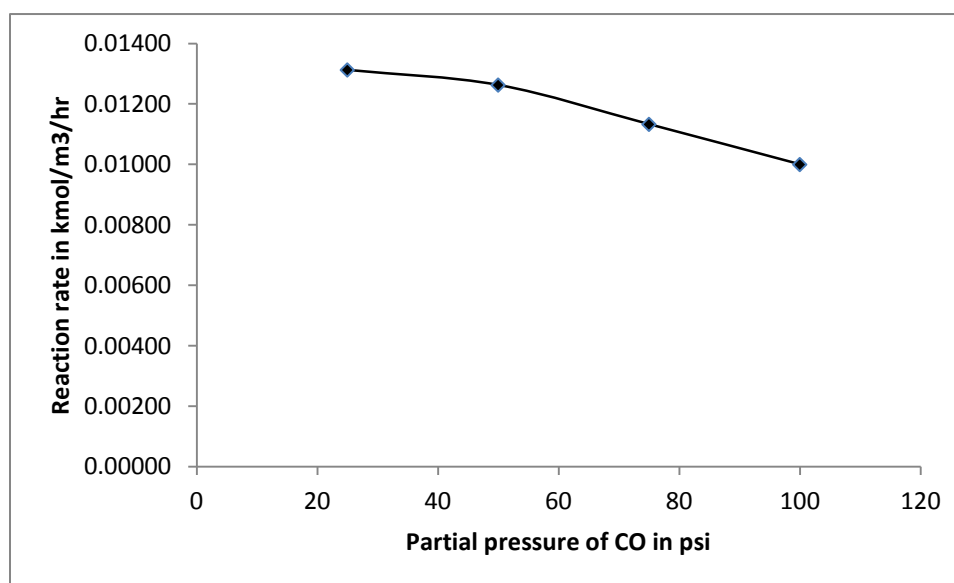


Figure 13: Effect of CO partial pressure on reaction rate

Reaction Conditions: Rh(CO)₂(acac) – 19.2 mg (0.074 mmol); (*R*)-BINAP: 94 mg (0.15 mmol); Styrene: 2.61 g (25 mmol); Solvent: Toluene; Total charge: 25 ml; H₂ partial pressure: 74 psi; Temperature: 60 °C (333 K); Agitation speed: 900 rpm

An increase in P_{CO} suppresses the formation of the active catalyst. The higher the partial pressure of CO, lower is the amount of rhodium available for hydroformylation. Moreover, higher CO partial pressure stabilizes the inactive resting state in the catalytic cycle^[3a], which lowers the rhodium available for catalysis further. However CO inhibition occurred at a very low P_{CO} in the present case^[4].

The effect of P_{CO} on selectivity is shown below:

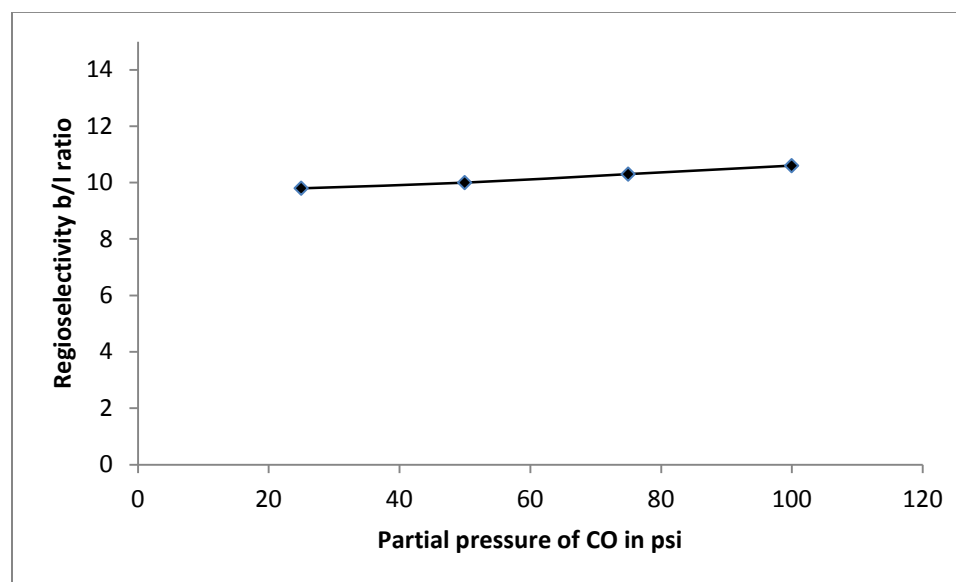


Figure 14: Effect of CO partial pressure on regioselectivity

Increase in P_{CO} increases the regioselectivity towards the branched aldehyde.

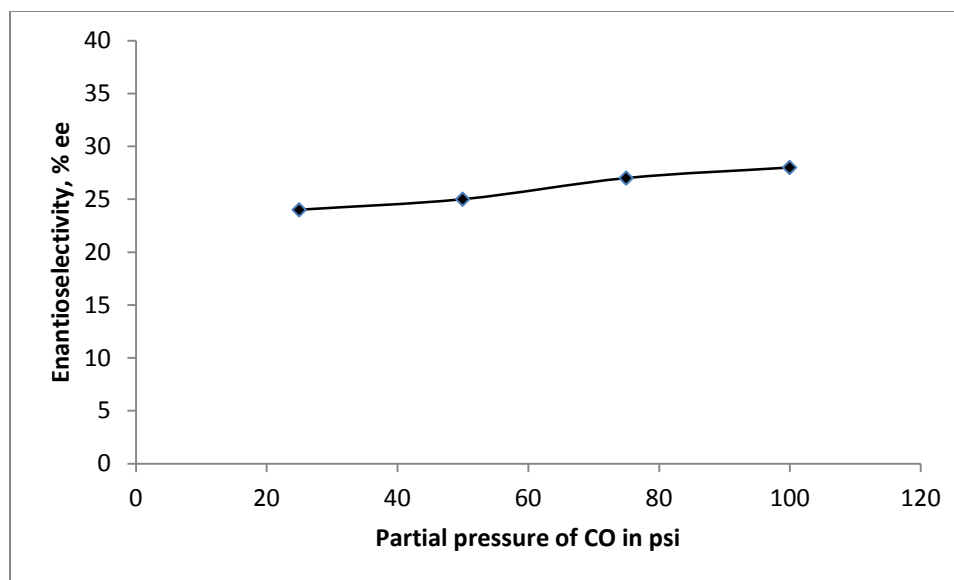


Figure 15: Effect of CO partial pressure on enantioselectivity

Enantiomeric excess increases with increase in partial pressure of CO.

2.3.3.5 Effect of H₂ partial pressure (P_{H2}):

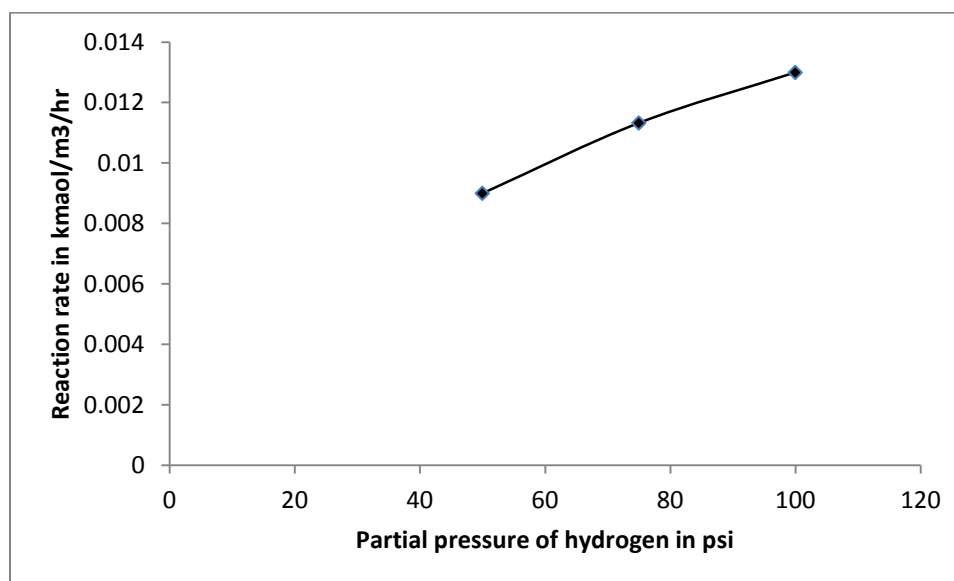


Figure 16: Effect of H₂ partial pressure on reaction rate

Reaction Conditions: Rh(CO)₂(acac) – 19.2 mg (0.074 mmol); (*R*)-BINAP: 94 mg (0.15 mmol); Styrene: 2.61 g (25 mmol); Solvent: Toluene; Total charge: 25 ml; CO partial pressure: 74 psi; Temperature: 60 °C (333 K); Agitation speed: 900 rpm

The partial pressure of H₂ shows an approximate linear effect on the rate of reaction, indicating first order kinetics.

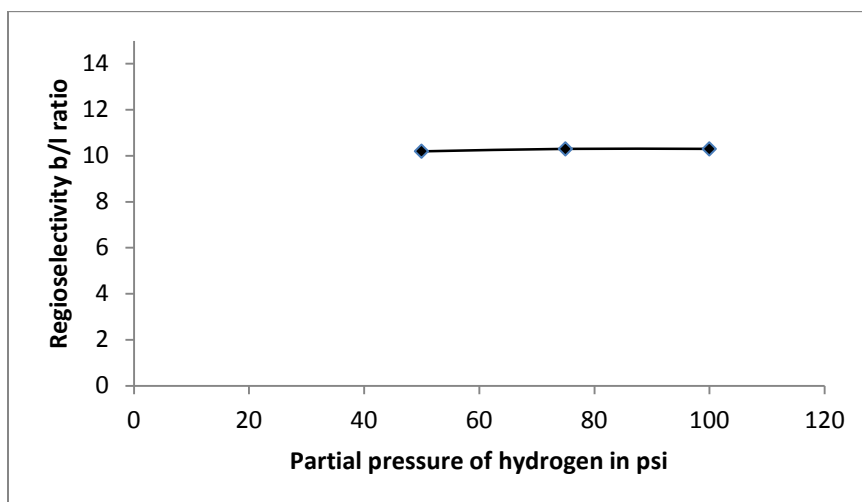


Figure 17: Effect of H₂ partial pressure on regioselectivity

The regioselectivity shows no dependence on P_{H₂}.

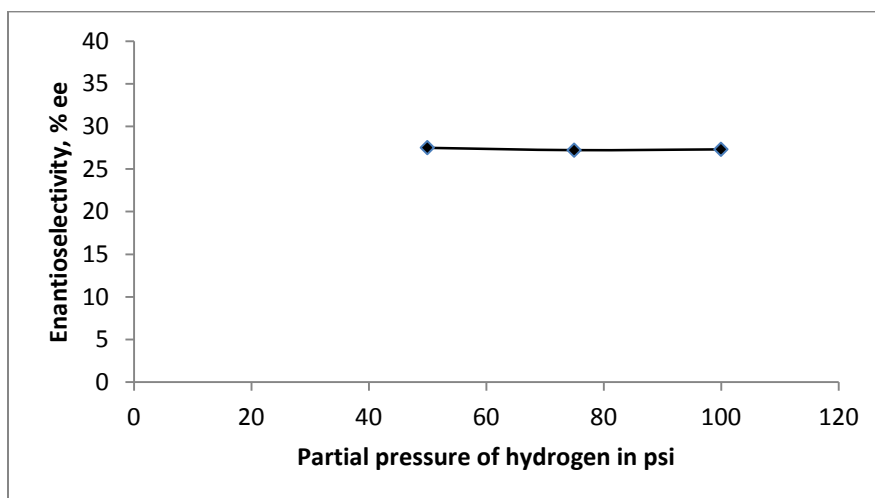


Figure 18: Effect of H₂ partial pressure on enantioselectivity

The enantioselectivity also is independent of the hydrogen partial pressure.

2.3.3.6 Effect of styrene concentration:

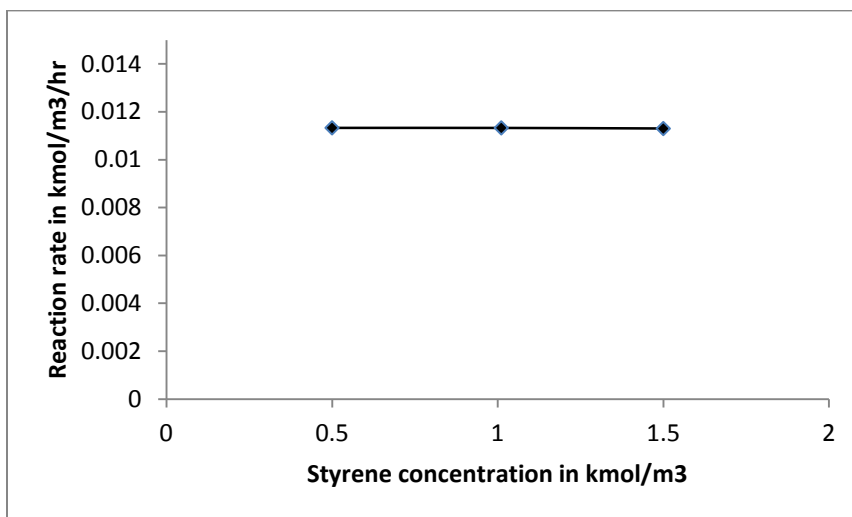


Figure 19: Effect of substrate concentration on reaction rate

Reaction Conditions: Rh(CO)₂(acac) – 19.2 mg (0.074 mmol); (*R*)-BINAP: 94 mg (0.15 mmol); Solvent: Toluene; Total charge: 25 ml; Syn gas (CO:H₂ = 1:1) pressure: 147 psi (10 atm); Temperature: 60 °C (333 K); Agitation speed: 900 rpm

The reaction rate was independent of the substrate concentration. This is probably because the concentration of the substrate is much higher than the catalyst concentration (Styrene/rhodium ratio is more than 300).

The substrate concentration also did not affect the selectivity of the reaction:

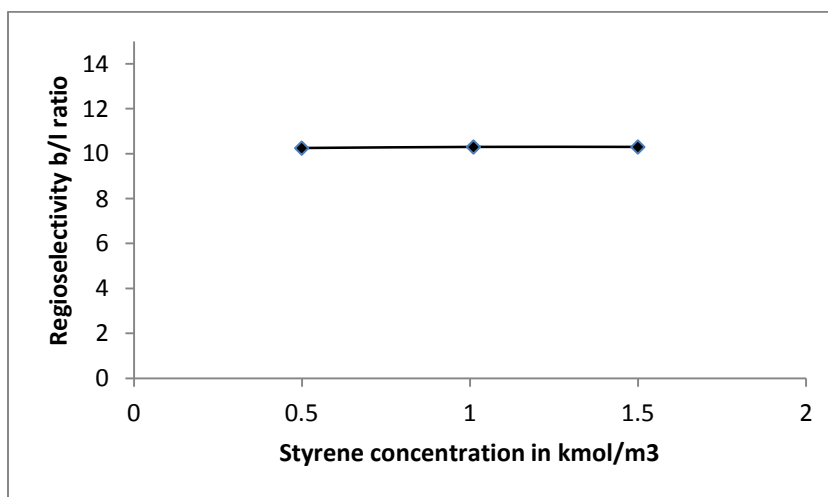


Figure 20: Effect of substrate concentration on regioselectivity

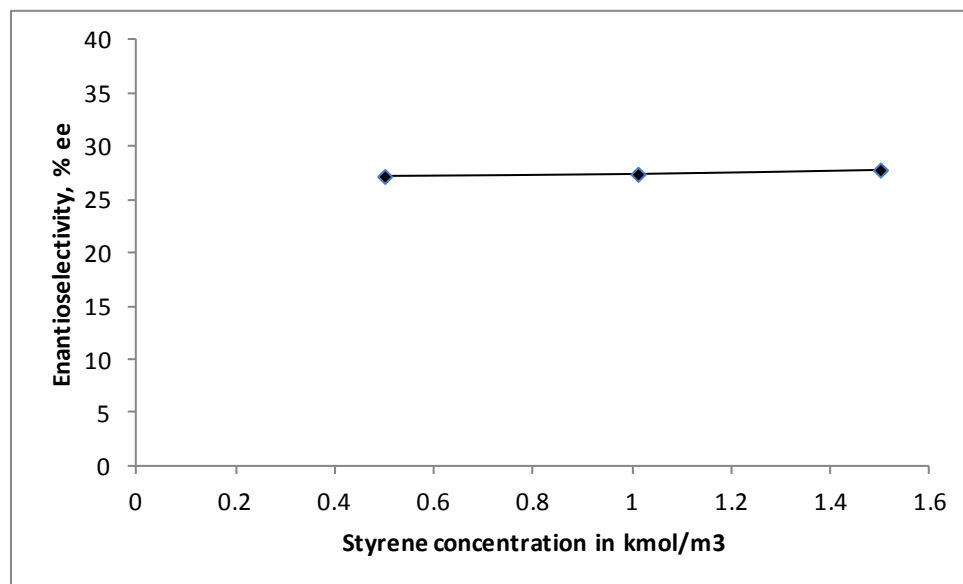


Figure 21: Effect of substrate concentration on enantioselectivity

2.3.3.7 Effect of temperature: The enantioselectivity decreased dramatically with increase in temperature. The regioselectivity (towards branched aldehyde) also decreased, but the effect was less pronounced than that for the enantioselectivity.

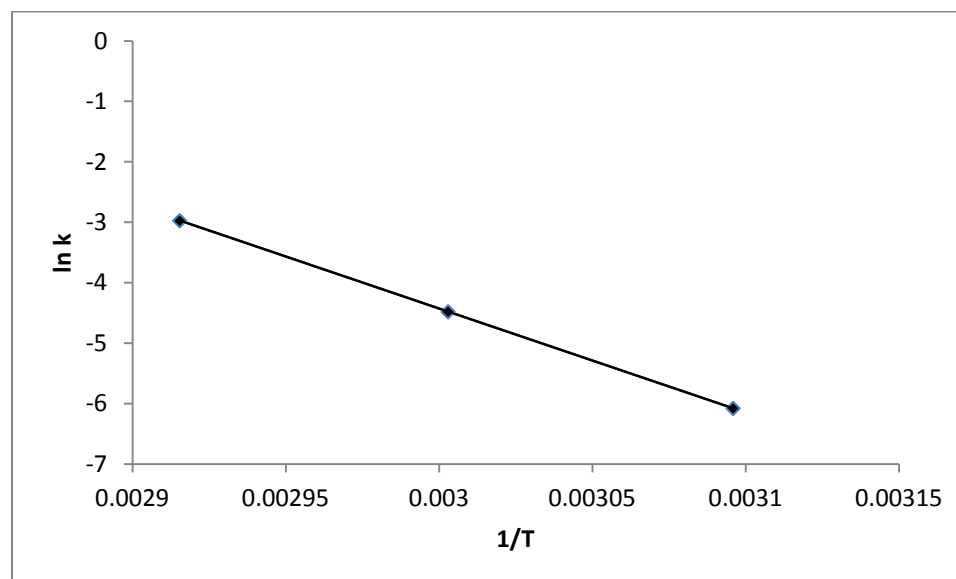


Figure 22: Arrhenius plot

Reaction Conditions: Rh(CO)₂(acac) – 19.2 mg (0.074 mmol); (*R*)-BINAP: 94 mg (0.15 mmol); Styrene: 2.61 g (25 mmol); Solvent: Toluene; Total charge: 25 ml; Syn gas (CO:H₂ = 1:1) pressure: 147 psi (10 atm); Temperature: 323 K, 333 K and 343 K; Agitation speed: 900 rpm

A plot of the natural logarithm of reaction rate versus the multiplicative inverse or reciprocal of temperature gave a straight line. The slope of this line was used to calculate the activation energy:

$$E_a = 143 \text{ kJ/mol} = 34.2 \text{ kcal/mol}$$

References

- [1] Y. S. Varshavskii, T. Cherkasova, *Zh. Neorg. Khim.* **1967**, *12*, 1709.
- [2] D. Han, X. Li, H. Zhang, Z. Liu, G. Hu, C. Li, *Journal of Molecular Catalysis A: Chemical* **2008**, *283*, 15-22.
- [3] aP. W. N. M. Van Leeuwen, C. Claver, *Rhodium catalyzed hydroformylation, Vol. 22*, Kluwer Academic Print on Demand, **2002**; bB. Cornils, W. A. Herrmann, *Applied homogeneous catalysis with organometallic compounds, Vol. 2*, VCH Weinheim etc., **1996**.
- [4] aV. S. Nair, S. P. Mathew, R. V. Chaudhari, *Journal of Molecular Catalysis A: Chemical* **1999**, *143*, 99-110; bA. van Rooy, E. N. Orij, P. C. J. Kamer, P. W. N. M. van Leeuwen, *Organometallics* **1995**, *14*, 34-43.

CHAPTER 3

**Computational study on asymmetric
hydroformylation of styrene using
(*R*)-BINAP modified rhodium catalyst**

3.1 Introduction

Very few literature reports are available on DFT studies on asymmetric hydroformylation^[1]. Moreover, these reports describe DFT studies either on a small part of the catalytic cycle or on model systems.

This chapter describes a DFT study on the entire catalytic cycle of asymmetric hydroformylation of styrene. The catalyst is (*R*)-BINAP modified rhodium.

3.2 Computational

Styrene can be hydroformylated to give three different products – (*S*)-2-phenylpropanal, (*R*)-2-phenylpropanal and 3-phenylpropanal. 2-phenylpropanals are the branched aldehydes whereas 3-phenylpropanal is the linear aldehyde. The branched aldehydes are chiral and the linear aldehyde is achiral. The following figure 1 shows formation of (*R*)-2-phenylpropanal, as per the Heck and Breslow mechanism. The overall mechanism of styrene hydroformylation can be imagined as a superimposition of three distinct catalytic cycles, each giving rise to one of the three aldehyde products.

The labels in the following figure 1 (“catalyst precursor”, catalyst, “step 1”, “step 2”, etc., the “side step”, the aldehyde product, transition states – TS1, TS2, etc) have been used consistently throughout this chapter. All molecules except the transition states have been termed as “stable molecules”.

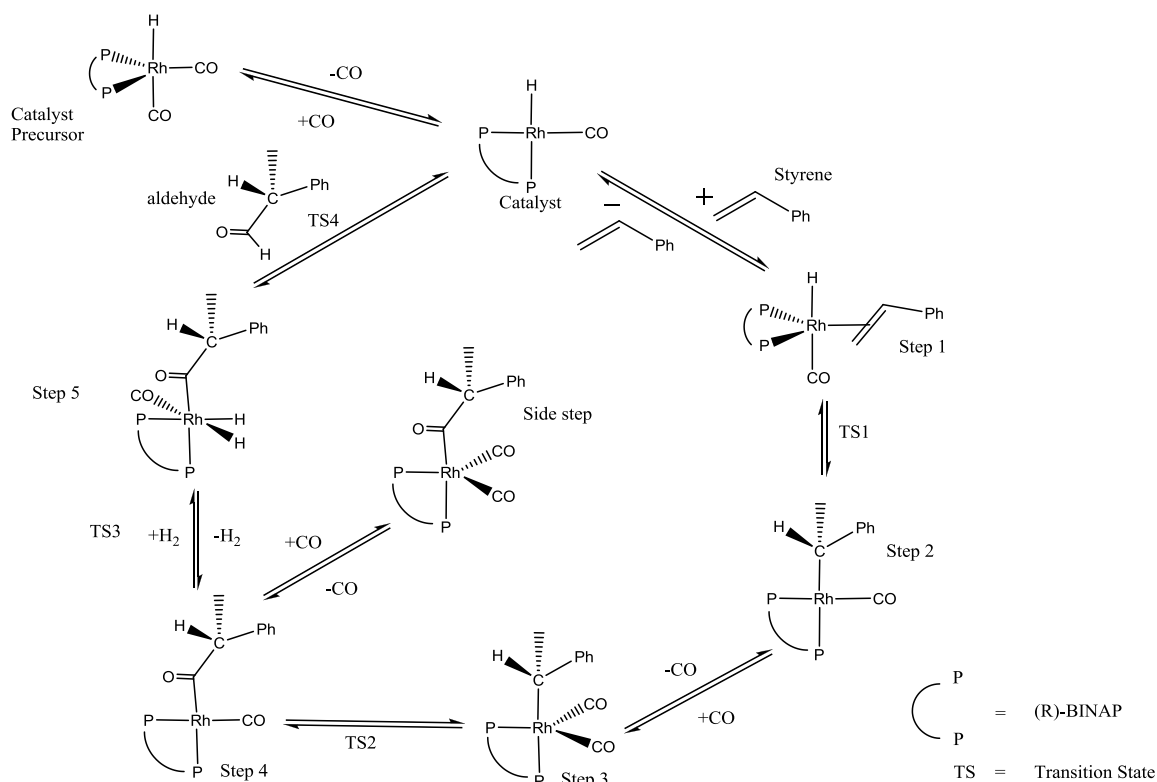


Figure 1: Heck and Breslow mechanism for asymmetric hydroformylation of styrene using (R)-BINAP modified rhodium catalyst

In the mechanism, the “catalyst precursor”, “step 1”, “step 3” and the “side step” are trigonal bipyramidal (TBP) complexes. The “catalyst”, “step 2” and “step 4” are square planar complexes. “Step 5” is an octahedral complex. There are four transition states in the catalytic cycle. Rhodium maintains an oxidation state of +1 in the catalytic cycle except for “step 5” where it has an oxidation state of +3. All molecules in figure 1 are diamagnetic ^[2].

The molecules on which this computational study has been done are very large (figure 1) and can have many conformers (and every conformer of a stable molecule corresponds to a local minimum on the energy hypersurface). The most stable conformer corresponds to the global minimum. To maximize the probability of finding the global minimum (or a local minimum that is energetically very close to the global minimum), all stable molecules (except simple molecules like CO, H₂ and styrene) were subjected to conformational search using torsion angle driving/ dihedral angle driving. This

conformational search/ analysis was done using molecular mechanics (MM+ force field) on HyperChem^[3].

For the typical conformational search of a stable molecule, as many independent torsion angles as possible, were chosen. This search was carried out on a desktop computer with an Intel Pentium 4 processor (3 GHz) and 1 GB RAM. The search was continued till the lowest energy conformer (on the list of conformers) was not replaced (by a more stable conformer) for more than 15 minutes. The conformational analysis of a typical stable molecule took a time of about 3 to 4 hours.

At least five of the lowest energy conformers so obtained from the conformational search were subjected to DFT calculations for geometry optimization. Thus the conformers were screened using molecular mechanics (MM) before subjecting them to quantum mechanical (QM) calculations. This was done to reduce the computational cost of the study. (DFT calculations are more compute-intensive than MM calculations and so using DFT for conformational search can be computationally very expensive.)

The DFT calculations were carried out on high performance clusters (HPCs). A typical configuration of a HPC is as follows:

- 8 nodes (1 management node + 7 compute nodes)
- Each node having 2 quad core Intel Nehalem processors (2.6 GHz, 3MB cache, 64 bit) – total 56 cores available for computation.
- Each quad core processor accompanied by 8 GB RAM
- Each compute node accompanied by 80 GB SATA hard drive
- Gigabit interconnect
- Management node accompanied by 500 GB RAID drive (scratch drive) and 2 GB storage drive.
- Operating System: Free Rocks Cluster^[4] OS

The TURBOMOLE^[5] (version 5) program package was used for DFT calculations. The Molden program was used for visualization of the results obtained from TURBOMOLE. Unless otherwise specified, following were the conditions used for a typical DFT calculation:

- def-TZVP basis set was used for rhodium. TZVP basis set was used for all other atoms.
- Becke-Perdew (b-p) functional ^[6] was used.
- Resolution of identity (RI) ^[7] and multipole accelerated resolution of identity (MARI-J) ^[8] approximations were used to speed up the calculations.

A typical geometry optimization done using DFT was done employing a “first order” method. In a “first order” method, only the first derivative of energy with respect to the atomic coordinates is calculated. The electronic energy so obtained is only a part of the overall energy of a molecule. To find the free energy of the molecule, the vibrational energy, rotational energy, translational energy and the entropy effects are also needed. For finding the vibrational energy, calculation of the Hessian is essential. The Hessian is a matrix of second derivatives of the energy with respect to the atomic coordinates. However, calculation of the Hessian matrix is a highly compute intensive job. Therefore only the important molecules (e.g. the lowest energy conformers of all stable molecules – as determined by the first order DFT calculations and all transition state geometries) were subjected to Hessian calculation. It is important to note though, that the first order method is adequate to give qualitative trends of energy differences between the molecules. This is because the electronic energy constitutes the most important part of the overall energy of any molecule.

The solvation effect was calculated for important molecules using COSMO. Toluene was assumed to be the solvent for the reaction. Here the optimized geometry obtained from the gas phase calculation was subjected to a single point COSMO calculation assuming the solvent to be a dielectric continuum.

The calculations were run on multiple cores (parallel computing ^[9]) to reduce the time required for getting the results. A typical geometry optimization job took a time of about two days to complete, on 16 cores (cores of a processor).

The transition states (saddle points on the energy hypersurface) were derived from the optimized geometries of the stable molecules in the catalytic cycle. A typical transition state (TS) calculation job took a time of about six days to complete, on 16 cores.

3.3 Results of the computational study

3.3.1 Conformational search: To justify the use of a MM based conformational search for screening of conformers of stable molecules, a study was done on a model system where n-decane molecule was subjected to torsion angle driving.

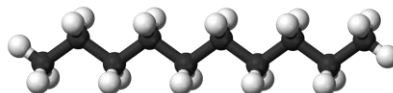


Figure 2: n-decane

181 conformers were generated over a period of about 3 hours. These conformers were listed in increasing order of strain energy. Ten equidistantly placed conformers in the list (viz. 1st, 21st, 41st, etc) were subjected to DFT calculations and their strain energies and electronic energies were plotted:

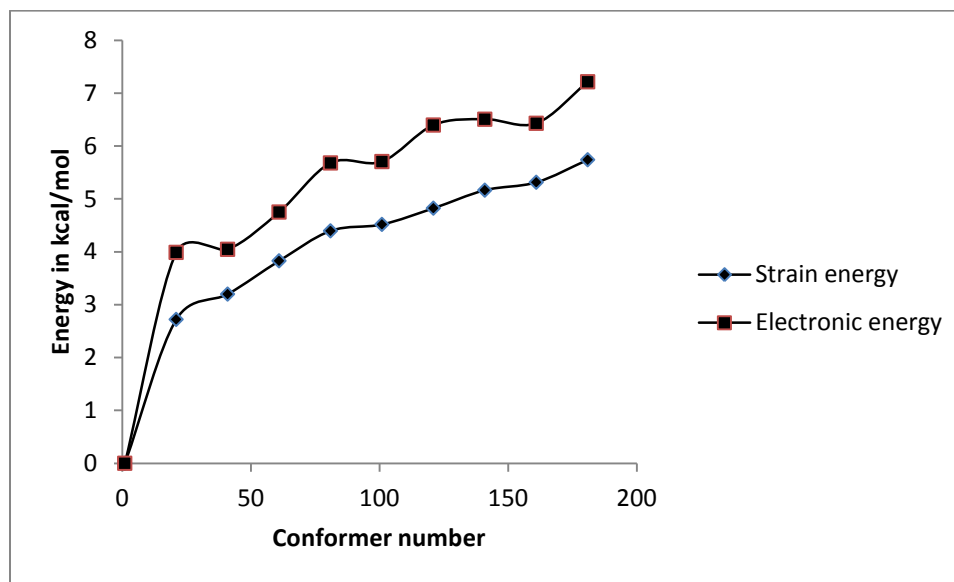


Figure 3: Plot of strain energy and electronic energy versus the conformer number of n-decane

As shown in the plot (figure 3), the trends for the strain energy and the electronic energy match very well. The lowest energy conformer given by MM (conformational search) is also the lowest energy conformer as per the DFT calculation. However n-decane is a

simple organic molecule, whereas the molecules in the catalytic cycle under study are complex.

The following figure 4 shows a plot of strain energy and electronic energy for the conformers of “step 2” molecule in the catalytic cycle that gives rise to the linear aldehyde.

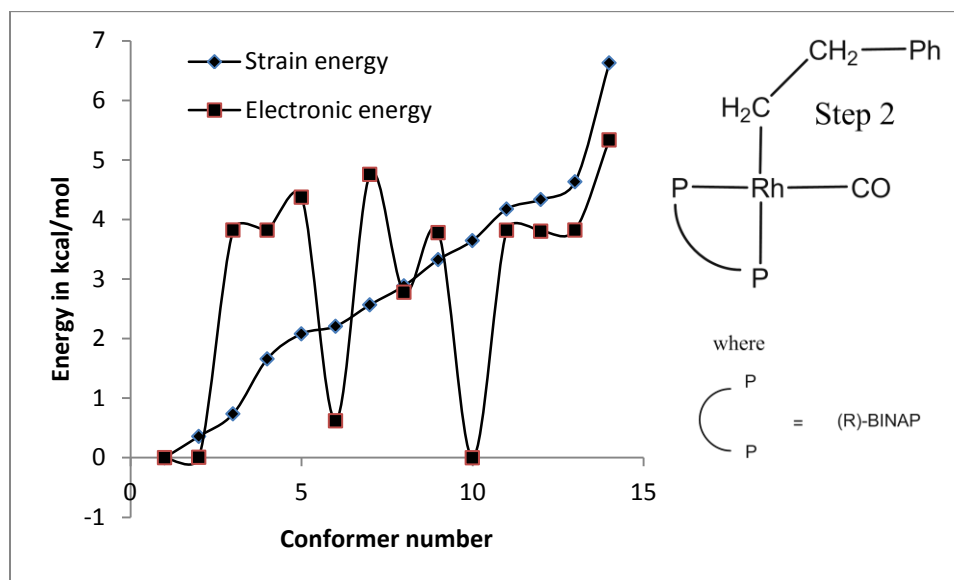


Figure 4: Plot of strain energy and electronic energy versus the conformer number of the “step 2” molecule (in the catalytic cycle that gives rise to 3-phenylpropanal)

As figure 4 depicts, the real life situation is more complicated than a model system (n-decane). So to maximize the probability of getting the global minima, at least five of the lowest energy conformers (given by MM) of all the stable molecules in the catalytic cycle, were subjected to DFT calculations.

The following figure 5 shows optimized structures of two conformers of free (*R*)-BINAP ligand:

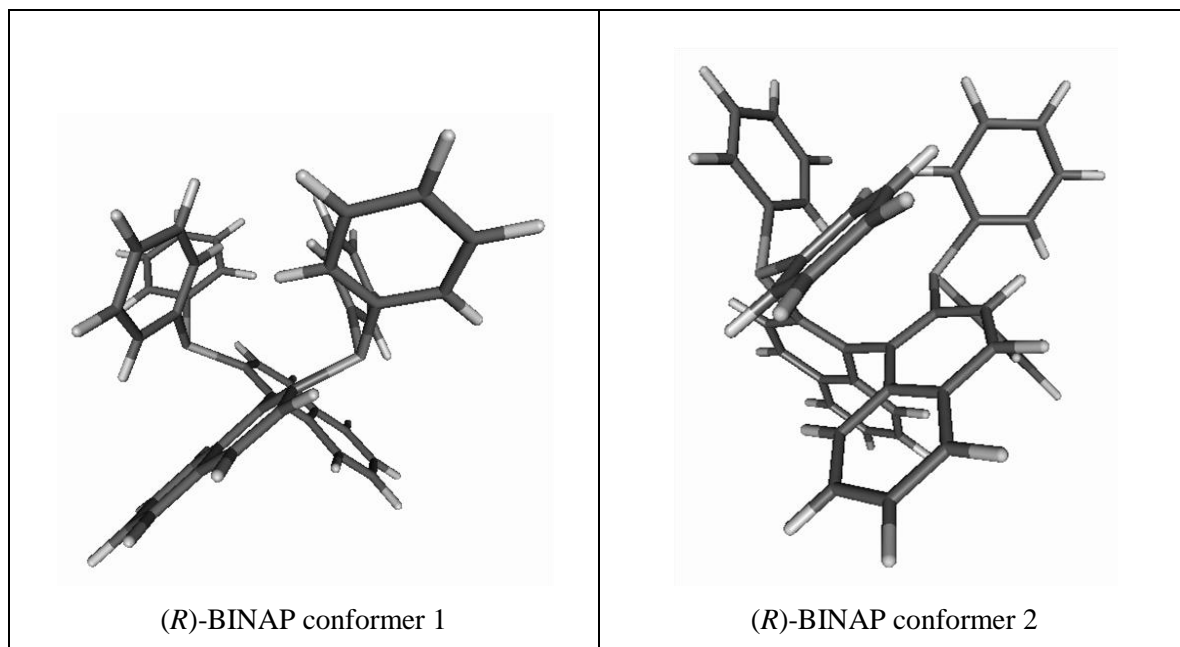


Figure 5: The two conformers of (*R*)-BINAP ligand

A conformational search for (*R*)-BINAP gave only two conformers. The electronic energy difference between the two conformers is 5.4 kcal/mol. Conformer 2 is more stable than conformer 1. In case of conformer 1, the lone pairs of electrons on the two phosphorus atoms point in opposite directions, whereas in conformer 2, the lone pairs point in the same direction.

In the present computational study, it was assumed that (*R*)-BINAP is not a trans-chelating or trans-spanning ligand^[10].

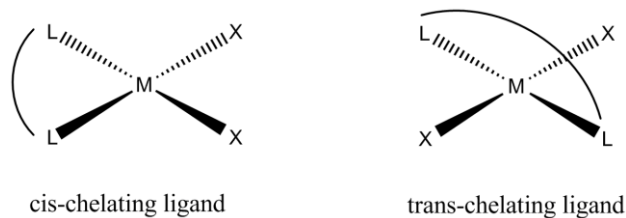


Figure 6: Cis and trans-chelating ligands

The metal complexes that have trigonal bipyramidal (TBP) and octahedral geometry can have many geometric isomers (isomers created due to change in relative positions of

various ligands). This necessitates conformational search for every geometric isomer in every step of the mechanism. However, while doing the conformational search using torsion angle driving, it was observed that the TBP complexes can undergo a “virtual” Berry pseudorotation^[11] (the conformational search itself generates the various geometric isomers).

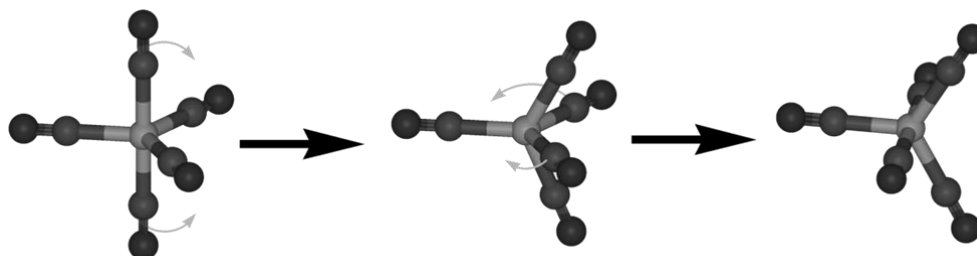


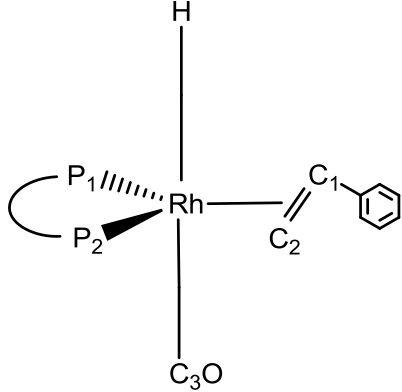
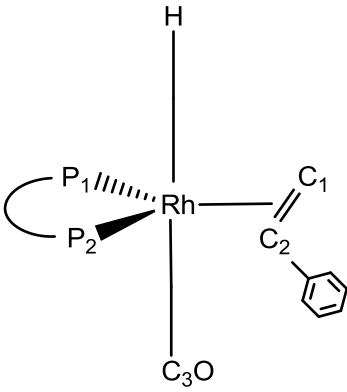
Figure 7: Berry pseudorotation in Iron pentacarbonyl

The octahedral metal complexes (“step 5”) also undergo similar virtual pseudorotation during torsion angle driving. This eliminated the need for a separate conformational search for every geometric isomer.

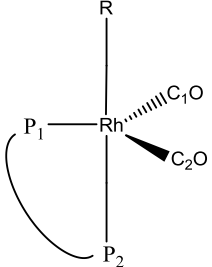
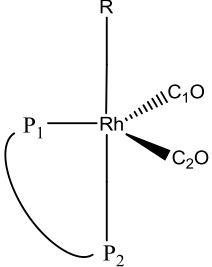
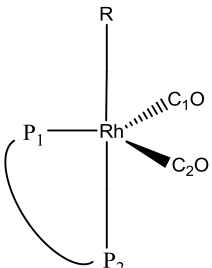
3.3.2 Results of DFT study on the catalytic cycle (Heck and Breslow mechanism): As described earlier, the overall catalytic cycle was assumed to be a superimposition of three catalytic cycles, each giving rise to one of the aldehyde products. The catalyst precursor, catalyst, substrate (styrene), H₂ and CO molecules are common for all the three catalytic cycles. The enantio-differentiation takes place when styrene approaches the rhodium atom in the catalyst, either through the re-face or the si-face (“step 1”). The approach through the re-face can give rise to (*R*)-2-phenylpropanal or 3-phenylpropanal. The approach through the si-face can give rise to (*S*)-2-phenylpropanal or 3-phenylpropanal. The regio-differentiation takes place when styrene inserts in the Rh-H bond. (The transition state TS1 decides whether branched or linear aldehyde would be formed.) The following table 1 describes the optimized geometries of the rhodium metal complexes (stable molecules) having the lowest free energies in each step in the three parallel catalytic cycles:

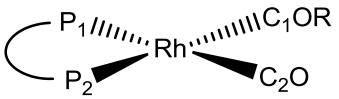
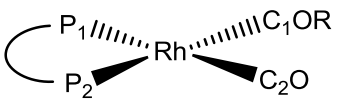
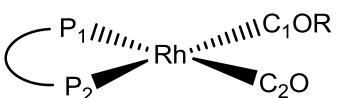
Table 1: Description of optimized geometries of lowest free energy stable molecules (Heck and Breslow mechanism)

| Code of the conformer of the metal complex | Positions of the core atoms | Metal complex belongs to the catalytic cycle that gives rise to: | Description of geometry |
|--|-----------------------------|--|---|
| <i>Catalyst precursor</i> | | | |
| complex5 | | All the three aldehydes | $P_1\text{-Rh-}P_2$ bite angle = 96.6° Rh- C_1 distance = 1.90 \AA Rh- C_2 distance = 1.93 \AA Rh-H distance = 1.61 \AA Rh- P_1 distance = 2.38 \AA Rh- P_2 distance = 2.39 \AA |
| <i>Catalyst</i> | | | |
| cc5 | | All the three aldehydes | $P_1\text{-Rh-}P_2$ bite angle = 95.1° Rh-C distance = 1.87 \AA Rh-H distance = 1.61 \AA Rh- P_1 distance = 2.34 \AA Rh- P_2 distance = 2.36 \AA |

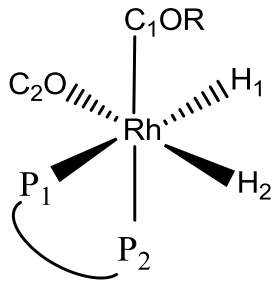
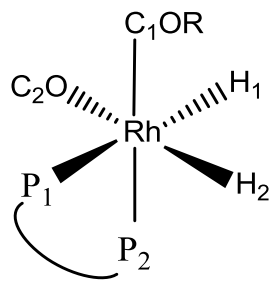
| Code of the conformer of the metal complex | Positions of the core atoms | Metal complex belongs to the catalytic cycle that gives rise to: | Description of geometry |
|--|--|--|--|
| <i>Step 1</i> | | | |
| eeeS1 |  | (S)-2-phenylpropanal and 3-phenylpropanal | P ₁ -Rh-P ₂ bite angle = 97.0° Rh-C ₁ distance = 2.28 Å Rh-C ₂ distance = 2.18 Å Rh-C ₃ distance = 1.93 Å Rh-H distance = 1.61 Å Rh-P ₁ distance = 2.37 Å Rh-P ₂ distance = 2.37 Å C ₁ -C ₂ distance = 1.42 Å C ₁ and C ₂ in equatorial plane |
| eeeR3 |  | (R)-2-phenylpropanal and 3-phenylpropanal | P ₁ -Rh-P ₂ bite angle = 97.0° Rh-C ₁ distance = 2.20 Å Rh-C ₂ distance = 2.24 Å Rh-C ₃ distance = 1.93 Å Rh-H distance = 1.61 Å Rh-P ₁ distance = 2.36 Å Rh-P ₂ distance = 2.37 Å C ₁ -C ₂ distance = 1.43 Å C ₁ and C ₂ in equatorial plane |

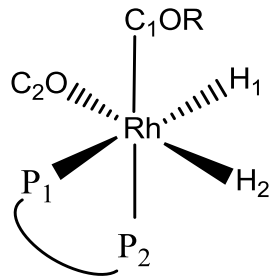
| Code of the conformer of the metal complex | Positions of the core atoms | Metal complex belongs to the catalytic cycle that gives rise to: | Description of geometry |
|--|-----------------------------|--|---|
| <i>Step 2</i> | | | |
| 2brS6 | | (<i>S</i>)-2-phenylpropanal | P_1 -Rh- P_2 bite angle = 92.1° Rh-C(-R) distance = 2.16 \AA Rh-C(-CO) distance = 1.88 \AA Rh- P_1 distance = 2.36 \AA Rh- P_2 distance = 2.36 \AA |
| 2brR1 | | (<i>R</i>)-2-phenylpropanal | P_1 -Rh- P_2 bite angle = 92.3° Rh-C(-R) distance = 2.18 \AA Rh-C(-CO) distance = 1.87 \AA Rh- P_1 distance = 2.35 \AA Rh- P_2 distance = 2.37 \AA |
| 2li3 | | 3-phenylpropanal | P_1 -Rh- P_2 bite angle = 93.4° Rh-C(-R) distance = 2.15 \AA Rh-C(-CO) distance = 1.87 \AA Rh- P_1 distance = 2.36 \AA Rh- P_2 distance = 2.35 \AA |

| Code of the conformer of the metal complex | Positions of the core atoms | Metal complex belongs to the catalytic cycle that gives rise to: | Description of geometry |
|--|---|--|---|
| <i>Step 3</i> | | | |
| 3brS2 |  | (S)-2-phenylpropanal | $P_1\text{-Rh-}P_2$ bite angle = 89.1° Rh- C_1 distance = 1.91 \AA Rh- C_2 distance = 1.91 \AA Rh-C(-R) distance = 2.25 \AA Rh- P_1 distance = 2.48 \AA Rh- P_2 distance = 2.40 \AA |
| 3brR2 |  | (R)-2-phenylpropanal | $P_1\text{-Rh-}P_2$ bite angle = 88.6° Rh- C_1 distance = 1.91 \AA Rh- C_2 distance = 1.90 \AA Rh-C(-R) distance = 2.27 \AA Rh- P_1 distance = 2.50 \AA Rh- P_2 distance = 2.40 \AA |
| 3li3 |  | 3-phenylpropanal | $P_1\text{-Rh-}P_2$ bite angle = 90.1° Rh- C_1 distance = 1.90 \AA Rh- C_2 distance = 1.91 \AA Rh-C(-R) distance = 2.20 \AA Rh- P_1 distance = 2.46 \AA Rh- P_2 distance = 2.40 \AA |

| Code of the conformer of the metal complex | Positions of the core atoms | Metal complex belongs to the catalytic cycle that gives rise to: | Description of geometry |
|--|---|--|--|
| <i>Step 4</i> | | | |
| 4brS2 |  | (S)-2-phenylpropanal | P ₁ -Rh-P ₂ bite angle = 93.2° Rh-C ₁ distance = 2.06 Å Rh-C ₂ distance = 1.88 Å Rh-P ₁ distance = 2.36 Å Rh-P ₂ distance = 2.40 Å |
| 4brR3 |  | (R)-2-phenylpropanal | P ₁ -Rh-P ₂ bite angle = 94.5° Rh-C ₁ distance = 2.02 Å Rh-C ₂ distance = 1.87 Å Rh-P ₁ distance = 2.36 Å Rh-P ₂ distance = 2.40 Å |
| 4li9 |  | 3-phenylpropanal | P ₁ -Rh-P ₂ bite angle = 94.0° Rh-C ₁ distance = 2.03 Å Rh-C ₂ distance = 1.87 Å Rh-P ₁ distance = 2.36 Å Rh-P ₂ distance = 2.40 Å |

| Code of the conformer of the metal complex | Positions of the core atoms | Metal complex belongs to the catalytic cycle that gives rise to: | Description of geometry |
|--|-----------------------------|--|--|
| <i>Side Step</i> | | | |
| sbrS2 | | (<i>S</i>)-2-phenylpropanal | $P_1\text{-Rh-}P_2$ bite angle = 88.8° Rh- C_1 distance = 2.12 Å Rh- C_2 distance = 1.91 Å Rh- C_3 distance = 1.92 Å Rh- P_1 distance = 2.50 Å Rh- P_2 distance = 2.45 Å |
| sbrR2 | | (<i>R</i>)-2-phenylpropanal | $P_1\text{-Rh-}P_2$ bite angle = 88.5° Rh- C_1 distance = 2.12 Å Rh- C_2 distance = 1.91 Å Rh- C_3 distance = 1.92 Å Rh- P_1 distance = 2.51 Å Rh- P_2 distance = 2.45 Å |
| sli2 | | 3-phenylpropanal | $P_1\text{-Rh-}P_2$ bite angle = 89.0° Rh- C_1 distance = 2.12 Å Rh- C_2 distance = 1.91 Å Rh- C_3 distance = 1.92 Å Rh- P_1 distance = 2.49 Å Rh- P_2 distance = 2.44 Å |

| Code of the conformer of the metal complex | Positions of the core atoms | Metal complex belongs to the catalytic cycle that gives rise to: | Description of geometry |
|--|--|--|--|
| <i>Step 5</i> | | | |
| 5brS8 |  | (S)-2-phenylpropanal | P ₁ -Rh-P ₂ bite angle = 92.8° Rh-C ₁ distance = 2.09 Å Rh-C ₂ distance = 1.93 Å Rh-H ₁ distance = 1.58 Å Rh-H ₂ distance = 1.62 Å Rh-P ₁ distance = 2.45 Å Rh-P ₂ distance = 2.44 Å |
| 5brR8 |  | (R)-2-phenylpropanal | P ₁ -Rh-P ₂ bite angle = 92.6° Rh-C ₁ distance = 2.09 Å Rh-C ₂ distance = 1.93 Å Rh-H ₁ distance = 1.58 Å Rh-H ₂ distance = 1.62 Å Rh-P ₁ distance = 2.46 Å Rh-P ₂ distance = 2.44 Å |

| Code of the conformer of the metal complex | Positions of the core atoms | Metal complex belongs to the catalytic cycle that gives rise to: | Description of geometry |
|--|---|--|---|
| 5li8 |  | 3-phenylpropanal | $P_1\text{-Rh-P}_2$ bite angle = 92.6° Rh-C ₁ distance = 2.10 Å Rh-C ₂ distance = 1.93 Å Rh-H ₁ distance = 1.58 Å Rh-H ₂ distance = 1.62 Å Rh-P ₁ distance = 2.45 Å Rh-P ₂ distance = 2.44 Å |

In table 1, the “step 1” molecules (eeeS1 and eeeR3) have (*R*)-BINAP in equatorial-equatorial position. Geometric isomers (generated by virtual pseudorotation in the conformational search) having (*R*)-BINAP in equatorial-axial position were unstable compared to those having (*R*)-BINAP in equatorial-equatorial position. The hydride and carbonyl groups are in axial positions in eeeS1 and eeeR3 molecules. The phenyl group of styrene is not in the equatorial plane of the metal complex and is away from the hydride and closer to the carbonyl. In free styrene, the double bond has a bond length of 1.34 Å. This bond length increases when styrene is coordinated with rhodium.

The “step 2” and “step 4” molecules in table 1 have distorted square planar geometries. These geometries are somewhere in between a perfect square planar and a perfect tetrahedral geometry.

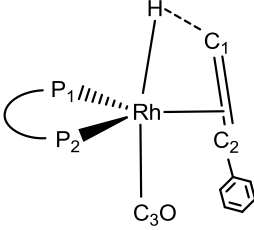
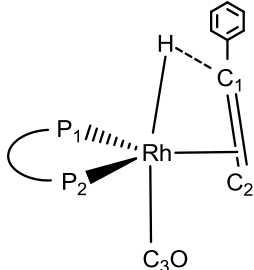
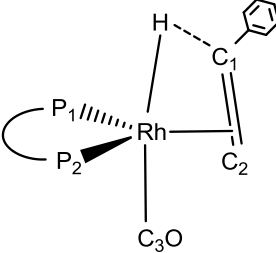
The “step 3” and the “side step” geometries (3brS2, 3brR2, 3li3, sbrS2, sbrR2 and sli2 molecules) have the (*R*)-BINAP in equatorial-axial position.

In the “step 5” geometries (5brS8, 5brR8 and 5li8 molecules), the acyl group (-COR) is opposite to one of the phosphorus atoms of (*R*)-BINAP. The carbonyl is opposite to one of the hydrides. The hydrides are mutually adjacent (*cis*). Geometric isomers having mutually opposite hydrides (*trans*) were unstable than those having mutually adjacent hydrides.

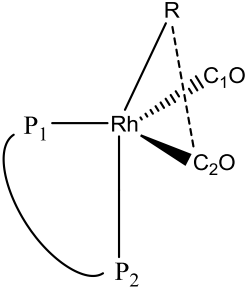
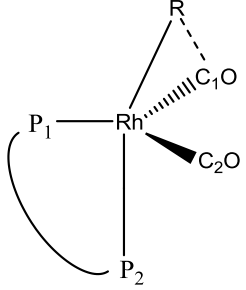
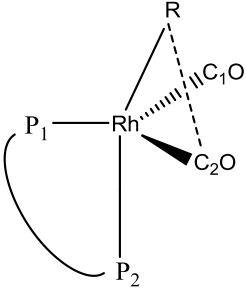
The following table 2 describes the optimized geometries of the various transition states in the three parallel catalytic cycles:

Table 2: Description of optimized geometries of transition states (Heck and Breslow mechanism)

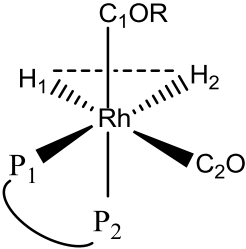
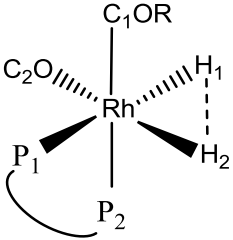
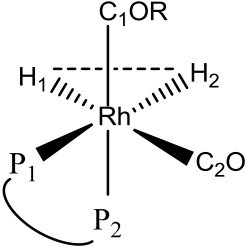
| Code of the transition state | Positions of the core atoms | Transition state belongs to the catalytic cycle that gives rise to: | Description of geometry |
|--|-----------------------------|---|---|
| <i>Transition state 1 (styrene insertion in the Rh-H bond)</i> | | | |
| SbTS1 | | (<i>S</i>)-2-phenylpropanal | P ₁ -Rh-P ₂ bite angle = 98.0° H-Rh-C ₂ -C ₁ dihedral = 28.9° H-C ₁ distance = 1.61 Å C ₁ -C ₂ distance = 1.44 Å |
| SbTS1o | | (<i>S</i>)-2-phenylpropanal | P ₁ -Rh-P ₂ bite angle = 96.2° H-Rh-C ₂ -C ₁ dihedral = -22.5° H-C ₁ distance = 1.63 Å C ₁ -C ₂ distance = 1.43 Å |
| RbTS1 | | (<i>R</i>)-2-phenylpropanal | P ₁ -Rh-P ₂ bite angle = 97.5° H-Rh-C ₂ -C ₁ dihedral = 27.2° H-C ₁ distance = 1.60 Å C ₁ -C ₂ distance = 1.43 Å |

| Code of the transition state | Positions of the core atoms | Transition state belongs to the catalytic cycle that gives rise to: | Description of geometry |
|------------------------------|--|---|---|
| RbTS1o |  | (R)-2-phenylpropanal | $P_1\text{-Rh-}P_2$ bite angle = 94.9° $\text{H-Rh-C}_2\text{-C}_1$ dihedral = -29.3° H-C_1 distance = 1.62 \AA $\text{C}_1\text{-C}_2$ distance = 1.44 \AA |
| SITS1 |  | 3-phenylpropanal | $P_1\text{-Rh-}P_2$ bite angle = 97.7° $\text{H-Rh-C}_2\text{-C}_1$ dihedral = 24.6° H-C_1 distance = 1.63 \AA $\text{C}_1\text{-C}_2$ distance = 1.44 \AA |
| SITS1o |  | 3-phenylpropanal | $P_1\text{-Rh-}P_2$ bite angle = 93.7° $\text{H-Rh-C}_2\text{-C}_1$ dihedral = -24.5° H-C_1 distance = 1.61 \AA $\text{C}_1\text{-C}_2$ distance = 1.44 \AA |

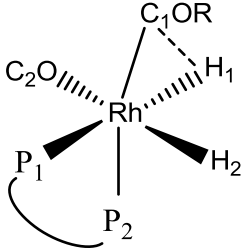
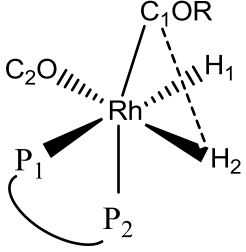
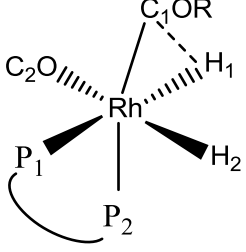
| Code of the transition state | Positions of the core atoms | Transition state belongs to the catalytic cycle that gives rise to: | Description of geometry |
|---|-----------------------------|---|---|
| RITS1 | | 3-phenylpropanal | $P_1\text{-Rh-}P_2$ bite angle = 93.6° $\text{H-Rh-C}_2\text{-C}_1$ dihedral = 23.6° H-C_1 distance = 1.64 \AA $\text{C}_1\text{-C}_2$ distance = 1.44 \AA |
| RITS1o | | 3-phenylpropanal | $P_1\text{-Rh-}P_2$ bite angle = 93.6° $\text{H-Rh-C}_2\text{-C}_1$ dihedral = -31.2° H-C_1 distance = 1.59 \AA $\text{C}_1\text{-C}_2$ distance = 1.44 \AA |
| Transition state 2 (carbonyl insertion in Rh-R bond) | | | |
| STS2 | | (S)-2-phenylpropanal | $P_1\text{-Rh-}P_2$ bite angle = 99.6° $P_1\text{-Rh-R}$ angle = 109.6° Rh-C(-R) distance = 2.68 \AA Rh-C_1 distance = 1.89 \AA Rh-C_2 distance = 1.95 \AA C_1O inserts in Rh-R bond |

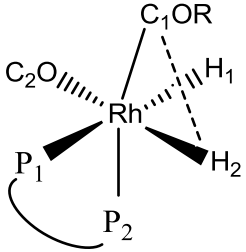
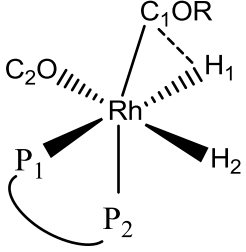
| Code of the transition state | Positions of the core atoms | Transition state belongs to the catalytic cycle that gives rise to: | Description of geometry |
|------------------------------|---|---|--|
| STS2o |  | (S)-2-phenylpropanal | P ₁ -Rh-P ₂ bite angle = 95.9° P ₁ -Rh-R angle = 106.8° Rh-C(-R) distance = 2.53 Å Rh-C ₁ distance = 1.93 Å Rh-C ₂ distance = 1.89 Å C ₂ O inserts in Rh-R bond |
| RTS2 |  | (R)-2-phenylpropanal | P ₁ -Rh-P ₂ bite angle = 97.1° P ₁ -Rh-R angle = 111.0° Rh-C(-R) distance = 2.52 Å Rh-C ₁ distance = 1.89 Å Rh-C ₂ distance = 1.94 Å C ₁ O inserts in Rh-R bond |
| RTS2o |  | (R)-2-phenylpropanal | P ₁ -Rh-P ₂ bite angle = 94.9° P ₁ -Rh-R angle = 109.1° Rh-C(-R) distance = 2.54 Å Rh-C ₁ distance = 1.93 Å Rh-C ₂ distance = 1.89 Å C ₂ O inserts in Rh-R bond |

| Code of the transition state | Positions of the core atoms | Transition state belongs to the catalytic cycle that gives rise to: | Description of geometry |
|--|-----------------------------|---|---|
| ITS2 | | 3-phenylpropanal | $P_1\text{-Rh-P}_2$ bite angle = 93.5° $P_1\text{-Rh-R}$ angle = 102.0° Rh-C(-R) distance = 2.40 \AA Rh-C_1 distance = 1.87 \AA Rh-C_2 distance = 1.95 \AA C_1O inserts in Rh-R bond |
| ITS2o | | 3-phenylpropanal | $P_1\text{-Rh-P}_2$ bite angle = 93.3° $P_1\text{-Rh-R}$ angle = 101.9° Rh-C(-R) distance = 2.41 \AA Rh-C_1 distance = 1.94 \AA Rh-C_2 distance = 1.88 \AA C_2O inserts in Rh-R bond |
| Transition state 3 (oxidative addition of hydrogen) | | | |
| STS3 | | (S)-2-phenylpropanal | $P_1\text{-Rh-P}_2$ bite angle = 91.4° Rh-H_1 distance = 1.65 \AA Rh-H_2 distance = 1.69 \AA $\text{H}_1\text{-H}_2$ distance = 1.07 \AA |

| Code of the transition state | Positions of the core atoms | Transition state belongs to the catalytic cycle that gives rise to: | Description of geometry |
|------------------------------|--|---|--|
| STS3o |  | (S)-2-phenylpropanal | P ₁ -Rh-P ₂ bite angle = 90.4° Rh-H ₁ distance = 1.68 Å Rh-H ₂ distance = 1.65 Å H ₁ -H ₂ distance = 1.09 Å |
| RTS3 |  | (R)-2-phenylpropanal | P ₁ -Rh-P ₂ bite angle = 91.4° Rh-H ₁ distance = 1.65 Å Rh-H ₂ distance = 1.69 Å H ₁ -H ₂ distance = 1.09 Å |
| RTS3o |  | (R)-2-phenylpropanal | P ₁ -Rh-P ₂ bite angle = 90.4° Rh-H ₁ distance = 1.68 Å Rh-H ₂ distance = 1.65 Å H ₁ -H ₂ distance = 1.07 Å |

| Code of the transition state | Positions of the core atoms | Transition state belongs to the catalytic cycle that gives rise to: | Description of geometry |
|---|-----------------------------|---|--|
| ITS3 | | 3-phenylpropanal | P_1 -Rh- P_2 bite angle = 91.9° Rh-H ₁ distance = 1.64 Å Rh-H ₂ distance = 1.67 Å H ₁ -H ₂ distance = 1.13 Å |
| ITS3o | | 3-phenylpropanal | P_1 -Rh- P_2 bite angle = 90.9° Rh-H ₁ distance = 1.68 Å Rh-H ₂ distance = 1.65 Å H ₁ -H ₂ distance = 1.06 Å |
| <i>Transition state 4 (reductive elimination of aldehyde)</i> | | | |
| STS4 | | (S)-2-phenylpropanal | P_1 -Rh- P_2 bite angle = 92.9° P_2 -Rh-C ₁ angle = 138.2° Rh-H ₁ distance = 1.59 Å Rh-H ₂ distance = 1.72 Å H ₂ combines with C ₁ OR |

| Code of the transition state | Positions of the core atoms | Transition state belongs to the catalytic cycle that gives rise to: | Description of geometry |
|------------------------------|--|---|--|
| STS4o |  | (S)-2-phenylpropanal | P ₁ -Rh-P ₂ bite angle = 99.1° P ₂ -Rh-C ₁ angle = 144.8° Rh-H ₁ distance = 1.71 Å Rh-H ₂ distance = 1.60 Å H ₁ combines with C ₁ OR |
| RTS4 |  | (R)-2-phenylpropanal | P ₁ -Rh-P ₂ bite angle = 92.8° P ₂ -Rh-C ₁ angle = 139.0° Rh-H ₁ distance = 1.59 Å Rh-H ₂ distance = 1.72 Å H ₂ combines with C ₁ OR |
| RTS4o |  | (R)-2-phenylpropanal | P ₁ -Rh-P ₂ bite angle = 99.3° P ₂ -Rh-C ₁ angle = 141.3° Rh-H ₁ distance = 1.71 Å Rh-H ₂ distance = 1.60 Å H ₁ combines with C ₁ OR |

| Code of the transition state | Positions of the core atoms | Transition state belongs to the catalytic cycle that gives rise to: | Description of geometry |
|------------------------------|---|---|--|
| ITS4 |  <p>The diagram shows a central Rhodium (Rh) atom coordinated to two phosphorus atoms (P1 and P2) in a bidentate fashion. P1 is on the left and P2 is at the bottom. The Rh atom is also coordinated to a carbonyl oxygen (C1OR) at the top, a carbonyl oxygen (C2O) on the left, and two hydrogens (H1 and H2) on the right. H1 is shown with a dashed bond to Rh, while H2 is shown with a solid wedge bond. A curved arrow indicates the interaction between H2 and C1OR.</p> | 3-phenylpropanal | P ₁ -Rh-P ₂ bite angle = 92.9° P ₂ -Rh-C ₁ angle = 137.2° Rh-H ₁ distance = 1.59 Å Rh-H ₂ distance = 1.72 Å H ₂ combines with C ₁ OR |
| ITS4o |  <p>The diagram shows a central Rhodium (Rh) atom coordinated to two phosphorus atoms (P1 and P2) in a bidentate fashion. P1 is on the left and P2 is at the bottom. The Rh atom is also coordinated to a carbonyl oxygen (C1OR) at the top, a carbonyl oxygen (C2O) on the left, and two hydrogens (H1 and H2) on the right. H1 is shown with a dashed bond to Rh, while H2 is shown with a solid wedge bond. A curved arrow indicates the interaction between H1 and C1OR.</p> | 3-phenylpropanal | P ₁ -Rh-P ₂ bite angle = 98.9° P ₂ -Rh-C ₁ angle = 141.8° Rh-H ₁ distance = 1.72 Å Rh-H ₂ distance = 1.60 Å H ₁ combines with C ₁ OR |

In table 2, the “transition state 1” (TS1) geometries show that one of the carbons from the carbon-carbon double bond in styrene, moves out of the equatorial plane, and approaches the hydride. If the carbon attached to the phenyl ring in styrene approaches the hydride (SITS1, SITS1o, RITS1 and RITS1o), 3-phenylpropanal is formed. Else 2-phenylpropanal is formed. Transition states SbTS1, SbTS1o, SITS1 and SITS1o are formed when the si-face of styrene is towards the rhodium. Transition states RbTS1, RbTS1o, RITS1 and RITS1o are formed when the re-face of styrene is towards the rhodium. SbTS1 and SbTS1o give rise to (*S*)-2-phenylpropanal. SbTS1o has less free energy than SbTS1. RbTS1 and RbTS1o give rise to (*R*)-2-phenylpropanal. RbTS1o has less free energy than RbTS1. SITS1, SITS1o, RITS1 and RITS1o give rise to 3-phenylpropanal. RITS1 has less free energy than SITS1, SITS1o and RITS1o.

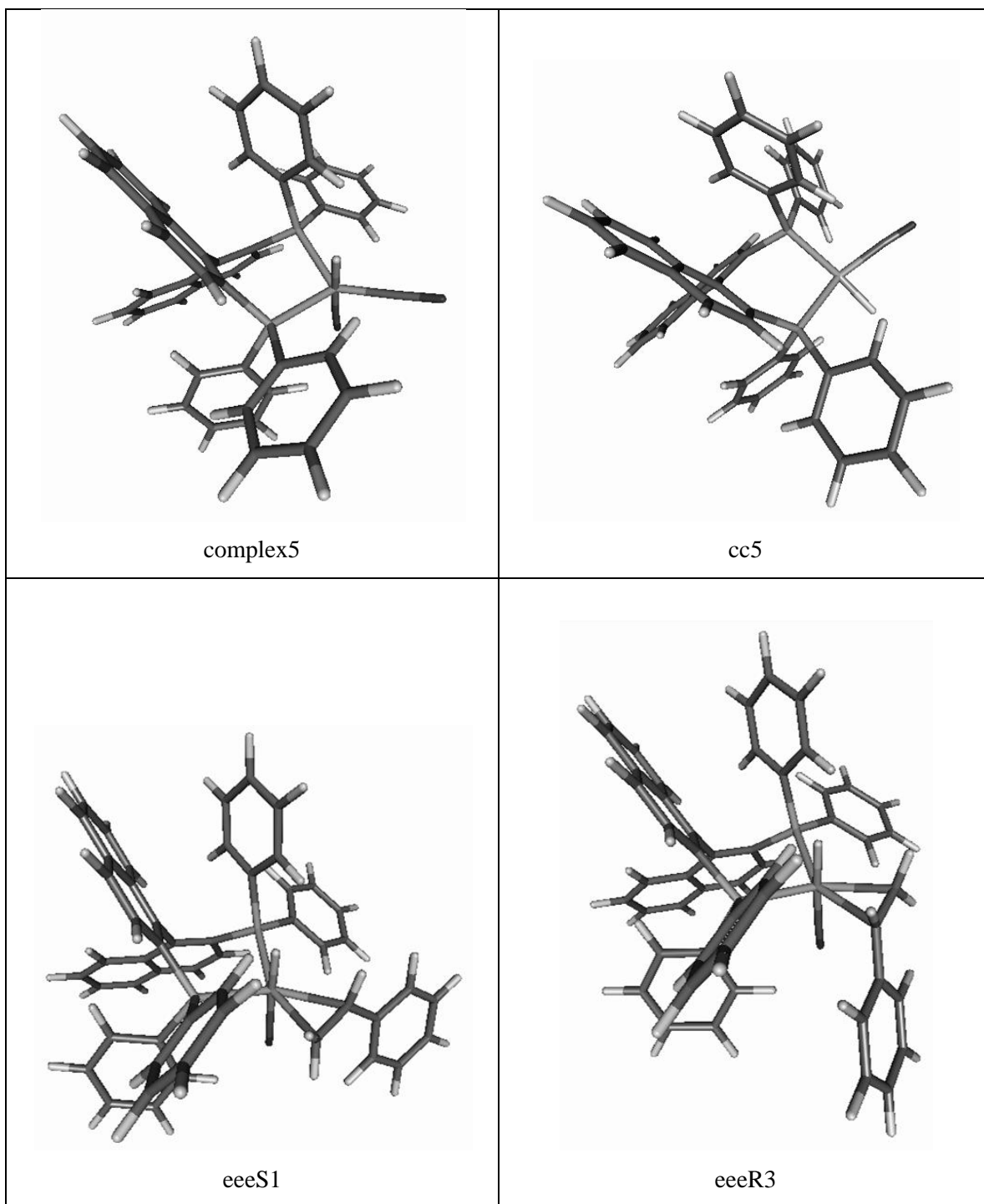
In case of “transition state 2” (TS2) geometries, STS2o has less free energy than STS2. RTS2 has less free energy than RTS2o. ITS2 has less free energy than ITS2o.

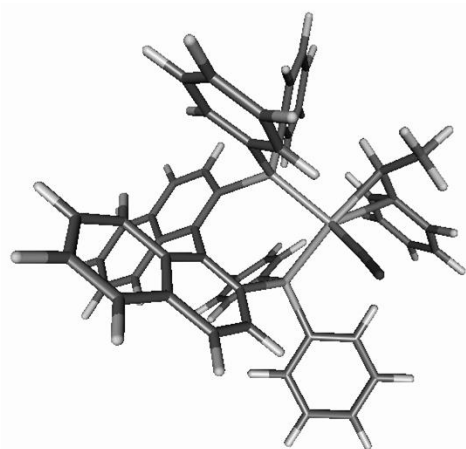
In case of “transition state 3” (TS3) geometries, STS3 has less free energy than STS3o. RTS3o has less free energy than RTS3. ITS3o has less free energy than ITS3. In a free hydrogen gas molecule, the hydrogen-hydrogen bond distance is 0.75 Å. This distance increases to more than 1 Å in TS3 geometries.

In case of “transition state 4” (TS4) geometries, STS4o has less free energy than STS4. RTS4 has less free energy than RTS4o. ITS4o has less free energy than ITS4.

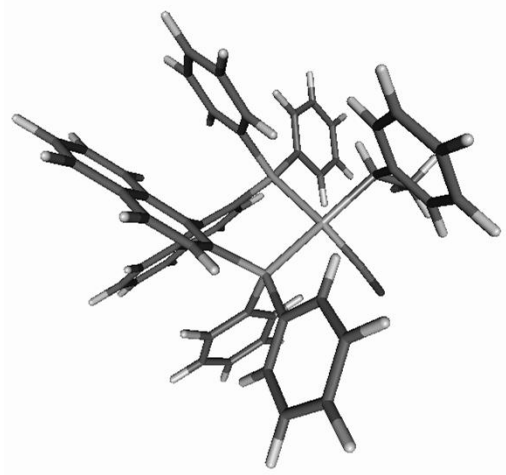
The following table 3 shows the optimized structures of the molecules listed in table 1 and table 2:

Table 3: Structures of molecules described in table 1 and table 2

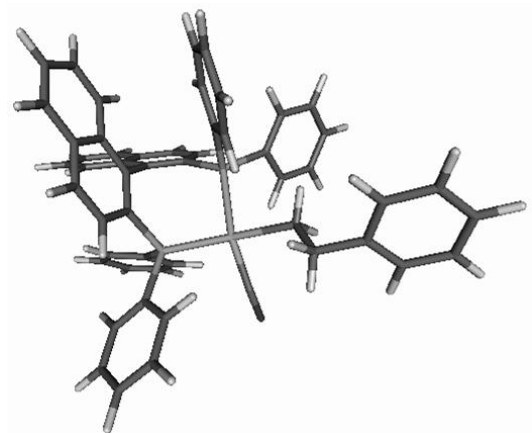




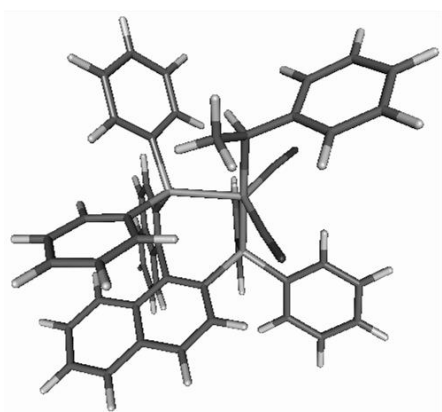
2brS6



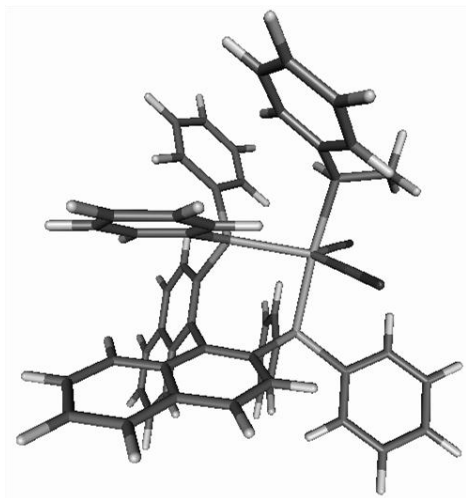
2brR1



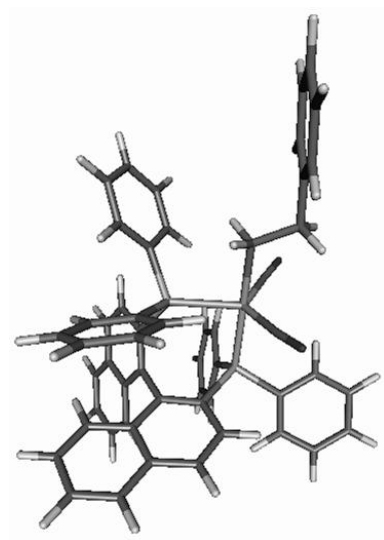
2li3



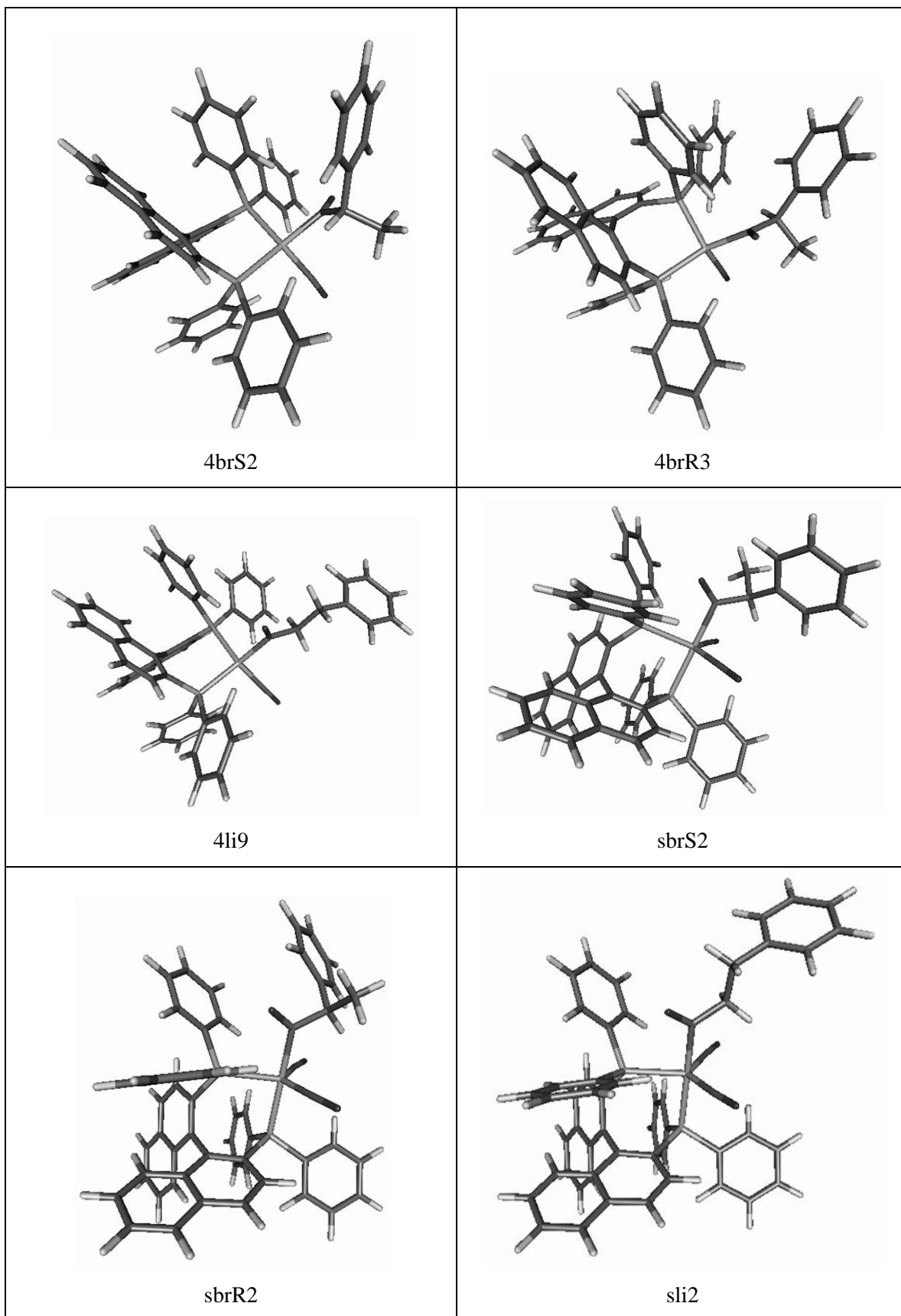
3brS2

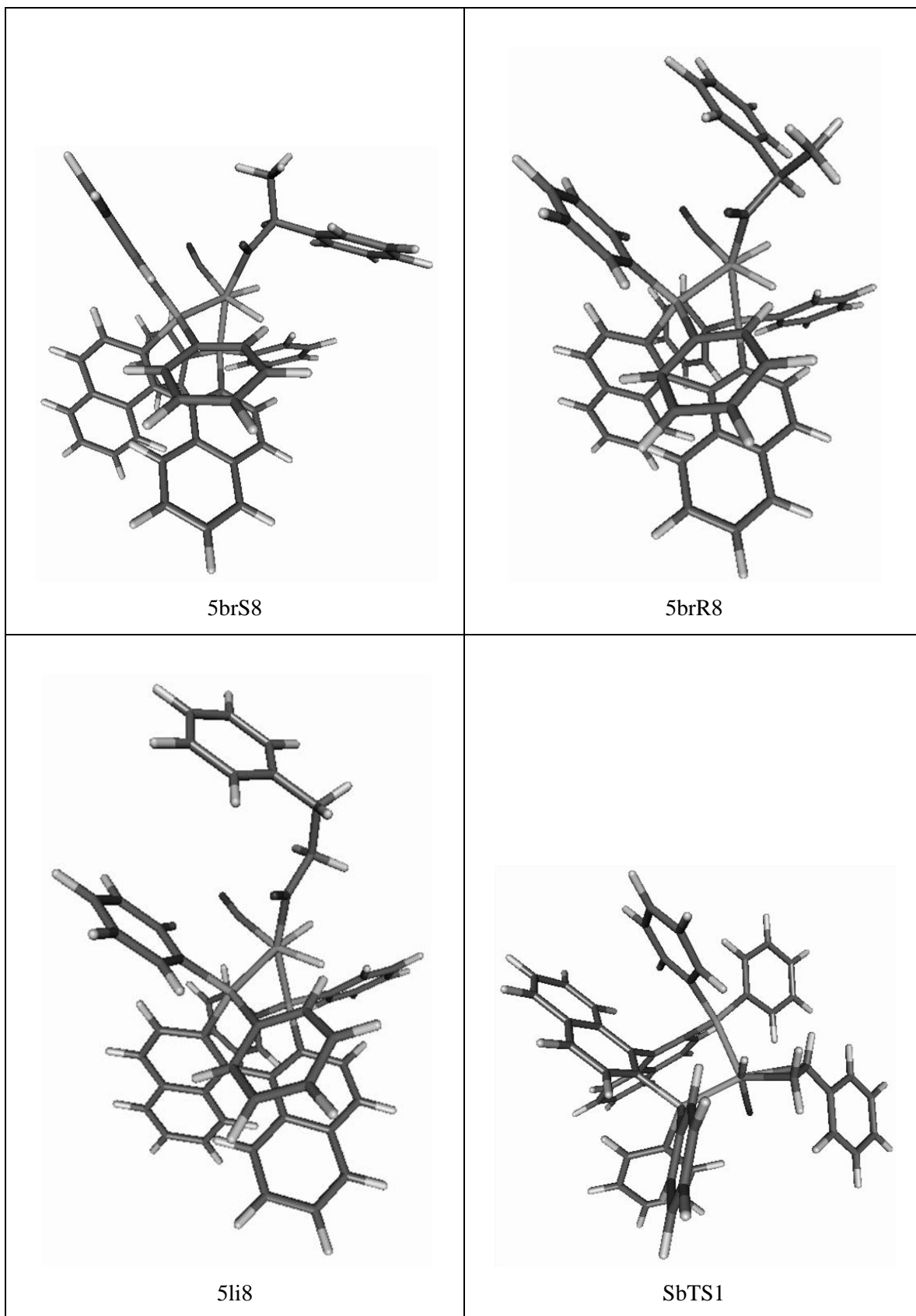


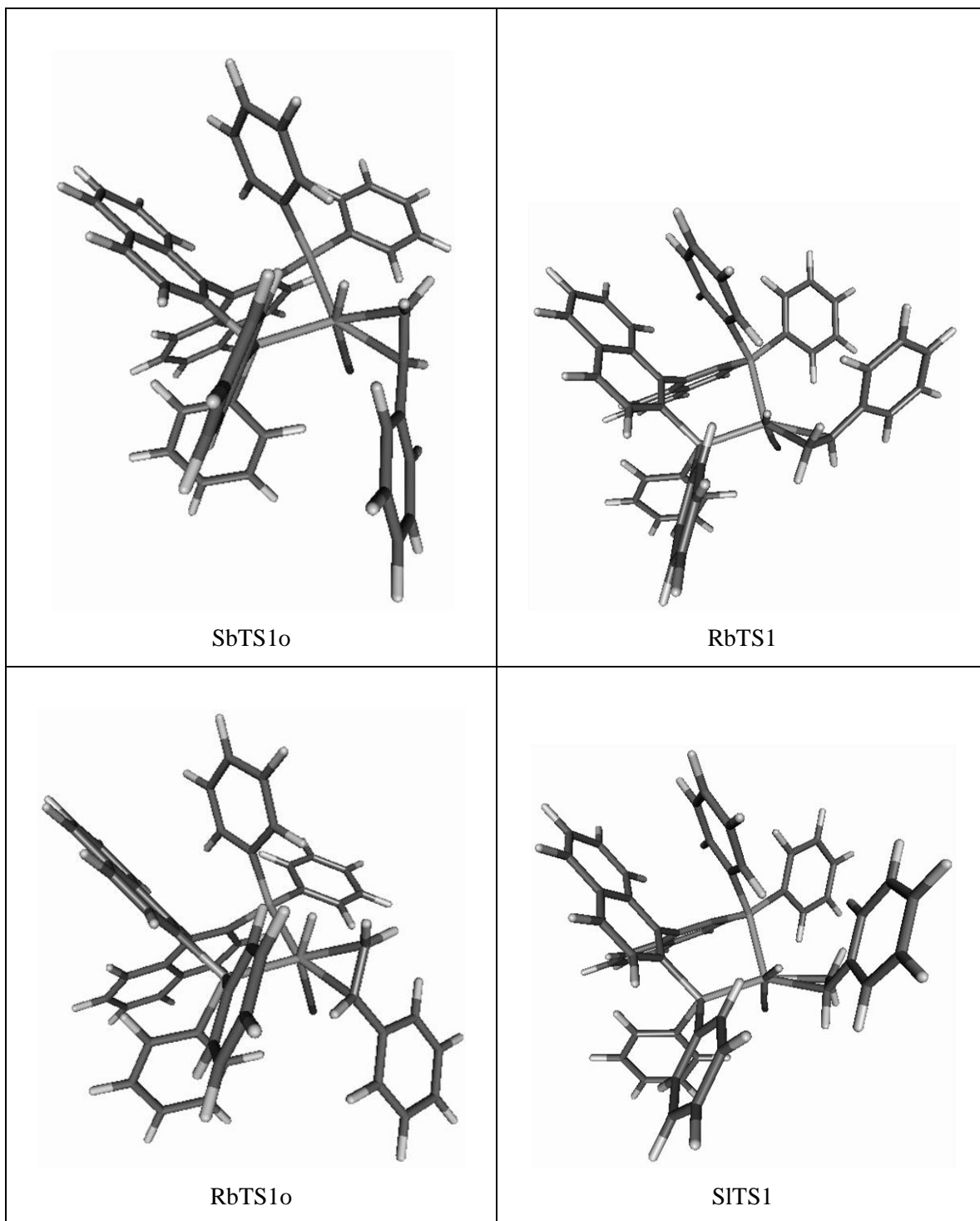
3brR2

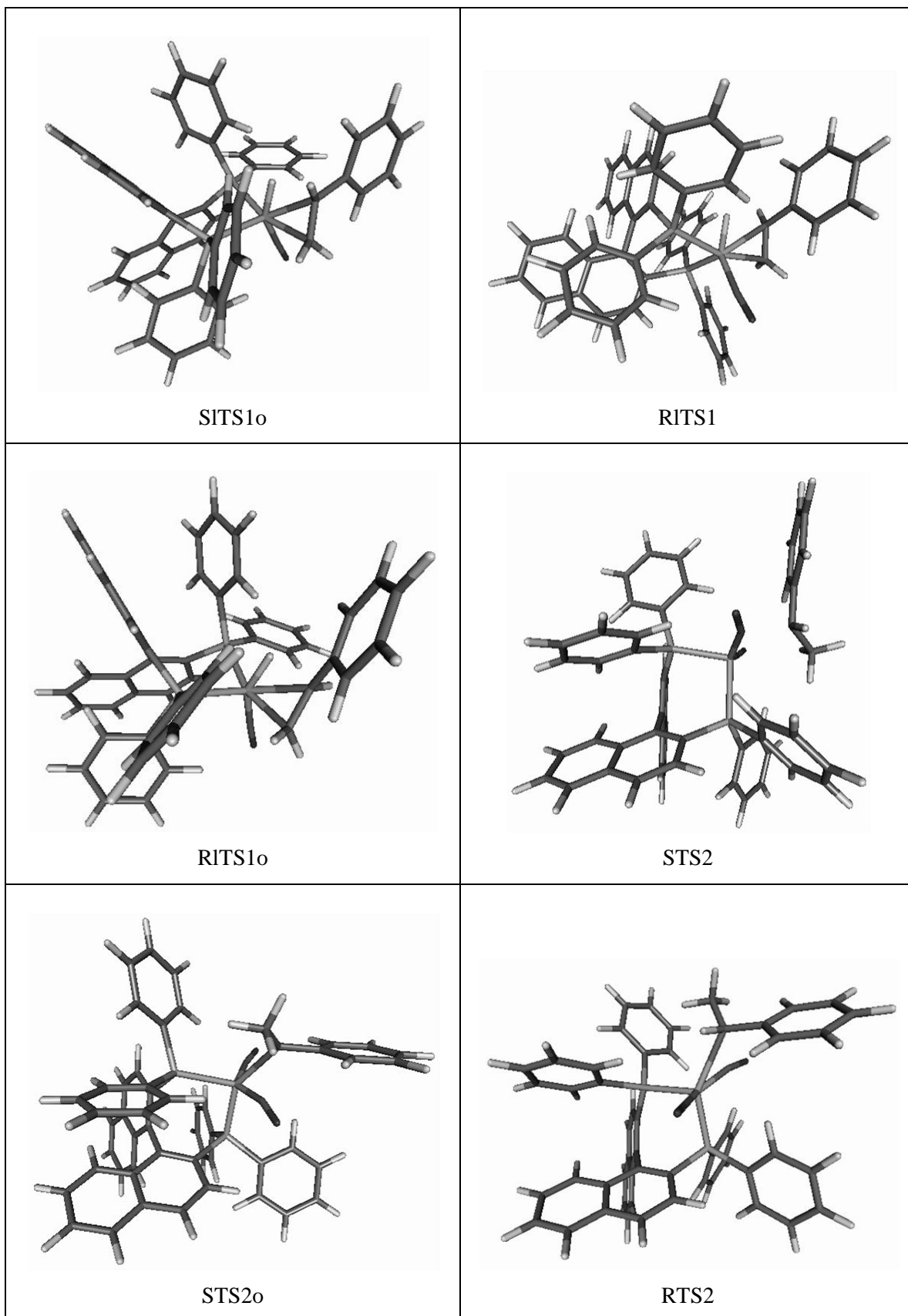


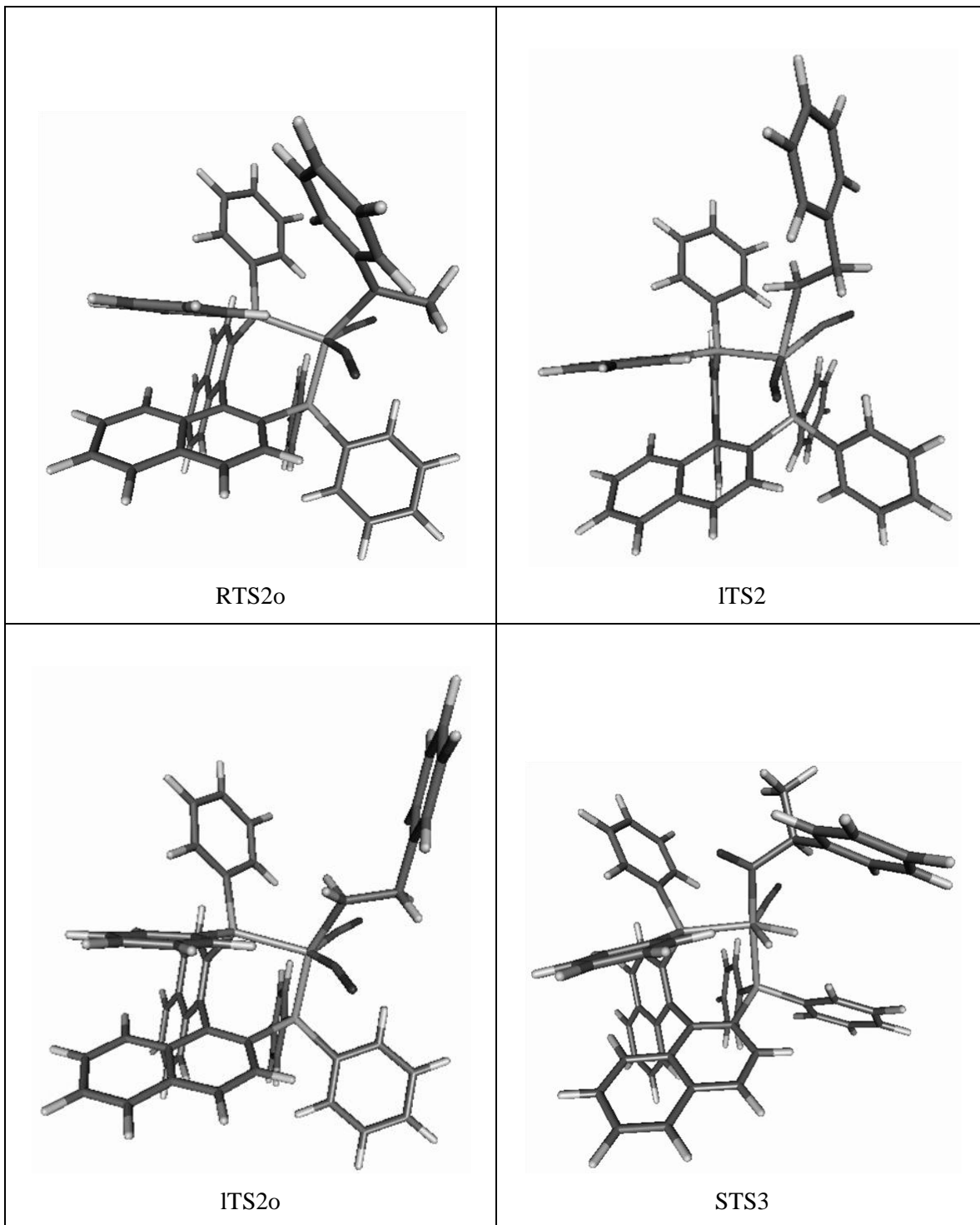
3li3

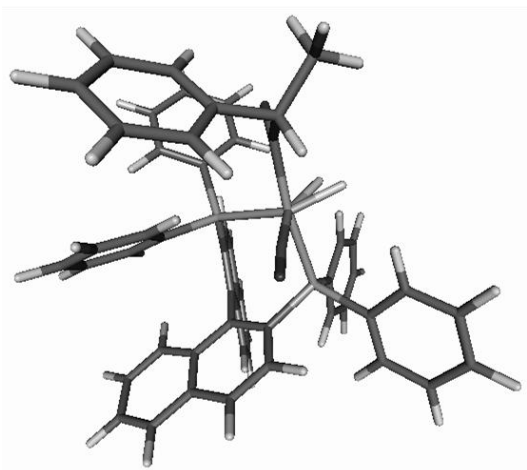




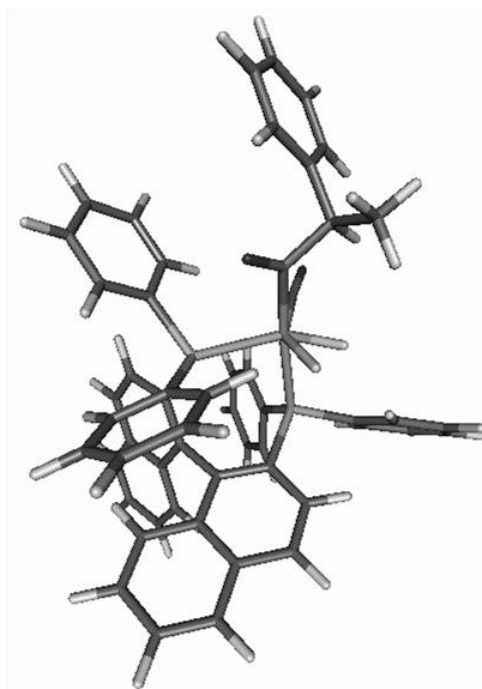




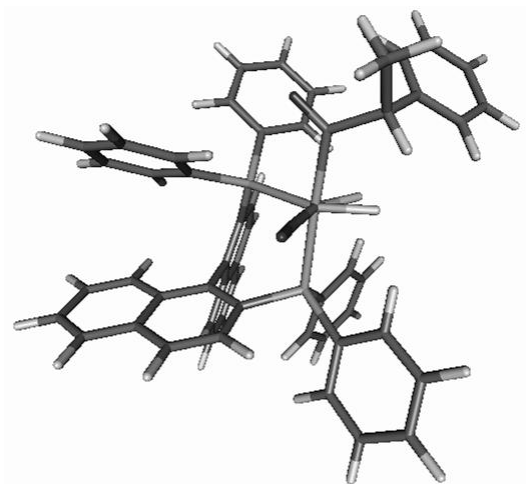




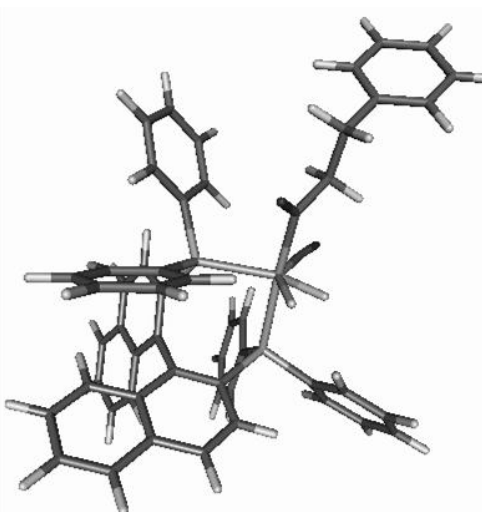
STS3o



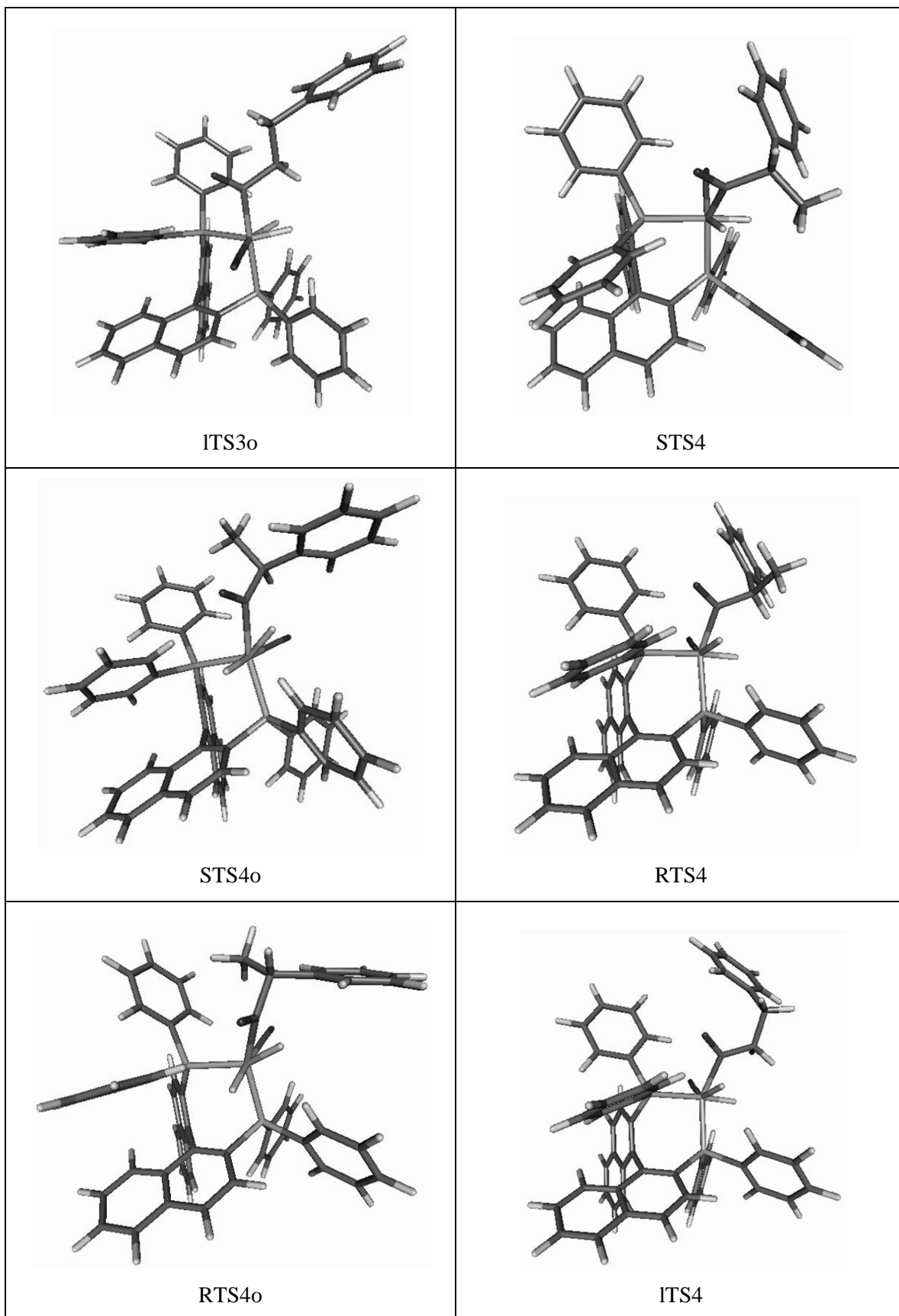
RTS3

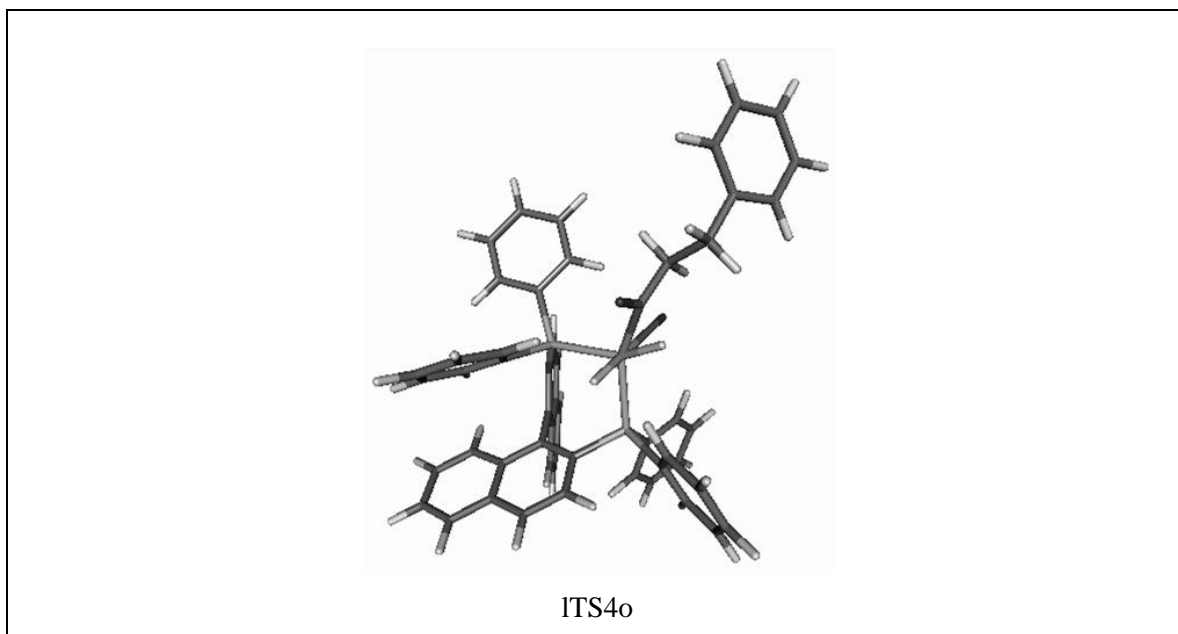


RTS3o



ITS3





3.3.2.1 Energy profile of the catalytic cycle (Heck and Breslow mechanism): In each of the three catalytic cycles giving rise to the three aldehyde products, molecules having the lowest free energies (both the stable molecules in every step and the transition states) were chosen and free energy profiles were plotted.

The free energy profile (gas phase) for formation of (*S*)-2-phenylpropanal at 60 °C (333 K) is as follows:

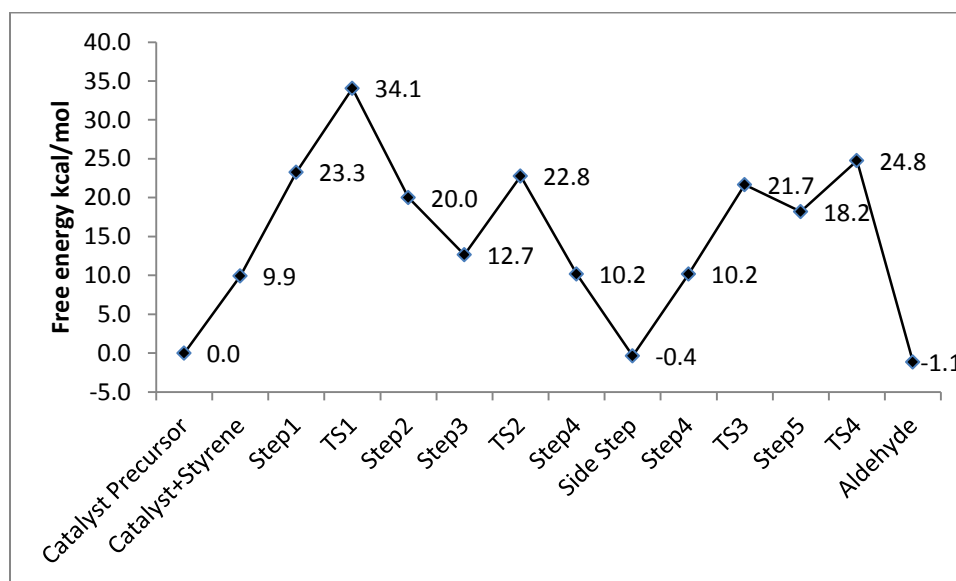


Figure 8: Free energy profile (gas phase) for formation of (*S*)-2-phenylpropanal

The free energy profile (gas phase) for formation of (*R*)-2-phenylpropanal at 60 °C (333 K) is as follows:

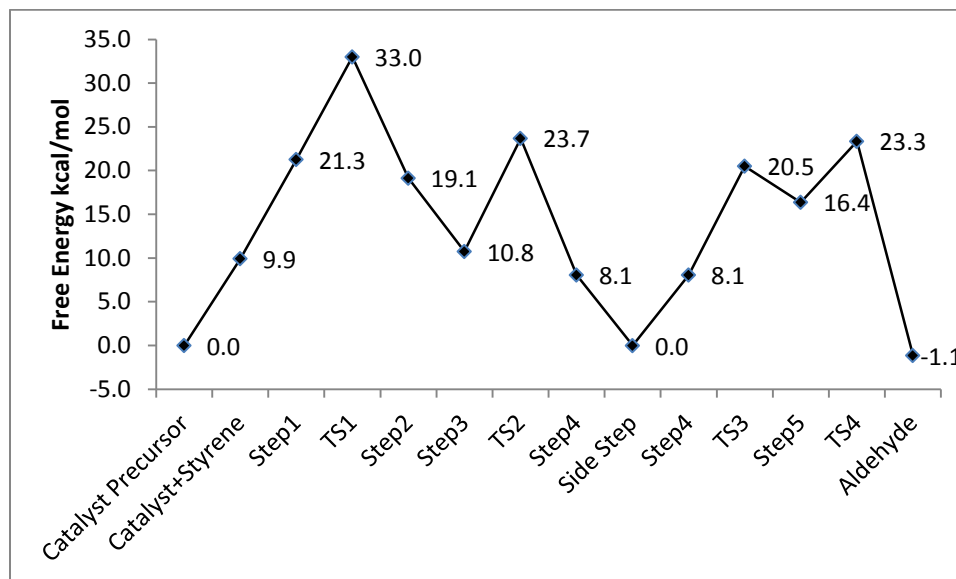


Figure 9: Free energy profile (gas phase) for formation of (*R*)-2-phenylpropanal

The free energy profile (gas phase) for formation of 3-phenylpropanal at 60 °C (333 K) is as follows:

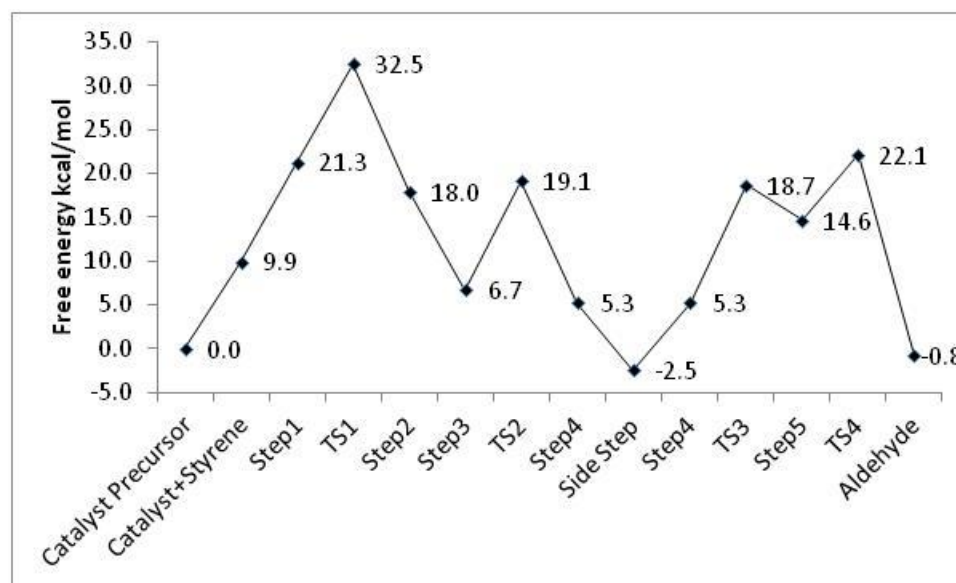


Figure 10: Free energy profile (gas phase) for formation of 3-phenylpropanal

As depicted in the free energy profiles (gas phase) for formation of the three aldehydes (Heck and Breslow mechanism), TS1 is the rate determining step (RDS). The activation energies are close to the one determined experimentally in chapter 2 (34.2 kcal/mol).

TS1 is also the step that determines the regioselectivity (b/l ratio) and the enantioselectivity (ee %).

When the energies of TS1 in the three profiles are compared, formation of 3-phenylpropanal has the lowest activation energy and formation of (*S*)-2-phenylpropanal has the highest activation energy. This means that the linear aldehyde should be formed in excess over the branched ones. Moreover the enantiomeric excess should be in favor of (*R*)-2-phenylpropanal. This is in contradiction to the experimental results in chapter 2 where (*S*)-2-phenylpropanal is formed in excess over (*R*)-2-phenylpropanal and the branched aldehydes are formed in excess over the linear one.

However the energy profiles described above are for gas phase calculations. To see if solvation makes any change in the activation energy trends for the formation of the three aldehydes, free energy profiles for solvated molecules (toluene solvent) were plotted.

The free energy profile (solvated) for formation of (*S*)-2-phenylpropanal at 60 °C (333 K) is as follows:

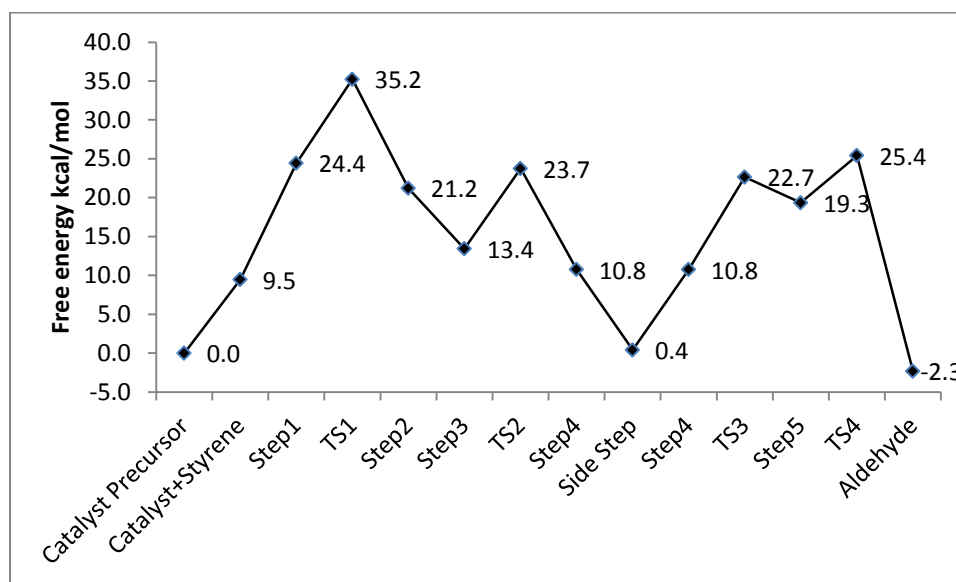


Figure 11: Free energy profile (solvated in toluene) for formation of (*S*)-2-phenylpropanal

The free energy profile (solvated) for formation of (*R*)-2-phenylpropanal at 60 °C (333 K) is as follows:

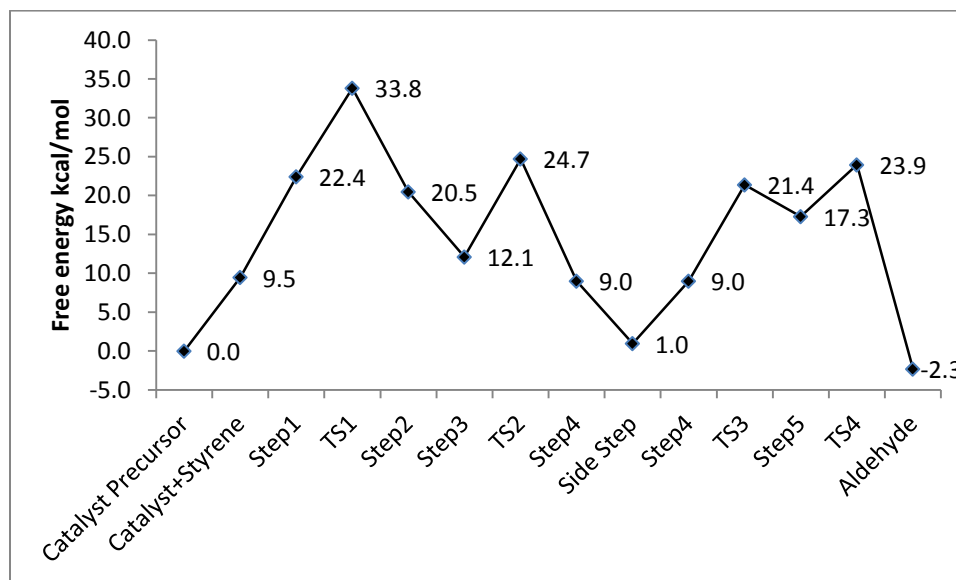


Figure 12: Free energy profile (solvated in toluene) for formation of (*R*)-2-phenylpropanal

The free energy profile (solvated) for formation of 3-phenylpropanal at 60 °C (333 K) is as follows:

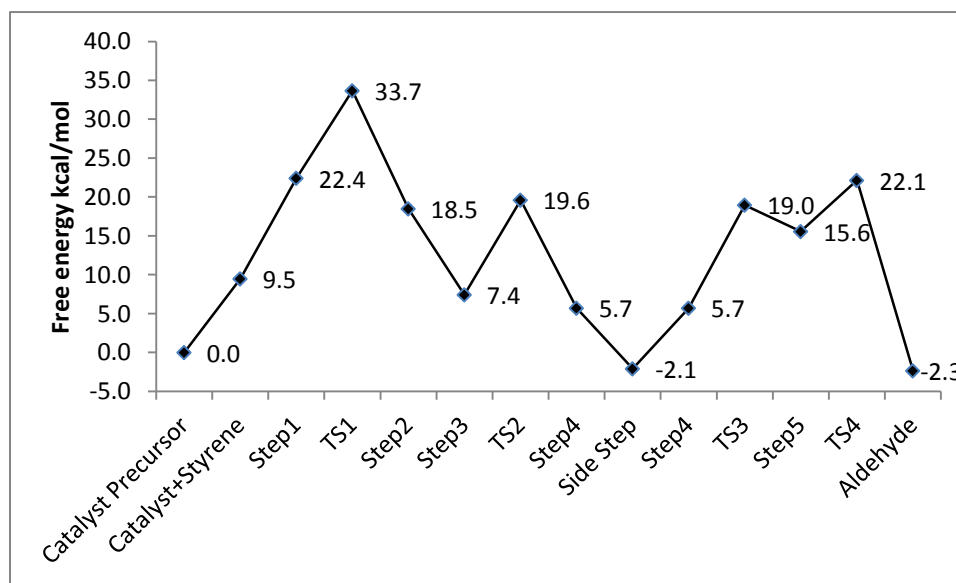


Figure 13: Free energy profile (solvated in toluene) for formation of 3-phenylpropanal

The free energy profiles (solvated) are almost identical to the gas phase free energy profiles. This indicated that solvation is not reversing the regioselectivity and enantioselectivity patterns of the gas phase calculations. This is because toluene is a non-polar solvent (dielectric constant of toluene is 2.379 at 25 °C).

So the question remained why the DFT calculations were giving results that are exactly opposite to experimental observations.

3.3.3 Finding the reasons for the anomalous results of the DFT calculations: There were many approximations and assumptions made while screening the molecules and calculating their free energies. The final results of any calculation can be only as good as the assumptions and approximations made while calculating.

So to find the reasons for the anomalous results of the DFT calculations, some of the assumptions and approximations were tested for their validity.

3.3.3.1 Testing the validity of the resolution of identity (RI) approximation: RI and MARI-*J* (multipole accelerated resolution of identity) approximations were used to speed up the DFT calculations.

SbTS1o, RbTS1o and RITS1 were the RDS for the formation of (*S*)-2-phenylpropanal, (*R*)-2-phenylpropanal and 3-phenylpropanal respectively. The gas phase free energies of SbTS1o, RbTS1o and RITS1 were 34.1 kcal/mol, 33.0 kcal/mol and 32.5 kcal/mol respectively, with the RI and the MARI-*J* approximations.

Without RI and MARI-*J*, the gas phase free energies of SbTS1o, RbTS1o and RITS1 were 34.1 kcal/mol, 33.0 kcal/mol and 32.4 kcal/mol respectively.

Thus the results of DFT calculations with RI and MARI-*J* were almost identical to those without RI and MARI-*J*.

3.3.3.2 Conformational search for the transition states: In the DFT calculations described above, conformational search was done only for the stable molecules and the transition states were derived from the stable molecules. The transition states themselves were not subjected to torsion angle driving because of the limitations of the HyperChem software.

To see if a conformational search can produce new transition state structures, the geometries of SbTS1o, RbTS1o and RITS1 were perturbed by rotating the phenyl ring on styrene by 90°. These perturbed structures were then subjected to transition state calculations. [The phenyl rings in the rhodium complexes tend to be at right angles to each other. So by perturbing the phenyl ring on styrene, one perturbs the phenyl rings on (*R*)-BINAP as well.]

At the end of the DFT calculations, it was found that the phenyl ring on styrene rotated back by 90° in each of the three cases. The final optimized geometries were identical to the geometries of SbTS1o, RbTS1o and RITS1.

3.3.3.3 Testing the validity of use of TZVP and def-TZVP basis sets: All the above DFT calculations were done using def-TZVP basis set for rhodium atom and TZVP basis set for all other atoms.

def-TZVP and TZVP are considered as high quality basis sets. The gas phase free energies of SbTS1o, RbTS1o and RITS1 were 34.1 kcal/mol, 33.0 kcal/mol and 32.5 kcal/mol respectively, with TZVP/ def-TZVP basis sets.

With def2-TZVP basis set (a basis set considered to be of higher quality than TZVP/ def-TZVP), the gas phase free energies of SbTS1o, RbTS1o and RITS1 were 34.0 kcal/mol, 33.0 kcal/mol and 32.4 kcal/mol respectively.

Thus increasing the quality of basis set did not change the final outcome of the DFT calculations.

3.3.3.4 Testing the validity of use of Becke-Perdew (b-p) functional: The free energies of SbTS1o, RbTS1o and RITS1 as depicted in the free energy profiles were calculated with b-p functional.

With Slater-Dirac exchange functional, the gas phase free energies of SbTS1o, RbTS1o and RITS1 were 34.3 kcal/mol, 33.3 kcal/mol and 32.6 kcal/mol respectively. With Perdew-Burke-Ernzerhof (PBE) ^[12] functional, the gas phase free energies were 34.2 kcal/mol, 33.1 kcal/mol and 32.4 kcal/mol respectively.

Thus use of different functional for DFT calculations did not change the free energy trend in the RDS of the three parallel catalytic cycles.

3.3.3.5 Testing the validity of use of DFT itself: Dispersion interactions are known to affect the accuracy of DFT calculations. To test whether dispersion interactions are important in the reaction system under study, the geometries of SbTS1o, RbTS1o and RITS1 were subjected to second order Møller–Plesset perturbation theory (MP2) ^[13] calculation (single point calculation).

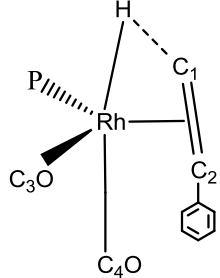
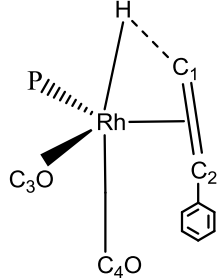
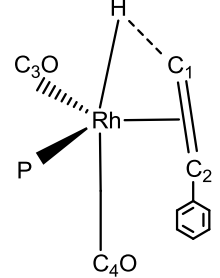
The trends of electronic energies given by MP2 calculations matched exactly with those given by DFT calculations. Thus the use of DFT was validated for the current study.

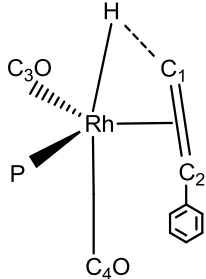
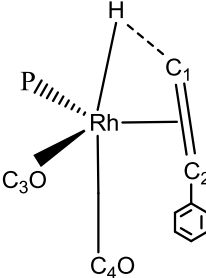
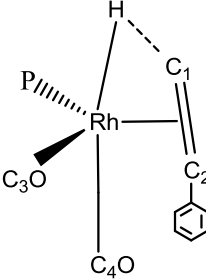
3.3.3.6 Testing the validity of the assumption that (*R*)-BINAP is a chelating ligand:

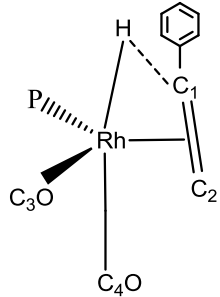
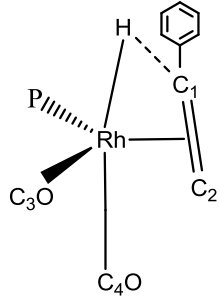
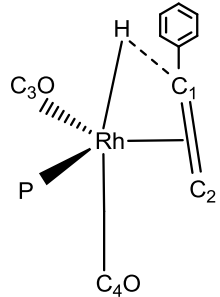
In all the calculations described till now, there was an implicit assumption that the bidentate ligand (*R*)-BINAP forms a chelate complex with rhodium. BINAP is also known to have monodentate coordination with metals ^[14]. The possibility of monodentate (*R*)-BINAP taking part in the rate determining step (styrene insertion in Rh-H bond) was tested.

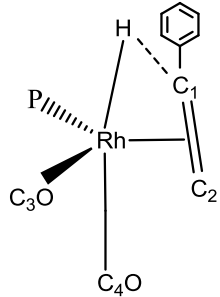
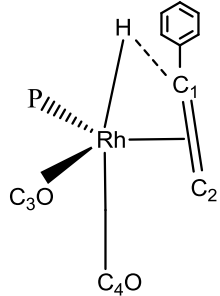
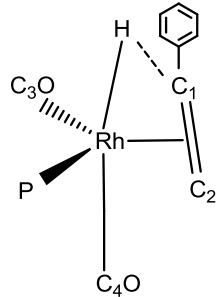
The following table 4 describes the optimized geometries of styrene insertion transition states with monodentate (*R*)-BINAP – rhodium catalyst:

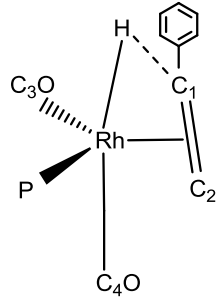
Table 4: Description of optimized geometries of styrene insertion transition states with monodentate (*R*)-BINAP – rhodium catalyst

| Code of transition state | Position of core atoms | Transition state belongs to the catalytic cycle that gives rise to: | Description of geometry |
|--------------------------|---|---|---|
| monoS11_b_TS1 |  | (S)-2-phenylpropanal | H-Rh-C ₂ -C ₁ dihedral = -20.1° H-C ₁ distance = 1.63 Å C ₁ -C ₂ distance = 1.42 Å |
| monoS12_b_TS1 |  | (S)-2-phenylpropanal | H-Rh-C ₂ -C ₁ dihedral = -10.1° H-C ₁ distance = 1.59 Å C ₁ -C ₂ distance = 1.42 Å |
| monoS21_b_TS1 |  | (S)-2-phenylpropanal | H-Rh-C ₂ -C ₁ dihedral = 32.0° H-C ₁ distance = 1.64 Å C ₁ -C ₂ distance = 1.43 Å |

| Code of transition state | Position of core atoms | Transition state belongs to the catalytic cycle that gives rise to: | Description of geometry |
|--------------------------|---|---|---|
| monoS22_b_TS1 |  | (S)-2-phenylpropanal | H-Rh-C ₂ -C ₁ dihedral = 31.9° H-C ₁ distance = 1.63 Å C ₁ -C ₂ distance = 1.44 Å |
| monoR11_b_TS1 |  | (R)-2-phenylpropanal | H-Rh-C ₂ -C ₁ dihedral = -33.4° H-C ₁ distance = 1.65 Å C ₁ -C ₂ distance = 1.44 Å |
| monoR12_b_TS1 |  | (R)-2-phenylpropanal | H-Rh-C ₂ -C ₁ dihedral = 7.7° H-C ₁ distance = 1.58 Å C ₁ -C ₂ distance = 1.42 Å |

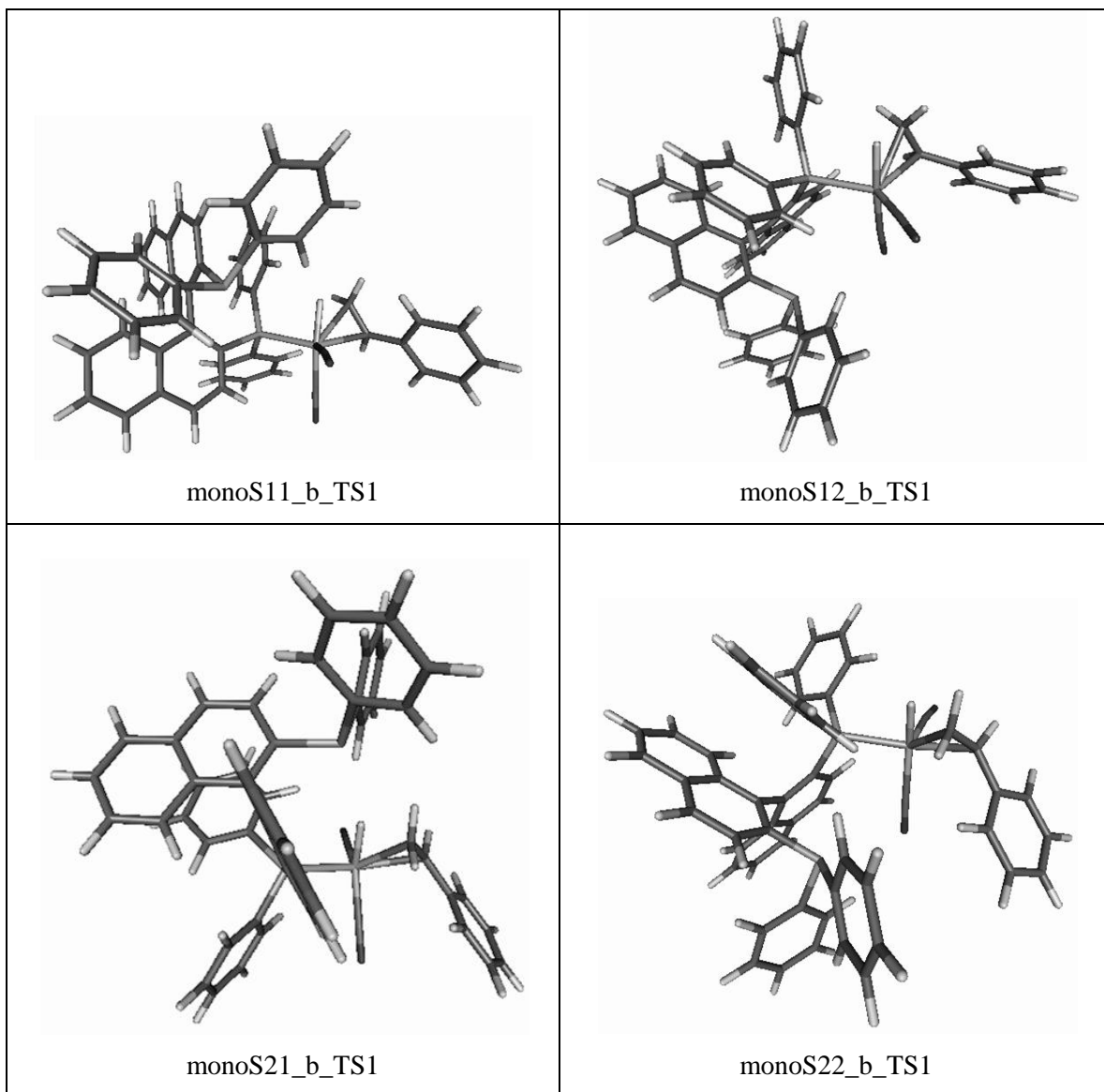
| Code of transition state | Position of core atoms | Transition state belongs to the catalytic cycle that gives rise to: | Description of geometry |
|--------------------------|---|---|--|
| monoR11_1_TS1 |  | 3-phenylpropanal | H-Rh-C ₂ -C ₁ dihedral = 22.6° H-C ₁ distance = 1.58 Å C ₁ -C ₂ distance = 1.44 Å |
| monoR12_1_TS1 |  | 3-phenylpropanal | H-Rh-C ₂ -C ₁ dihedral = 21.5° H-C ₁ distance = 1.62 Å C ₁ -C ₂ distance = 1.43 Å |
| monoR21_1_TS1 |  | 3-phenylpropanal | H-Rh-C ₂ -C ₁ dihedral = 23.1° H-C ₁ distance = 1.72 Å C ₁ -C ₂ distance = 1.43 Å |

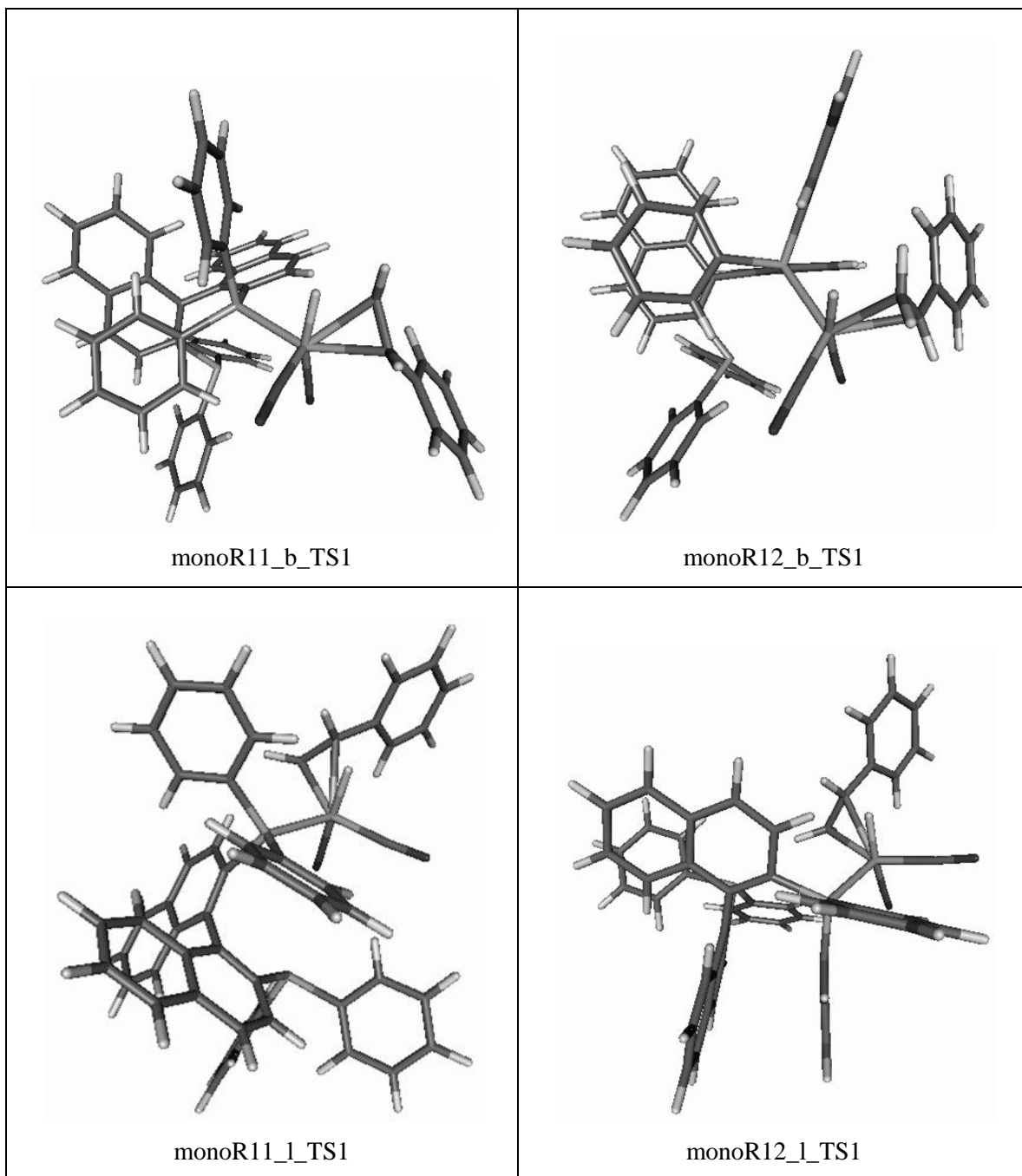
| Code of transition state | Position of core atoms | Transition state belongs to the catalytic cycle that gives rise to: | Description of geometry |
|--------------------------|---|---|---|
| monoS11_1_TS1 |  | 3-phenylpropanal | H-Rh-C ₂ -C ₁ dihedral = 31.0° H-C ₁ distance = 1.57 Å C ₁ -C ₂ distance = 1.44 Å |
| monoS12_1_TS1 |  | 3-phenylpropanal | H-Rh-C ₂ -C ₁ dihedral = 27.6° H-C ₁ distance = 1.64 Å C ₁ -C ₂ distance = 1.44 Å |
| monoS21_1_TS1 |  | 3-phenylpropanal | H-Rh-C ₂ -C ₁ dihedral = -23.9° H-C ₁ distance = 1.64 Å C ₁ -C ₂ distance = 1.44 Å |

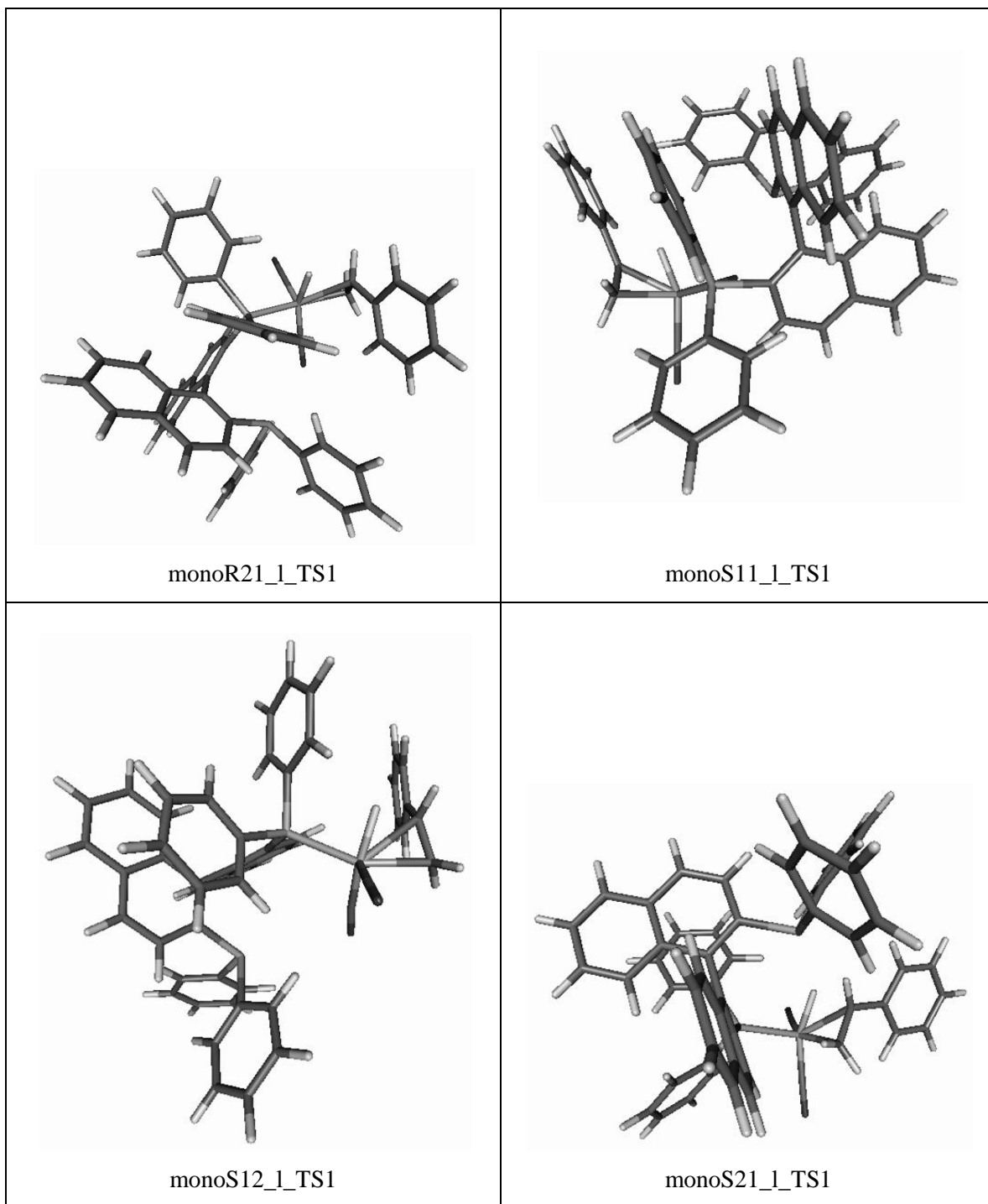
| Code of transition state | Position of core atoms | Transition state belongs to the catalytic cycle that gives rise to: | Description of geometry |
|--------------------------|---|---|---|
| monoS22_1_TS1 |  | 3-phenylpropanal | H-Rh-C ₂ -C ₁ dihedral = -14.6° H-C ₁ distance = 1.61 Å C ₁ -C ₂ distance = 1.43 Å |

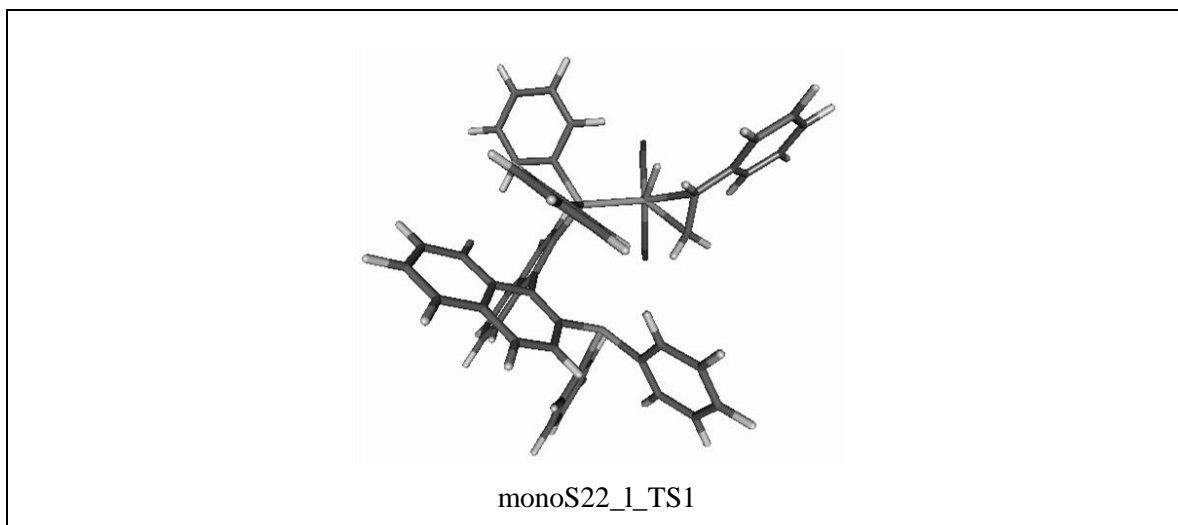
The following table 5 shows the optimized structures of the molecules listed in table 4:

Table 5: Structures of molecules described in table 4









It was found that the free energies of all transition states having monodentate (*R*)-BINAP were higher than the free energies of SbTS1o, RbTS1o and RITS1. Moreover the trends for the regio and the enantioselectivity given by the rhodium catalyst modified by monodentate (*R*)-BINAP were the same as that for chelating (*R*)-BINAP. Transition states with chelating (*R*)-BINAP had lower free energies because of the entropy effect [15].

Thus the possibility of monodentate (*R*)-BINAP taking part in the rate determining step (styrene insertion in Rh-H bond) was ruled out.

3.3.3.7 Testing the validity of use of Heck and Breslow mechanism: It was assumed that the reaction system under study followed the Heck and Breslow mechanism. To investigate the possibility of presence of alternate mechanisms, the process of formation of aldehyde from alkene was broken down into smaller steps.

Hydroformylation is addition of two hydrogen atoms and one carbonyl to an alkene. The Heck and Breslow mechanism can be broken down into three basic steps:

- Addition of the first hydrogen atom (to the alkene)
- Addition of carbonyl
- Addition of the second hydrogen atom (to form the aldehyde)

Any permutation of these three basic steps should give rise to the aldehyde from the alkene:

- Addition of the two hydrogen atoms followed by addition of carbonyl would mean that the alkene is first hydrogenated to alkane and thereafter the alkane is carbonylated to the aldehyde. However this possibility was ruled out because complete mass balance for intermediate samples was established in the experimental study (chapter 2).
- Addition of one of the carbonyls from $\text{HRh}(\text{CO})_2[(R)\text{-BINAP}]$ (the “catalyst precursor” from Heck and Breslow mechanism) to the alkene (to form a four membered ring) followed by the addition of the two hydrogen atoms can give rise to two distinct possibilities:

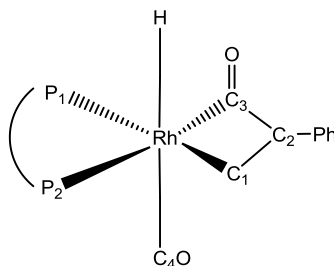


Figure 14: Complex that can be formed by insertion of styrene in the Rh-CO bond of $\text{HRh}(\text{CO})_2[(R)\text{-BINAP}]$

The first possibility is that the hydrogen on rhodium is added to C_3 and the Rh- C_3 bond is broken. The problem with this possible mechanism is that the complex so formed will give rise to a resting state (analogous to the “side step” in the Heck and Breslow mechanism), the structure similar to which has never been reported in any hydroformylation study.

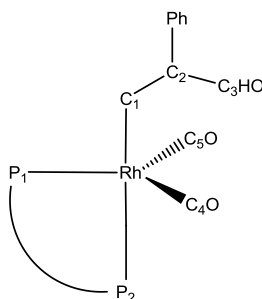


Figure 15: The structure of the "resting state" when H is added to C_3 in figure 14

- The second possibility is that the hydrogen on rhodium is added to C₁ and the Rh-C₁ bond (in figure 14) is broken. This possible mechanism will give rise to a resting state that is identical to the one found in the Heck and Breslow mechanism. The following figure gives a schematic representation of this possible mechanism (henceforth will be referred to as “mechanism 2”):

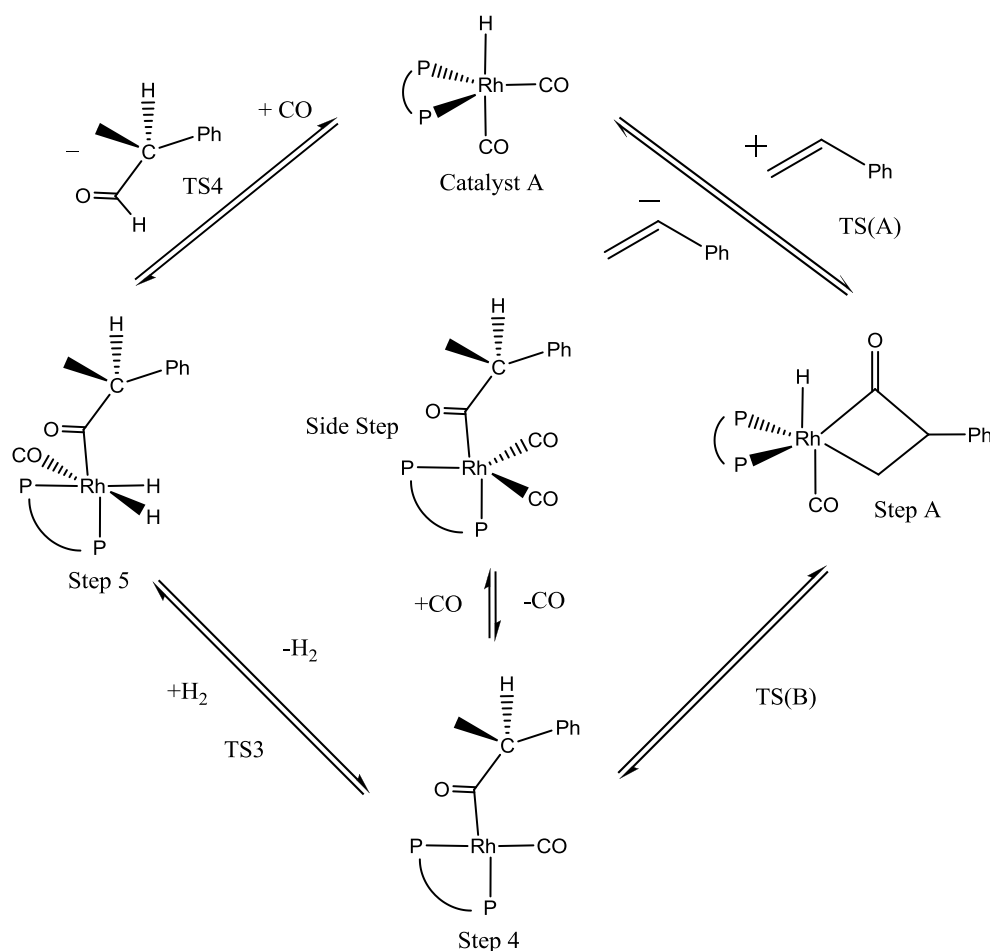


Figure 16: “Mechanism 2” for hydroformylation

The labels - “step 4”, “step 5”, “side step”, TS3 and TS4 have been borrowed from the Heck and Breslow mechanism. The only difference between the Heck and Breslow mechanism and the “mechanism 2” is the formation of “step A” and the transition states TS(A) and TS(B). The “catalyst precursor” in the Heck and Breslow mechanism is the active catalyst in “mechanism 2” and has been labeled as “catalyst A”.

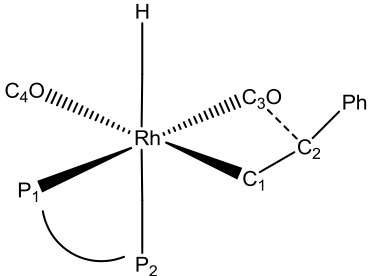
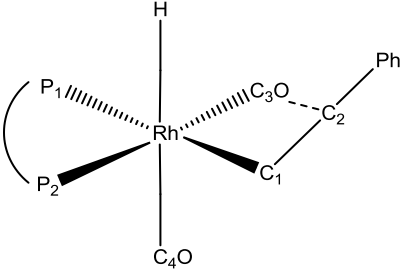
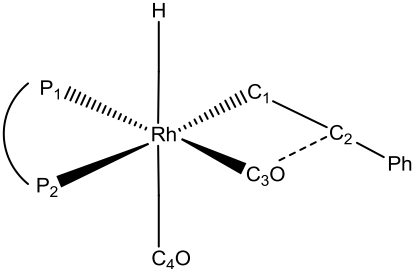
The “step A” geometry has never been reported in any literature on hydroformylation. But this could be justified by the fact that the carbonyl frequency of “step A” molecules (as calculated by the Hessian) match exactly with the carbonyl frequency of the corresponding aldehyde products. This means that “Step A” (or analogous) molecules would have possibly remained undetected in any *in situ* IR study^[16].

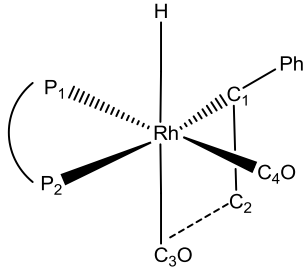
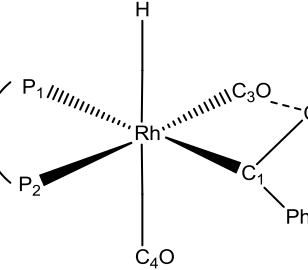
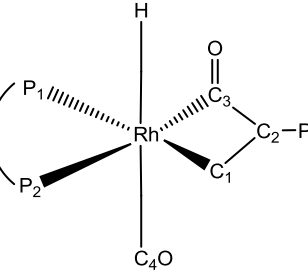
A computational study was done on the “mechanism 2”. The following table 6 describes the optimized geometries of TS(A), the lowest free energy “step A” molecules and TS(B) for all the three parallel catalytic cycles in “mechanism 2”:

Table 6: Description of optimized geometries of TS(A), the lowest free energy "step A" molecules and TS(B) in "mechanism 2"

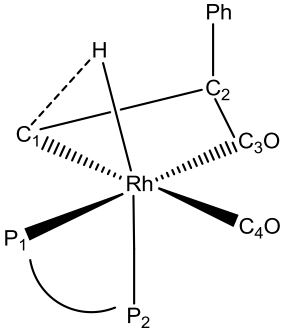
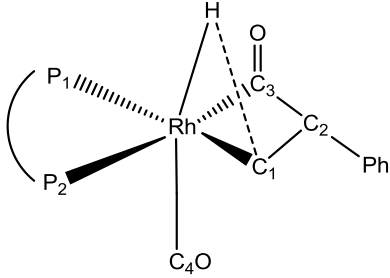
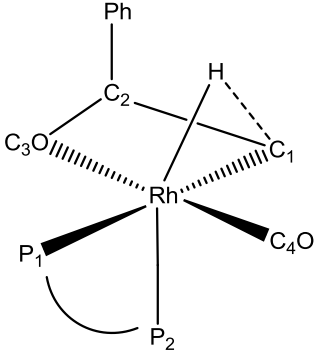
| Code of the complex molecule | Positions of core atoms | Metal complex belongs to the catalytic cycle that gives rise to: | Description of geometry |
|---------------------------------|-------------------------|--|---|
| <i>Transition state - TS(A)</i> | | | |
| m2STS1_2 | | (S)-2-phenylpropanal | P ₁ -Rh-P ₂ bite angle = 88.3° Rh-C ₁ distance = 2.23 Å C ₂ -C ₃ distance = 2.28 Å |
| m2STS1_3 | | (S)-2-phenylpropanal | P ₁ -Rh-P ₂ bite angle = 91.1° Rh-C ₁ distance = 2.20 Å C ₂ -C ₃ distance = 2.32 Å |
| m2STS1_4 | | (S)-2-phenylpropanal | P ₁ -Rh-P ₂ bite angle = 92.0° Rh-C ₁ distance = 2.24 Å C ₂ -C ₃ distance = 2.26 Å |

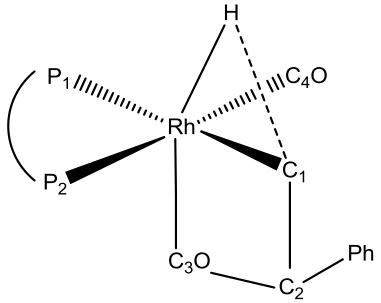
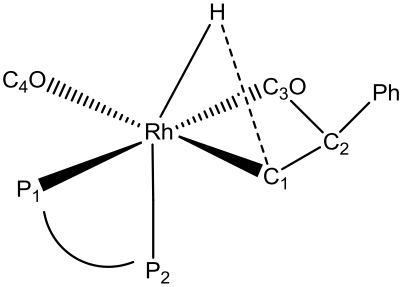
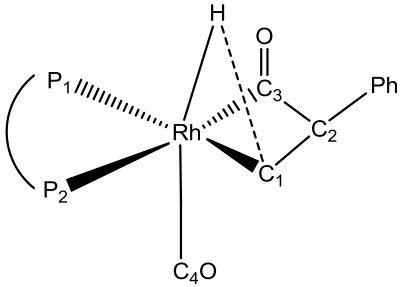
| Code of the complex molecule | Positions of core atoms | Metal complex belongs to the catalytic cycle that gives rise to: | Description of geometry |
|------------------------------|-------------------------|--|--|
| m2STS1_5 | | (S)-2-phenylpropanal | $P_1\text{-Rh-P}_2$ bite angle = 95.0° Rh-C ₁ distance = 2.20 Å C ₂ -C ₃ distance = 2.55 Å |
| m2RTS1_1 | | (R)-2-phenylpropanal | $P_1\text{-Rh-P}_2$ bite angle = 88.4° Rh-C ₁ distance = 2.17 Å C ₂ -C ₃ distance = 2.23 Å |
| m2RTS1_2 | | (R)-2-phenylpropanal | $P_1\text{-Rh-P}_2$ bite angle = 90.3° Rh-C ₁ distance = 2.23 Å C ₂ -C ₃ distance = 2.26 Å |

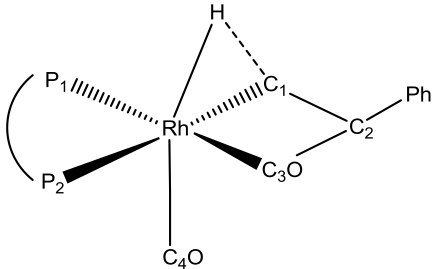
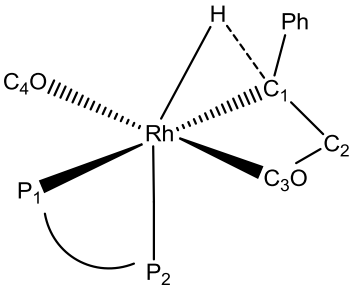
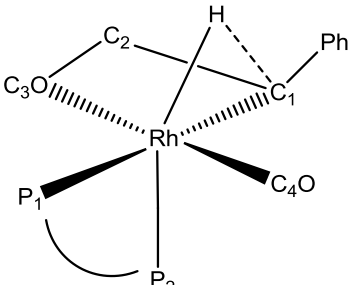
| Code of the complex molecule | Positions of core atoms | Metal complex belongs to the catalytic cycle that gives rise to: | Description of geometry |
|------------------------------|---|--|---|
| m2RTS1_3 |  | (R)-2-phenylpropanal | P ₁ -Rh-P ₂ bite angle = 92.4° Rh-C ₁ distance = 2.21 Å C ₂ -C ₃ distance = 2.31 Å |
| m2RTS1_4 |  | (R)-2-phenylpropanal | P ₁ -Rh-P ₂ bite angle = 91.7° Rh-C ₁ distance = 2.23 Å C ₂ -C ₃ distance = 2.27 Å |
| m2RTS1_5 |  | (R)-2-phenylpropanal | P ₁ -Rh-P ₂ bite angle = 89.5° Rh-C ₁ distance = 2.23 Å C ₂ -C ₃ distance = 2.22 Å |

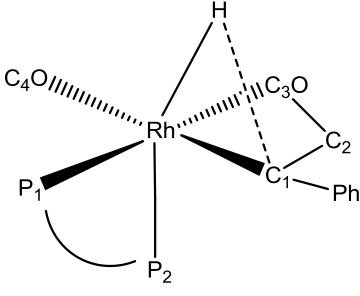
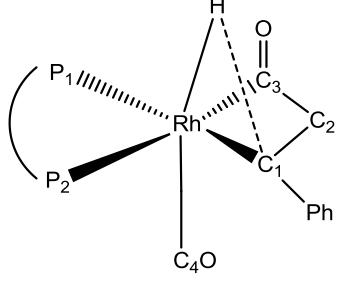
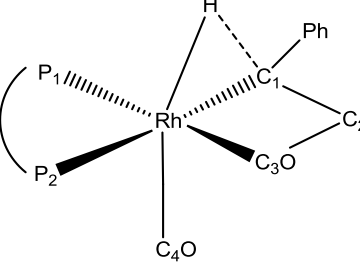
| Code of the complex molecule | Positions of core atoms | Metal complex belongs to the catalytic cycle that gives rise to: | Description of geometry |
|------------------------------|---|--|---|
| m2ITS1_2 |  | 3-phenylpropanal | $P_1\text{-Rh-}P_2$ bite angle = 94.9° Rh-C ₁ distance = 3.29 \AA C ₂ -C ₃ distance = 1.78 \AA |
| m2ITS1_7 |  | 3-phenylpropanal | $P_1\text{-Rh-}P_2$ bite angle = 91.5° Rh-C ₁ distance = 3.17 \AA C ₂ -C ₃ distance = 1.91 \AA |
| Step A | | | |
| m2_1S4 |  | (S)-2-phenylpropanal | $P_1\text{-Rh-}P_2$ bite angle = 92.6° C ₁ -Rh-C ₃ angle = 66.7° Rh-C ₁ distance = 2.16 \AA Rh-C ₃ distance = 2.09 \AA |

| Code of the complex molecule | Positions of core atoms | Metal complex belongs to the catalytic cycle that gives rise to: | Description of geometry |
|---------------------------------|-------------------------|--|---|
| m2_1R4 | | (R)-2-phenylpropanal | $P_1\text{-Rh-P}_2$ bite angle = 92.8° $C_1\text{-Rh-C}_3$ angle = 66.4° Rh-C_1 distance = 2.16 \AA Rh-C_3 distance = 2.08 \AA |
| m2_117 | | 3-phenylpropanal | $P_1\text{-Rh-P}_2$ bite angle = 92.8° $C_1\text{-Rh-C}_3$ angle = 66.4° Rh-C_1 distance = 2.23 \AA Rh-C_3 distance = 2.08 \AA |
| Transition state - TS(B) | | | |
| m2STS2_1 | | (S)-2-phenylpropanal | $P_1\text{-Rh-P}_2$ bite angle = 92.8° $C_1\text{-Rh-C}_3$ angle = 65.8° H-C_1 distance = 1.54 \AA Rh-C_1 distance = 2.27 \AA Rh-C_3 distance = 2.08 \AA |

| Code of the complex molecule | Positions of core atoms | Metal complex belongs to the catalytic cycle that gives rise to: | Description of geometry |
|------------------------------|---|--|---|
| m2STS2_3 |  | (S)-2-phenylpropanal | $P_1\text{-Rh-}P_2$ bite angle = 90.2° $C_1\text{-Rh-}C_3$ angle = 66.4° H-C_1 distance = 1.63 \AA Rh-C_1 distance = 2.27 \AA Rh-C_3 distance = 2.06 \AA |
| m2STS2_4 |  | (S)-2-phenylpropanal | $P_1\text{-Rh-}P_2$ bite angle = 91.9° $C_1\text{-Rh-}C_3$ angle = 65.7° H-C_1 distance = 1.60 \AA Rh-C_1 distance = 2.27 \AA Rh-C_3 distance = 2.07 \AA |
| m2RTS2_1 |  | (R)-2-phenylpropanal | $P_1\text{-Rh-}P_2$ bite angle = 95.8° $C_1\text{-Rh-}C_3$ angle = 66.4° H-C_1 distance = 1.57 \AA Rh-C_1 distance = 2.26 \AA Rh-C_3 distance = 2.07 \AA |

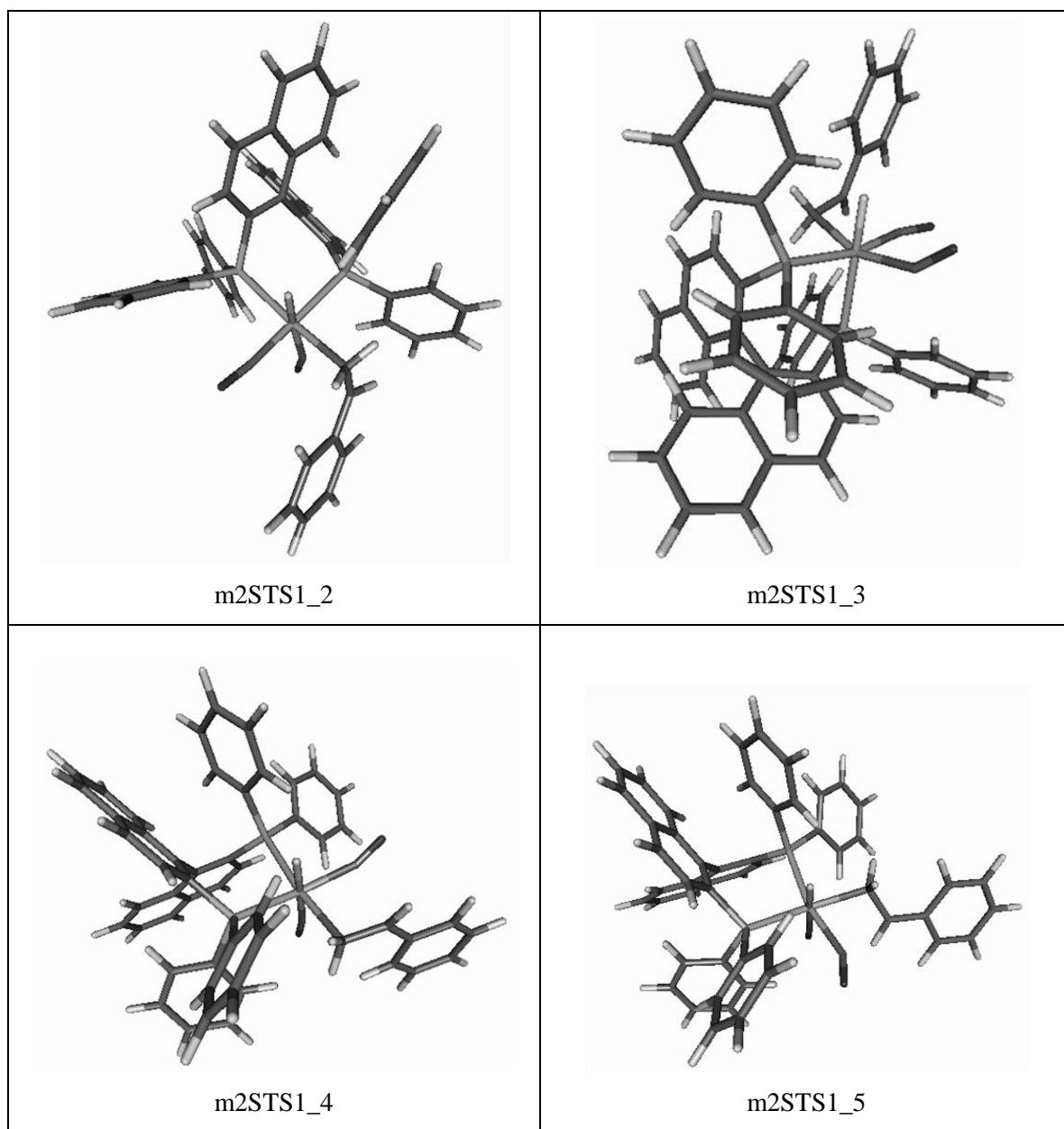
| Code of the complex molecule | Positions of core atoms | Metal complex belongs to the catalytic cycle that gives rise to: | Description of geometry |
|------------------------------|---|--|---|
| m2RTS2_2 |  | (R)-2-phenylpropanal | P ₁ -Rh-P ₂ bite angle = 89.0° C ₁ -Rh-C ₃ angle = 65.3° H-C ₁ distance = 1.83 Å Rh-C ₁ distance = 2.23 Å Rh-C ₃ distance = 2.12 Å |
| m2RTS2_3 |  | (R)-2-phenylpropanal | P ₁ -Rh-P ₂ bite angle = 91.0° C ₁ -Rh-C ₃ angle = 66.8° H-C ₁ distance = 1.62 Å Rh-C ₁ distance = 2.27 Å Rh-C ₃ distance = 2.05 Å |
| m2RTS2_4 |  | (R)-2-phenylpropanal | P ₁ -Rh-P ₂ bite angle = 91.5° C ₁ -Rh-C ₃ angle = 66.2° H-C ₁ distance = 1.58 Å Rh-C ₁ distance = 2.27 Å Rh-C ₃ distance = 2.08 Å |

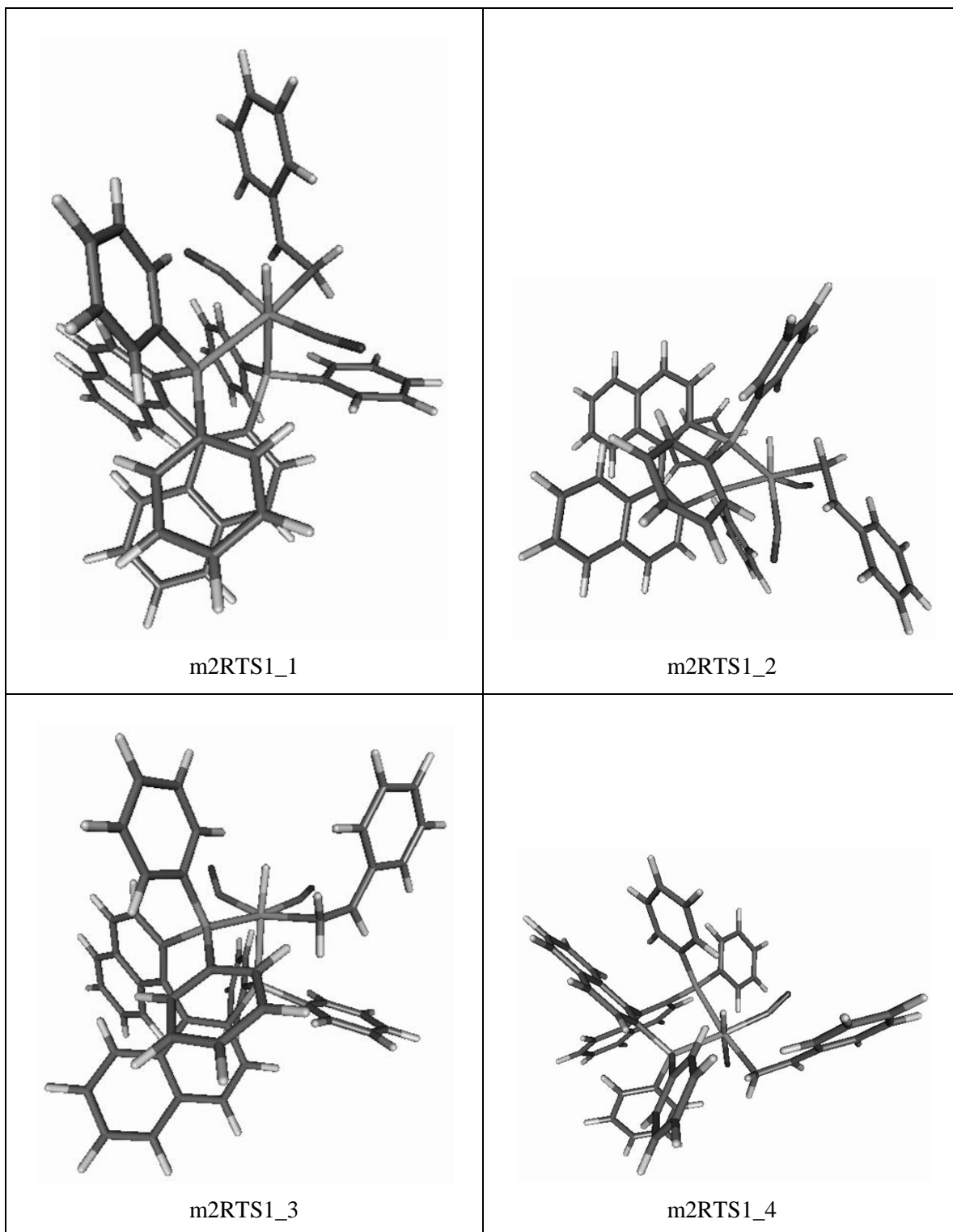
| Code of the complex molecule | Positions of core atoms | Metal complex belongs to the catalytic cycle that gives rise to: | Description of geometry |
|------------------------------|--|--|---|
| m2RTS2_5 |  | (R)-2-phenylpropanal | $P_1\text{-Rh-}P_2$ bite angle = 93.1° $C_1\text{-Rh-}C_3$ angle = 66.1° H-C_1 distance = 1.61 \AA Rh-C_1 distance = 2.27 \AA Rh-C_3 distance = 2.06 \AA |
| m2ITS2_1 |  | 3-phenylpropanal | $P_1\text{-Rh-}P_2$ bite angle = 95.4° $C_1\text{-Rh-}C_3$ angle = 65.5° H-C_1 distance = 1.59 \AA Rh-C_1 distance = 2.36 \AA Rh-C_3 distance = 2.07 \AA |
| m2ITS2_3 |  | 3-phenylpropanal | $P_1\text{-Rh-}P_2$ bite angle = 95.9° $C_1\text{-Rh-}C_3$ angle = 65.7° H-C_1 distance = 1.61 \AA Rh-C_1 distance = 2.35 \AA Rh-C_3 distance = 2.07 \AA |

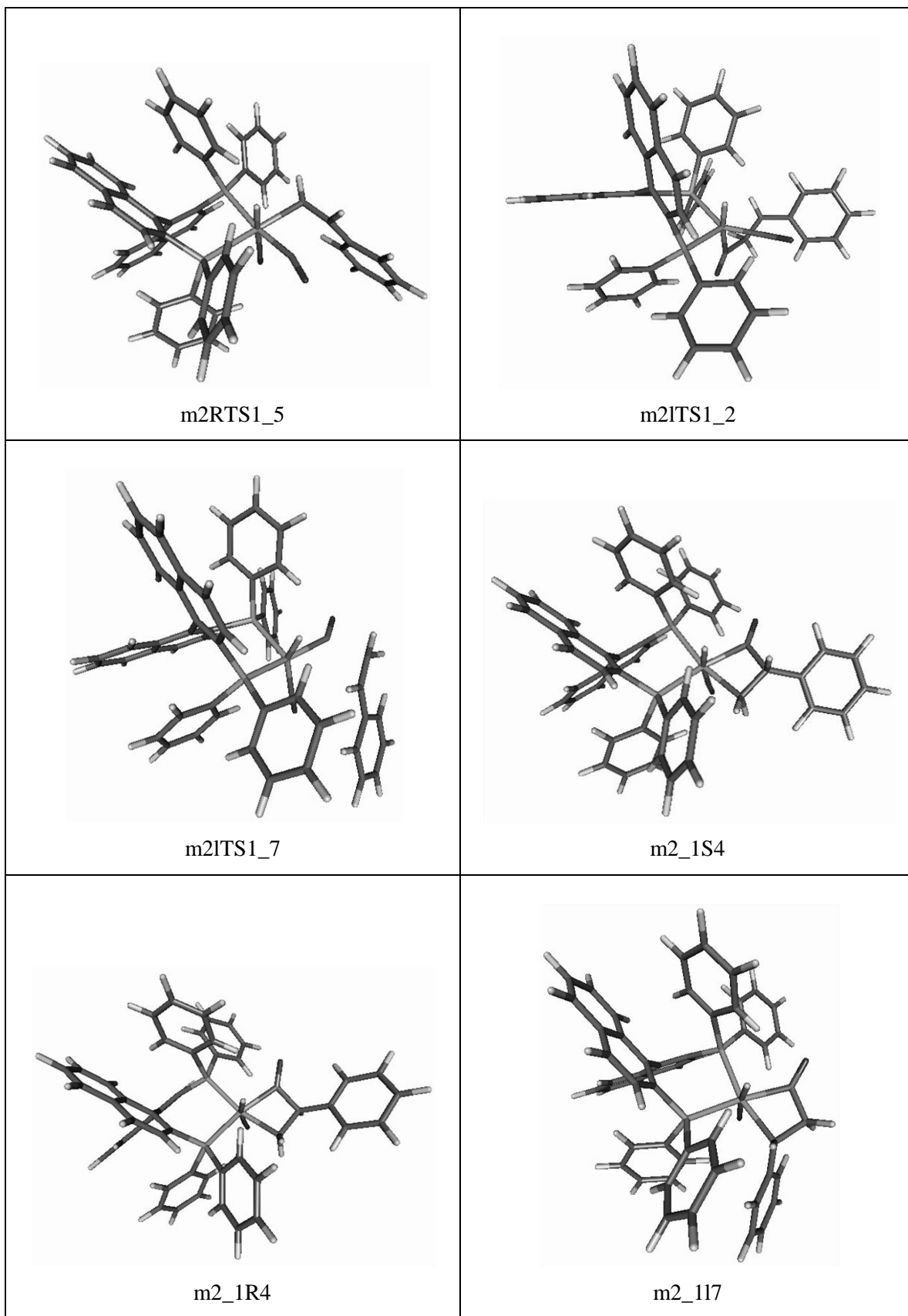
| Code of the complex molecule | Positions of core atoms | Metal complex belongs to the catalytic cycle that gives rise to: | Description of geometry |
|------------------------------|---|--|---|
| m2ITS2_5 |  | 3-phenylpropanal | $P_1\text{-Rh-}P_2$ bite angle = 90.8° $C_1\text{-Rh-}C_3$ angle = 65.7° H-C_1 distance = 1.68 \AA Rh-C_1 distance = 2.35 \AA Rh-C_3 distance = 2.06 \AA |
| m2ITS2_7 |  | 3-phenylpropanal | $P_1\text{-Rh-}P_2$ bite angle = 91.5° $C_1\text{-Rh-}C_3$ angle = 65.2° H-C_1 distance = 1.58 \AA Rh-C_1 distance = 2.37 \AA Rh-C_3 distance = 2.07 \AA |
| m2ITS2_8 |  | 3-phenylpropanal | $P_1\text{-Rh-}P_2$ bite angle = 93.4° $C_1\text{-Rh-}C_3$ angle = 65.5° H-C_1 distance = 1.66 \AA Rh-C_1 distance = 2.36 \AA Rh-C_3 distance = 2.06 \AA |

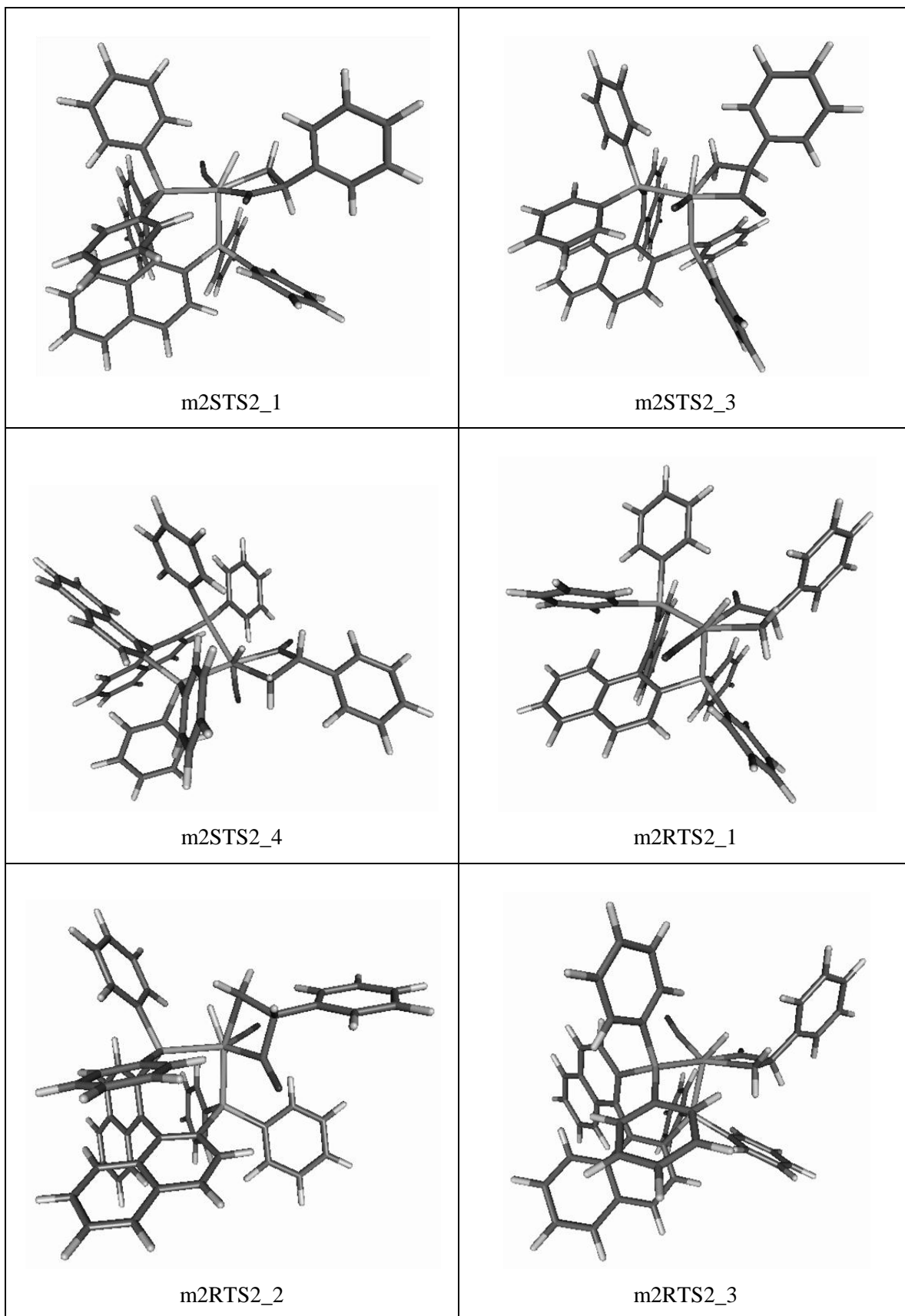
The following table 7 shows the optimized structures of the molecules listed in table 6:

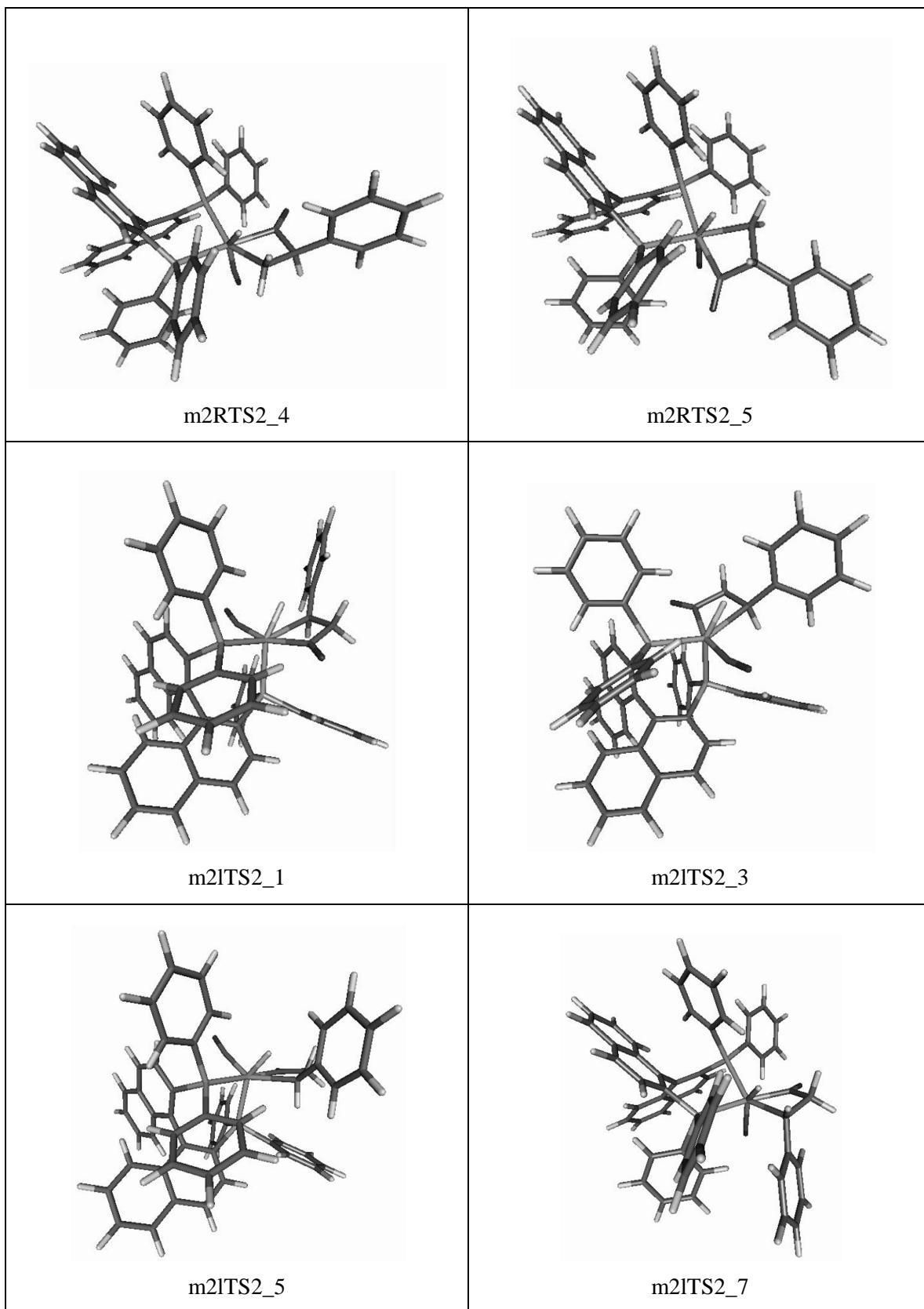
Table 7: Structures of molecules described in table 6

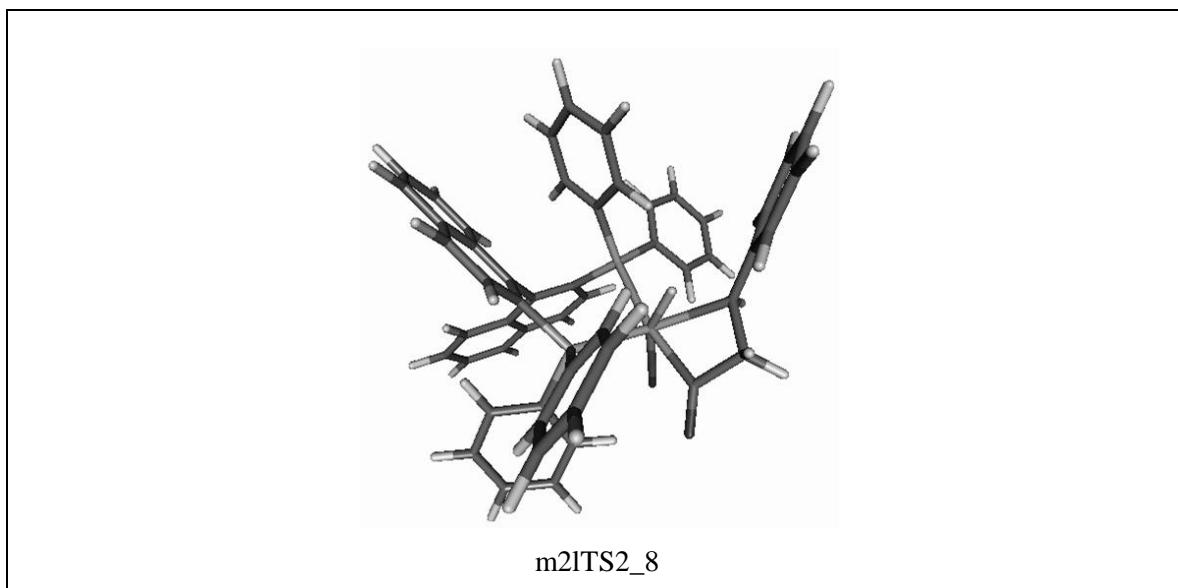












The molecules having the lowest free energies (both the stable molecules in every step and the transition states) were chosen and free energy profiles were plotted for all the three catalytic cycles of “mechanism 2”:

The free energy profile (solvated in toluene) as per “mechanism 2” for formation of (*S*)-2-phenylpropanal at 60 °C (333 K) is as follows:

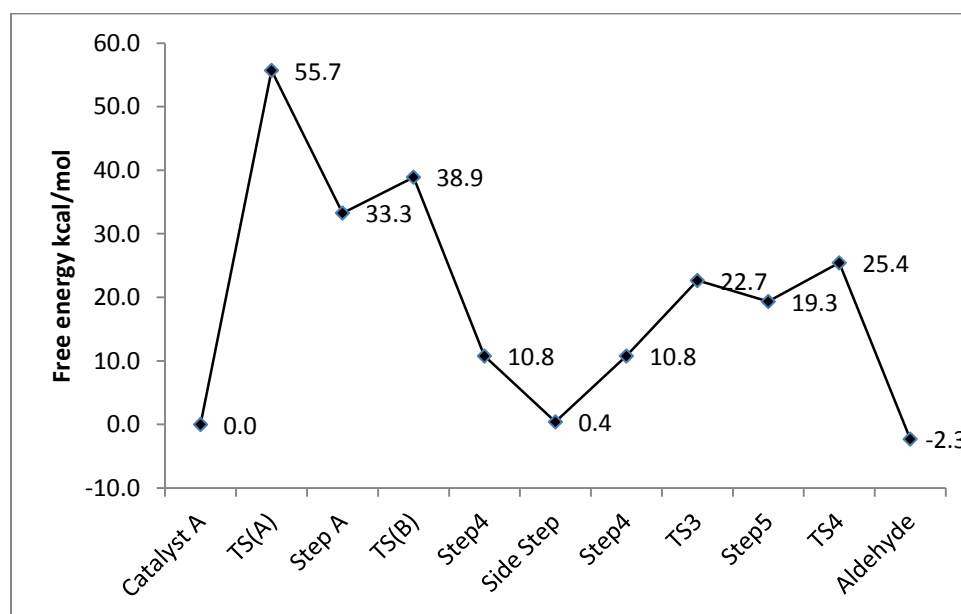


Figure 17: Free energy profile (solvated in toluene) for formation of (*S*)-2-phenylpropanal (“mechanism 2”)

The free energy profile (solvated in toluene) as per “mechanism 2” for formation of (*R*)-2-phenylpropanal at 60 °C (333 K) is as follows:

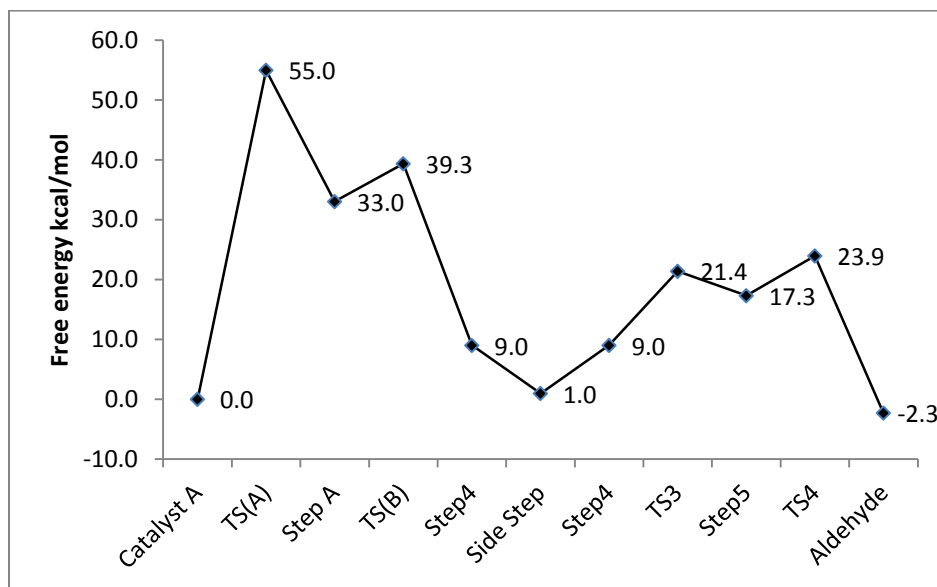


Figure 18: Free energy profile (solvated in toluene) for formation of (*R*)-2-phenylpropanal (“mechanism 2”)

The free energy profile (solvated in toluene) as per “mechanism 2” for formation of 3-phenylpropanal at 60 °C (333 K) is as follows:

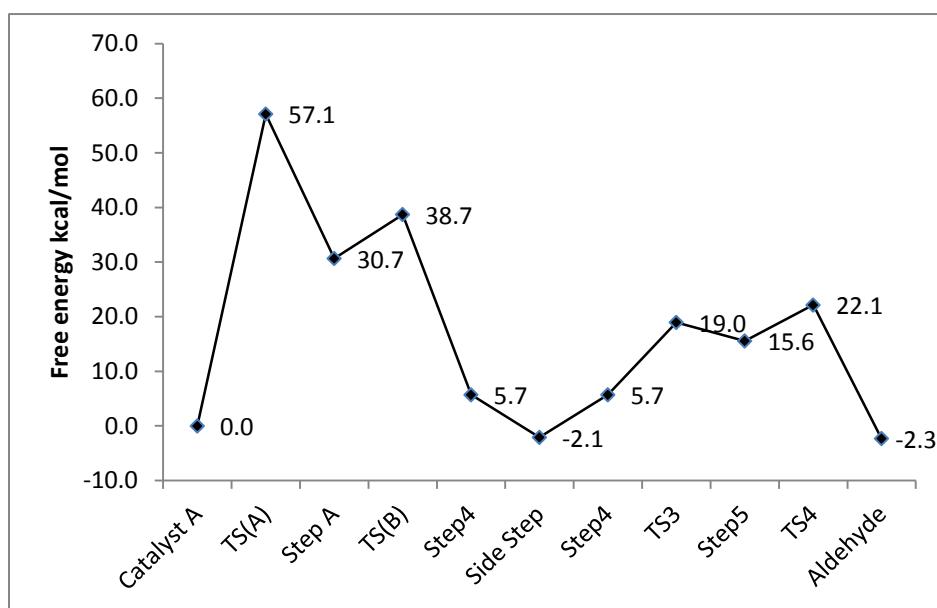


Figure 19: Free energy profile (solvated in toluene) for formation of 3-phenylpropanal (“mechanism 2”)

As depicted in the free energy profiles for “mechanism 2”, TS(A) is the rate determining step. 3-phenylpropanal has the highest activation energy and (*R*)-2-phenylpropanal has the lowest activation energy. Thus the “mechanism 2” can predict the trend for regioselectivity correctly (b/l ratio should be more than one). However it fails to predict the trend for enantioselectivity [enantiomeric excess is in favor of (*S*)-2-phenylpropanal as per the experimental study in chapter 2]. Moreover the activation energy of “mechanism 2” is prohibitive when compared to that of the Heck and Breslow mechanism.

So the possibility of the reaction following the “mechanism 2” was discarded.

One can make a small modification to “mechanism 2”, where instead of $\text{HRh}(\text{CO})_2[(R)\text{-BINAP}]$ acting as the catalyst, $\text{HRh}(\text{CO})[(R)\text{-BINAP}]$ is the catalyst. $\text{HRh}(\text{CO})[(R)\text{-BINAP}]$ is also the active catalyst in the Heck and Breslow mechanism.

In this “modified mechanism 2” the geometry for the first step (after addition of carbonyl to styrene) will be as follows:

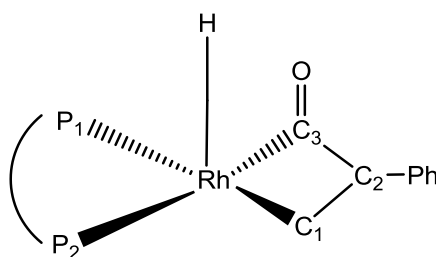


Figure 20: Complex that can be formed by insertion of styrene in the Rh-CO bond of $\text{HRh}(\text{CO})[(R)\text{-BINAP}]$

However even after the formation of the complex in figure 20, the reaction is likely to pass over the energy barrier of TS(B) and TS(B) (in all the three catalytic cycles) have higher free energy than TS1 of Heck and Breslow mechanism. So the “mechanism 2” cannot compete with the Heck and Breslow mechanism on energy basis, even after this modification.

3.3.3.8 Investigating the possibility of extra transition states in the Heck and Breslow mechanism: It was assumed that TS1, TS2, TS3 and TS4 are the only possible transition states in the Heck and Breslow mechanism. However there are reports in the

literature where uptake barriers play important role in the kinetics of catalytic reactions [17].

An attempt was made to find if there were any barriers for styrene uptake in the present reaction system. It was found that styrene indeed has an uptake barrier. When styrene approaches the catalyst molecule, the square planar geometry of the catalyst is disturbed. Moreover (*R*)-BINAP being a bulky ligand does not allow the styrene to approach the rhodium easily. The following figure 21 shows the structures of the transition states for styrene uptake:

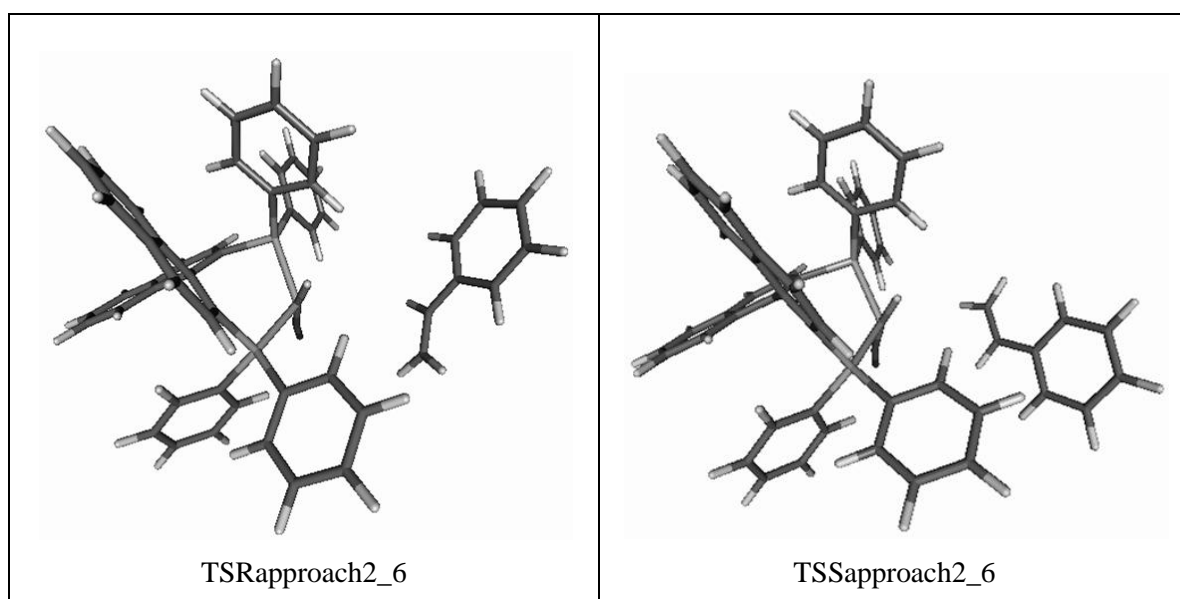


Figure 21: Styrene uptake transition states

The transition state - TSRapproach2_6 depicts the re-face of styrene approaching the rhodium atom. This transition state can give rise to (*R*)-2-phenylpropanal or 3-phenylpropanal.

TSSapproach2_6 depicts the si-face of styrene approaching the rhodium atom. This transition state can give rise to (*S*)-2-phenylpropanal or 3-phenylpropanal.

Using the information on styrene uptake barrier, modified energy profiles for the three parallel catalytic cycles were plotted for the Heck and Breslow mechanism.

The modified free energy profile (gas phase) for formation of (*S*)-2-phenylpropanal at 60°C (333 K) is as follows:

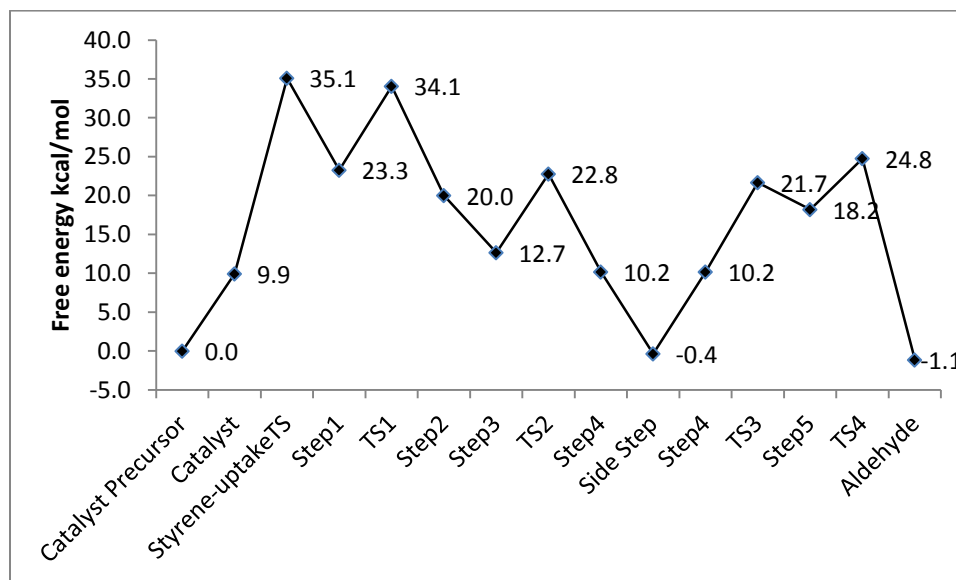


Figure 22: Modified free energy profile (gas phase) for formation of (*S*)-2-phenylpropanal

The modified free energy profile (gas phase) for formation of (*R*)-2-phenylpropanal at 60°C (333 K) is as follows:

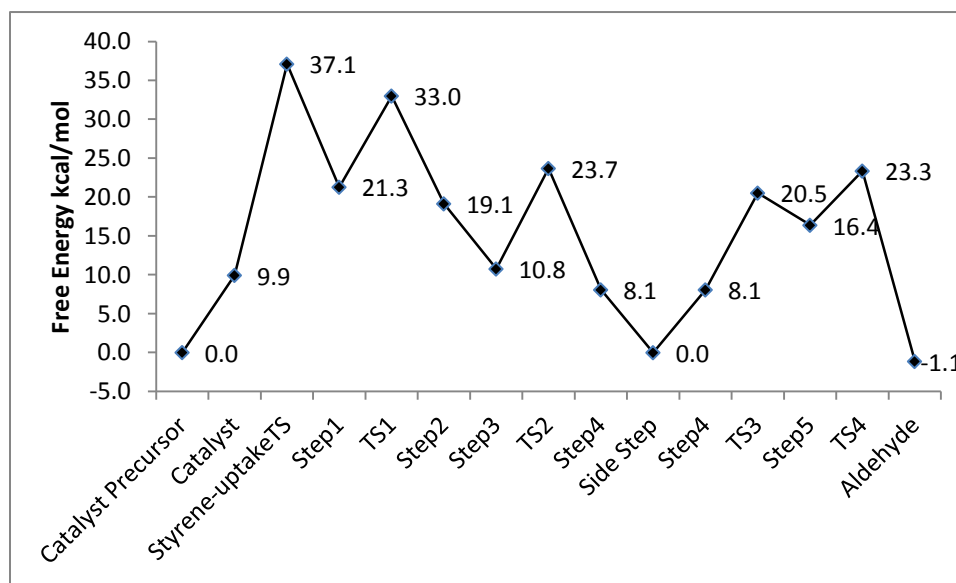


Figure 23: Modified free energy profile (gas phase) for formation of (*R*)-2-phenylpropanal

The free energy profile (gas phase) for formation of 3-phenylpropanal at 60 °C (333 K) is as follows:

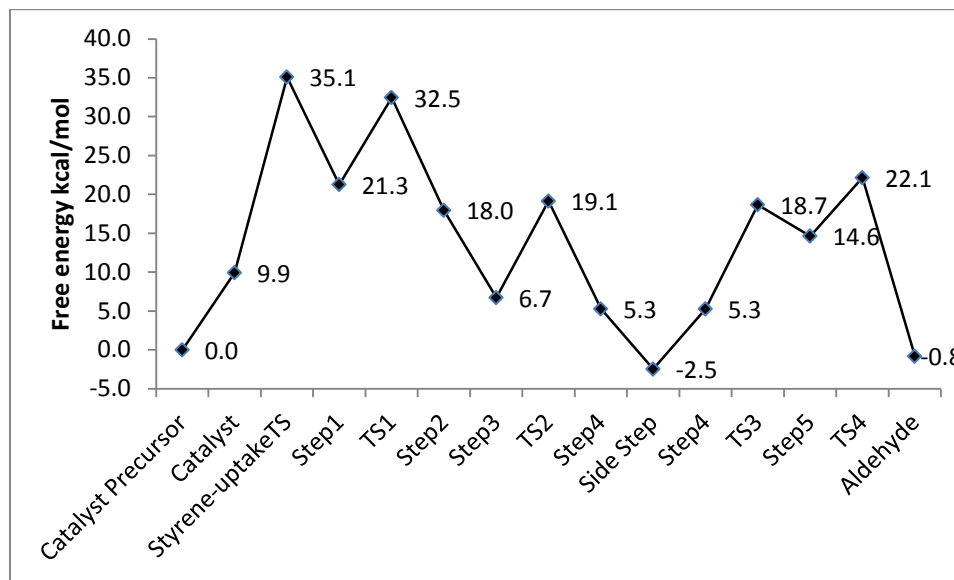


Figure 24: Modified free energy profile (gas phase) for formation of 3-phenylpropanal

As depicted in the styrene uptake modified free energy profiles for the three aldehydes, TSSApproach2_6 is the RDS for the formation of (*S*)-2-phenylpropanal and 3-phenylpropanal. TSRApproach2_6 is the RDS for the formation of (*R*)-2-phenylpropanal. The free energy of TSSApproach2_6 is lower than that of TSRApproach2_6 by 2.0 kcal/mol.

Thus the styrene uptake barrier (in combination with TS1) can explain the experimentally observed enantioselectivity [in favor of (*S*)-2-phenylpropanal]. However it cannot explain the experimentally observed regioselectivity which is in favor of the branched aldehyde.

Like there is an uptake barrier for the alkene, there can also be a barrier for removal of the aldehyde. However an attempt to find the aldehyde removal barrier was unsuccessful. A possible reason for the regioselectivity towards the branched aldehyde could be the stability of the “resting state” (“side step”) in the energy profile of the linear aldehyde in comparison to those of the branched ones.

3.4 Conclusions

A computational study on the entire catalytic cycle of asymmetric hydroformylation of styrene using (*R*)-BINAP modified rhodium catalyst was completed. Although a method of quantitative prediction of the activity/ selectivity of the catalyst could not be developed, an extremely important phenomenon of the uptake barrier of alkene being the RDS was discovered. This is the first time an alkene uptake barrier (and not the alkene insertion barrier) is being reported as the RDS for a hydroformylation reaction^[18].

It is important to note that this concept of the uptake barrier being the RDS can be applied to almost all asymmetric hydroformylation reactions. This is because almost all asymmetric hydroformylation reactions are carried out using ligands whose sizes are comparable to that of (*R*)-BINAP. Depending on which face of the prochiral alkene (re or si) has a smaller uptake barrier (and by knowing the alkene insertion barriers), one can qualitatively predict as to which enantiomer of the aldehyde product would be formed in excess.

Moreover, the concept of the alkene uptake barrier being the RDS can be extended even to achiral/ symmetric hydroformylation where large sized ligands are used to modify the metal catalyst. Larger the size of the ligand, larger would be the uptake barrier. Similarly, larger the size of the substrate, larger would be the uptake barrier. Which combination of various sizes of ligands and substrates will raise the alkene uptake barrier higher than the alkene insertion (into the Rh-H bond) barrier can be decided on a case to case basis using DFT study.

The results of the parametric study (chapter 2), like the first order dependence of the reaction rate on the hydrogen partial pressure and the negative order dependence of the reaction rate of the carbon monoxide partial pressure, can be predicted only after doing a stochastic simulation study or a energetic span model study^[19] on the energy profile obtained through DFT. However a stochastic simulation/ energetic span model study was out of the scope of this thesis.

References:

- [1] aC. J. Cobley, R. D. J. Froese, J. Klosin, C. Qin, G. T. Whiteker, K. A. Abboud, *Organometallics* **2007**, *26*, 2986-2999; bJ. Meeuwissen, A. J. Sandee, B. de Bruin, M. A. Siegler, A. L. Spek, J. N. H. Reek, *Organometallics* **2010**, *29*, 2413-2421.
- [2] M. Sparta, K. J. Børve, V. R. Jensen, *Journal of the American Chemical Society* **2007**, *129*, 8487-8499.
- [3] H. HyperChem, *Gainesville, FL*, 32601.
- [4] R. C. D. ROCKS.
- [5] R. Ahlrichs, F. Furche, C. Hättig, W. Klopper, M. Sierka, F. Weigend, *University of Karlsruhe: Karlsruhe, Germany* **2009**.
- [6] aP. A. M. Dirac, *Proceedings of the Royal Society of London. Series A* **1929**, *123*, 714; bJ. C. Slater, *Physical Review* **1951**, *81*, 385; cS. H. Vosko, L. Wilk, M. Nusair, *Canadian Journal of Physics* **1980**, *58*, 1200-1211; dA. D. Becke, *Physical Review A* **1988**, *38*, 3098; eJ. P. Perdew, *Physical Review B* **1986**, *33*, 8822.
- [7] M. Feyereisen, G. Fitzgerald, A. Komornicki, *Chemical physics letters* **1993**, *208*, 359-363.
- [8] M. Sierka, A. Hogekamp, R. Ahlrichs, *The Journal of chemical physics* **2003**, *118*, 9136.
- [9] G. S. Almasi, A. Gottlieb, *Redwood City, The* **1990**.
- [10] A. Von Zelewsky, *Stereochemistry of coordination compounds, Vol. 3*, John Wiley & Sons Inc, **1996**.
- [11] M. E. Cass, K. K. Hii, H. S. Rzepa, *Journal of Chemical Education* **2006**, *83*, 336.
- [12] aJ. Perdew, Y. Wang, *Wang Y (1992) Phys Rev B* **1992**, *45*, 13244; bJ. P. Perdew, K. Burke, M. Ernzerhof, *Physical Review Letters* **1996**, *77*, 3865-3868.
- [13] C. Møller, M. S. Plesset, *Physical Review* **1934**, *46*, 618.
- [14] F. Prestopino, R. Persson, M. Monari, N. Focci, E. Nordlander, *Inorganic Chemistry Communications* **1998**, *1*, 302-304.
- [15] C. S. Chung, *Journal of Chemical Education* **1984**, *61*, 1062.
- [16] K. Nozaki, T. Matsuo, F. Shibahara, T. Hiyama, *Organometallics* **2003**, *22*, 594-600.
- [17] aK. Vanka, Z. Xu, T. Ziegler, *Canadian journal of chemistry* **2003**, *81*, 1413-1429; bM. Bochmann, *Organometallics* **2010**; cZ. Flisak, T. Ziegler, *Proceedings of the National Academy of Sciences* **2006**, *103*, 15338.
- [18] E. Zuidema, L. Escorihuela, T. Eichelsheim, J. J. Carbó, C. Bo, P. C. J. Kamer, P. W. N. M. van Leeuwen, *Chemistry-A European Journal* **2008**, *14*, 1843-1853.
- [19] aS. Kozuch, S. Shaik, *Accounts of Chemical Research* **2010**; bA. Uhe, S. Kozuch, S. Shaik, *Journal of computational chemistry* **2010**; cS. Kozuch, J. M. L. Martin, *ACS Catalysis* **2011**, *1*, 246-253.